Feedback between a retinoid-related nuclear receptor and the *let-7* microRNAs controls the pace and number of molting cycles in *C. elegans.*

Ruhi Patel[1,3]*, Himani Galagali[2]*, John K. Kim[2]† and Alison R. Frand[1]†

*Equal contributions

[1] Department of Biological Chemistry, David Geffen School of Medicine
University of California, Los Angeles, Los Angeles, CA 90095

[2] Department of Biology, Johns Hopkins University
Baltimore, MD 21218

[3] Current address:
Department of Molecular Immunology and Microbiology, David Geffen School of Medicine
University of California, Los Angeles, Los Angeles, CA 90095

†To whom correspondence should be addressed:
jnkim@jhu.edu
afrand@mednet.ucla.edu

Keywords: molting cycle, gene expression oscillations, heterochronic pathway, ultradian and circadian rhythms

Abbreviations:

CCG	Clock Controlled Gene
ChIP	Chromatin Immunoprecipitation
CRISPR	Clustered Regularly Interspersed Short Palindromic Repeats
crRNA	CRISPR RNA
GFP	Green Fluorescent Protein
iCLIP	Individual-nucleotide resolution Crosslinking Immunoprecipitation
LCS	*let-7* Consensus Site
let	Lethal
MFE	Minimum Free Energy
Mlt	Molting Cycle Defective
NHR	Nuclear Hormone Receptor
nls	nuclear localization signal
PER	PERIOD gene
pri	Primary
qPCR	Quantitative Polymerase Chain Reaction
RE	Response Element
RNAi	RNA interference
ROR	Retinoid-related Orphan Receptor
RORE	Retinoid-related Orphan Receptor Response Element
siRNA	Short-interfering RNA
ssODN	Single Stranded Oligo DNA Nucleotide
tdTomato	Tandem Tomato
tracrRNA	Trans-activating crRNA
UTR	Untranslated Region

SUMMARY

Animal development requires coordination among cyclic processes, sequential cell fate specifications, and once-a-lifetime morphogenic events, but the underlying mechanisms are not well understood. *C. elegans* undergo four molts at regular 8–10 h intervals. The pace of the cycle is governed by PERIOD/*lin-42* and other as-yet unknown factors. Cessation of the cycle in young adults is controlled by the *let-7* family of microRNAs and downstream transcription factors in the heterochronic pathway. Here, we characterize a negative feedback loop between NHR-23, the worm homolog of mammalian retinoid-related orphan receptors (RORs), and the *let-7* family of microRNAs that regulates both the frequency and finite number of molts. The molting cycle is decelerated in *nhr-23* knockdowns, accelerated in *let-7(-)* mutants, and similar to wild type animals in *let-7(-) nhr-23(-)* double mutants. NHR-23 binds response elements (ROREs) in the *let-7* promoter and activates transcription. In turn, *let-7* dampens *nhr-23* expression across development via a complementary *let-7* binding site (LCS) in the *nhr-23* 3′ UTR. The molecular interactions between NHR-23 and *let-7* hold true for other *let-7* family microRNAs. Either derepression of *nhr-23* transcripts by LCS deletion or high gene dosage of *nhr-23* leads to protracted behavioral quiescence and extra molts in adults. NHR-23 and *let-7* also co-regulate scores of genes required for execution of the molts, including *lin-42.* In addition, ROREs and LCSs isolated from mammalian *ROR* and *let-7* genes function in *C. elegans*, suggesting conservation of this feedback mechanism. We propose that this feedback loop unites the molting timer and the heterochronic gene regulatory network possibly by functioning as a cycle counter.

Introduction

Timekeeping is a critical component of animal development. Developmental clocks, like the somitogenesis clocks of vertebrates and segmentation clocks of insects, govern the frequency of cyclic processes (Diaz-Cuadros et al., 2021; Uriu, 2016). Heterochronic gene pathways, like the microRNA-mRNA networks in *Caenorhabditis elegans* and other organisms, regulate sequential events and orchestrate the timing of development across tissue types (Ambros and Ruvkun, 2018; Galagali and Kim, 2020). The mechanism by which developmental clocks and heterochronic pathways interact to coordinate repeated developmental processes with cell fate transitions remains unknown.

Studies of circadian rhythms have provided a framework for understanding how biological clocks schedule rhythmic processes. The circadian clock governs diurnal physiologic rhythms in animals, for example, feeding-fasting and sleep-wake cycles, and helps coordinate the underlying cellular and molecular processes to predictable 24 hour (h) changes in the environment (Takahashi, 2016). The period of developmental clocks, unlike physiologic clocks, may vary based on changes in external environmental cues, such as temperature, nutrition and growth factors. Developmental clocks that regulate morphogenic processes may also need to stop after a finite number of iterations (Rensing et al., 2001; Tsiairis and Grosshans, 2021).

The mechanistic basis for both developmental and physiological clocks are molecular-genetic oscillators. Cyclical expression of the core components of oscillators and their target genes together underlie biological rhythms. Molecular-genetic oscillators are comprised of interconnected feedback loops among the core components. Theoretical studies indicate that negative feedback loops with intrinsic delays or interdependent positive and negative feedback loops with intrinsic delays can both set up self-sustaining genetic oscillators (Johnson and Day, 2000; Novak and Tyson, 2008; Tsiairis and Grosshans, 2021). In both cases, time delays are caused in part by unequal rates of RNA versus protein synthesis and degradation. For example, during somitogenesis, the Hes7 transcription factor represses its own transcription, setting up a negative feedback loop with a delay (Bessho et al., 2003).

The key components of the mammalian circadian clock in mammals also consists of transcriptional activators and repressors interacting through interlocked feedback loops. During the day, CLOCK and BMAL1 activate the transcription of *PERIOD/PER* and other genes. During the night, PER proteins interact with CLOCK and BMAL1 and repress their own transcription (Partch et al., 2014; Takahashi, 2016; 2017). The short half-life of the PER protein, in combination with the continued transcriptional repression of *PER*, results in decrease of PER proteins late in the night. The decrease in the levels of PER is accompanied by increases in the levels of CLOCK

113 and BMAL1 early in the morning. CLOCK and BMAL1 also activate transcription of *REV-ERB*α
114 and *REV-ERB*β. The competition between the transcriptional repressors, REV-ERBs, and the
115 transcriptional activators, the Retinoid-related Orphan Receptors (RORs), for the same binding
116 sites in the *BMAL1* promoter regulates rhythmic expression of *BMAL1* in peripheral organs and
117 the central nervous system (Cook et al., 2015; Zhang et al., 2017).

118 The components of the circadian clock are also subject to post-transcriptional and post-
119 translational regulation. The *bantam* microRNAs regulate the temporal expression of *Drosophila*
120 *clock* by directly binding the *clock* 3′ UTR and repressing translation (Kadener et al., 2009). In
121 mice, the microRNAs *miR-24* and *miR-30* regulate stability of *Per2* mRNA and repress translation
122 through interactions with the *Per2* 3′ UTR (Yoo et al., 2017). A few other microRNAs regulate the
123 expression of core clock components. However, the prevalence of microRNA-mediated post-
124 transcriptional feedback loops among biological clocks is not well understood (Alvarez-Saavedra
125 et al., 2011; Chen et al., 2013; Du et al., 2014).

126 Molting in *C. elegans* is a reiterated and periodic developmental process. Under favorable
127 conditions, *C. elegans* develop through four larval stages, L1–L4. Larvae molt from one stage to
128 the next at regular 8–10 h intervals and then emerge as adults. *C. elegans* enter and exit a state
129 of behavioral quiescence, termed lethargus, during each molt (Figure 1A). Across lethargus,
130 epithelia detach from the old cuticle and synthesize the new cuticle. The animal then escapes
131 from the old cuticle at ecdysis. Newly emerged larvae forage and feed during the intermolt. Prior
132 studies identified PER/LIN-42 as a key component of the underlying pacemaker (Monsalve et al.,
133 2011, McCulloch and Rougvie, 2014).

134 More recent work has identified and modeled a single genetic oscillator that governs the
135 oscillatory expression of more than 3,700 genes across *C. elegans* larval development, including
136 257 linked to specific aspects of molting (Hendriks et al., 2014; Kim et al., 2013; Meeuse et al.,
137 2020). Transcript levels of these genes oscillate with the same frequency as the molting cycle,
138 and the waveforms have a phase-locked peak once per larval stage, i.e., the genes peak at the
139 same relative time-point within each larval stage (Meeuse et al., 2020; Tsiairis and Großhans,
140 2021). It is not known whether the PER-based molting cycle timer and the genetic oscillator
141 represent the same timekeeping mechanism.

142 The heterochronic gene pathway regulates the timing of unidirectional cell fate transitions
143 during the development of *C. elegans*. Key heterochronic genes include the conserved *let-7*
144 microRNA, its paralogs, and stage-specific targets of the *let-7* family (Abbott et al., 2005; Ambros
145 and Ruvkun, 2018; Reinhart et al., 2000) (Figure 1B). Each larval stage is marked by stereotypic
146 divisions of the lateral epidermal stem cells, called seam cells. The *let-7* paralogs *mir-48, mir-84*,

147 and *mir-241* specify the L2 fate of the seam cells, wherein the cells undergo one symmetric and
148 one asymmetric division (Abbott *et al.*, 2005). The *let-7* microRNA specifies later L3 and L4 fates,
149 which include homotypic fusion of the seam cells into lateral syncytia and secretion of trilobed
150 structures in the worm cuticle called alae (Reinhart *et al.*, 2000; Vadla et al., 2012).

151 NHR-23, the only *C. elegans* homolog of mammalian ROR transcription factors, is
152 repeatedly expressed in the larval epidermis during each larval stage (Frand et al., 2005;
153 Kostrouchova et al., 1998). Predicted targets of NHR-23 are enriched for genes associated with
154 molting, including cuticle collagens and enzymes necessary for synthesis and degradation of the
155 cuticle (Kouns et al., 2011). LIN-42, the *C. elegans* homolog of the core circadian clock protein
156 and tumor suppressor PERIOD (Jeon et al., 1999), sustains the 8 h intervals between molts
157 (Monsalve *et al.*, 2011). LIN-42 and the *let-7* family mutually inhibit one another (Figure 1C)
158 (McCulloch and Rougvie, 2014; Perales et al., 2014; Reinhart *et al.*, 2000; Van Wynsberghe et
159 al., 2014). Moreover, homologs of genes involved in the maintenance of circadian rhythm in
160 *Drosophila* interact genetically with *let-7* and regulate the L4-to-adult transition in *C. elegans*
161 (Banerjee et al., 2005).

162 Further evidence of crosstalk between the molting cycle timer and the heterochronic
163 pathway comes from the observation that the levels of primary *let*-7 family transcripts cycle in
164 phase with the molts (McCulloch and Rougvie, 2014; Van Wynsberghe et al., 2011). The cyclical
165 expression profile of primary *let*-7 family transcripts is consistent with temporally reiterated, as
166 well as stage-specific, function(s). However, the transcriptional activator responsible for the
167 oscillatory expression of *let-7* remains unknown.

168 Here, we show that both NHR-23 and the *let*-7 family of microRNAs (the *let*-7s) are key
169 components of a simple regulatory circuit that operates within the molecular-genetic oscillator
170 underlying the molting cycle and also within the heterochronic gene regulatory network. Using
171 longitudinal studies of the biorhythm of molting in relevant genetic backgrounds, molecular and
172 cell biological analyses, and bioinformatic approaches, we show that NHR-23 transcriptionally
173 activates the *let-7s* and, in turn, the *let-7s* post-transcriptionally repress *nhr-23* mRNA. In addition,
174 NHR-23 positively autoregulates its own transcription. Together, NHR-23/ROR and the *let-7s*
175 establish a transcriptional–post-transcriptional feedback loop that governs the pace and extinction
176 of the cycle after four iterations. As both the key components and *cis*-regulatory elements
177 comprising this feedback loop are conserved from nematodes to mammals, our findings may
178 apply to specific developmental and circadian clocks of humans and related pathologies including
179 birth defects, malignancies, sleep disorders, and metabolic syndromes (Oyama et al., 2017; Patke
180 et al., 2017; Puram et al., 2016; Roenneberg and Merrow, 2016).

181

182 **RESULTS**

183

184 **Larval molting cycles lengthen in *nhr-23* knockdowns and shorten in *let-7* family mutants.**

185 To determine the role of *nhr-23* and *let-7* in timing the molting cycle, we measured and
186 compared the length of molting cycles in *nhr-23* knockdowns, *let-7* mutants, and control larvae
187 through a series of longitudinal studies. Each experiment captured one iteration of the molting
188 cycle. The full set captured emergence of L2s, L3s, L4s and young adults. In each experiment,
189 we measured 1) the interval of physical activity in the target stage (defined as the time elapsed
190 between successive episodes of lethargus); 2) the interval of lethargus associated with the molt;
191 and 3) the wake-to-wake interval (defined as the time elapsed between two sequential transitions
192 from lethargus to activity) (Figure 2A).

193 Feeding L1 stage hatchlings bacteria that express dsRNAs complementary to *nhr-23*
194 (*nhr-23(RNAi)*) usually leads to severe molting defects and larval arrest in the L2 stage. To
195 circumvent L2 arrest and determine how knockdown of *nhr-23* affects the timing of the L3 and L4
196 stages, we maintained worms on control bacteria for 6 h and 14 h, respectively, and then moved
197 the worms to *nhr-23(RNAi)* bacteria. This strategy ensured that all test subjects emerged in the
198 target stage superficially normal, but none of the test subjects fully shed the cuticle from the
199 ensuing molt—signifying complete penetrance of the molting-defective (Mlt) phenotype
200 associated with *nhr-23(RNAi)*. Age-matched, wild-type larvae fed the same bacterial strain
201 transformed with an empty vector served as controls.

202 The actograms in Figure 2 display the results of these longitudinal studies. Each actogram
203 corresponds to an isogenic cohort of animals. Therein, each column represents a single animal
204 that emerged in the target stage (L4 in Figure 2B and L3 in Figure 2C), developed, and underwent
205 the ensuing molt. Each animal was isolated during the preceding molt to achieve stringent
206 synchronization at the outset. After it emerged, the worm was observed for approximately 1 min
207 at regular 1-h intervals. At each timepoint, the worm was "active" if both pharyngeal muscle
208 contractions (pumps) and sinusoidal locomotion were observed. Conversely, the subject was
209 "lethargic" if neither pharyngeal pumps nor sinusoidal locomotion were observed, and its body
210 posture resembled a hockey stick (Iwanir et al., 2013; Raizen et al., 2008). Separation of the
211 preexisting cuticle from the body and detection of the shed cuticle on the culture plate signified
212 the commencement and completion of ecdysis, respectively (Singh and Sulston, 1978).

213 As expected, the cohort of wild-type (control) animals first emerged as L4s, then entered
214 and exited lethargus, shed the larval cuticle (ecdysed), and emerged as young adults almost

synchronously (Figure 2B and Supplemental Table 1). The cohort of *nhr-23(RNAi)* animals that emerged as L4s entered lethargus later and remained lethargic for twice as long as the control cohort. All of the *nhr-23(RNAi)* animals began to pump and locomote once again, but oftentimes at lower rates than wild-type adults. In principle, this intermittent sluggishness might result from incomplete arousal or hindrance by unshed parts of the L4-stage cuticle. Regardless, the wake-to-wake interval of the L4-stage *nhr-23(RNAi)* cohort was 13 ± 1.1 h as compared with 10.3 ± 0.4 h for the control cohort ($p \leq 0.0001$). Following this trend, the L3-stage cohort of *nhr-23(RNAi)* larvae also entered lethargus later and remained in lethargus twice as long as the age-matched wild-type cohort (Figure 2C). Similarly, the cohort of *nhr-23(RNAi)* larvae molting from L2 to L3 were in lethargus 3-fold longer than the age-matched controls (Supplemental Table 1). Thus, delayed and protracted lethargi were associated with knockdown of *nhr-23* across three larval stages.

To evaluate the role of the *let-7s*, we tracked cohorts of *let-7(n2853)*, *let-7(mg279)* and *let-7(mg279); mir-84(tm1304)* double mutants across late larval stages. Both *n2853* and *mg279* are associated with lower levels of mature *let-7*, relative to wild-type animals. However, *n2853* is a substitution in the seed sequence, whereas *mg279* is a 27 bp deletion upstream of the mature microRNA (Bracht et al., 2004; Reinhart *et al.*, 2000). The null allele of *mir-84* enhances relevant phenotypes associated with *let-7(mg279)* (Hayes and Ruvkun, 2006). We also tracked *mir-48 mir-241(nDf51); mir-84(n4037)* triple mutants across L2, when the corresponding microRNAs are expressed but mature *let-7* is not yet detected (McCulloch and Rougvie, 2014). In contrast to animals subjected to *nhr-23(RNAi)*, *let-7(n2853)* mutants both entered and exited lethargus more quickly than wild-type animals. For example, the wake-to-wake interval for the *let-7(n2853)* cohort developing from L4s into adults was only 7.9 ± 0.6 h, an acceleration of 2.9 ± 0.7 h relative to the wild-type cohort (Figure 2B). All of the *let-7(n2853)* animals subsequently ruptured at the vulva, a hallmark of this strong loss-of-function allele (Ecsedi et al., 2015). In complementary studies, L4-stage cohorts of both *let-7(mg279)* single and *let-7(mg279); mir-84(tm1304)* double mutants also entered lethargus ahead of wild-type L4s (Supplemental Table 1). Moreover, the cohort of *let-7(n2853)* mutants observed from emergence in L3 onward passed through two consecutive lethargic phases and emerged as young adults ahead of the entire wild-type cohort (Figure 2C). As such, repetition of the L3 stage, a retarded heterochronic phenotype, cannot explain the acceleration of the L4 stage observed in *let-7(n2853)* mutants, because both the L3 and L4 stages of the mutants were shorter than those of wild-type larvae. Thus, lethargus was advanced and larval development was accelerated in three distinct mutants of the *let-7* family.

248 When we combined stage-specific *nhr-23(RNAi)* with *let-7(n2853)*, the altered pace of
249 molting associated with each single mutant was partially co-suppressed (Figure 2B, C and
250 Supplemental Table 1). Strikingly, none of the *let-7(n2853)* mutants ruptured on *nhr-23(RNAi)*,
251 suggesting that the *let-7*-mediated suppression of *nhr-23* regulates both lethargus and the
252 morphogenesis of the vulva. (Figure 2B). The L4-stage cohort of *nhr-23(RNAi) let-7(n2853)*
253 double mutants entered lethargus later than *let-7(n2853)* single mutants but emerged from
254 lethargus earlier than *nhr-23(RNAi)* single mutants. As a result, the wake-to-wake interval of the
255 L4-stage cohort of *nhr-23(RNAi) let-7(n2853)* double mutants was 10.6 ± 0.8 h, similar to the
256 value of the wild-type cohort ($p \geq 0.9$). Notably, *nhr-23(RNAi) let-7(n2853)* double mutants
257 underwent aberrant ecdysis, indicating that the role of *nhr-23* in lethargus and ecdysis are
258 genetically separable.
259 Partial co-suppression of the altered pace of molting was also apparent during the L2 and
260 L3 stages. The wake-to-wake interval of the *nhr-23(RNAi) let-7(n2853)* double mutants during the
261 L3 stage was 1.4 ± 1.4 h shorter than *nhr-23(RNAi)* alone ($p=0.0002$). Moreover, the triple
262 knockout of the *let-7* sisters, *mir-48 mir-241(nDf51); mir-84(n4037),* partially suppressed the
263 prolonged lethargy associated with *nhr-23(RNAi)* across the L2/L3 molt, shortening the lethargic
264 interval by 0.9 ± 1.0 h ($p=0.002$, Supplemental Table 1) to that of wild-type animals.
265 Taken together, these longitudinal data suggest a model whereby NHR-23 accelerates
266 the molting cycle, partly by directly activating the expression of the *let-7s*, and the *let-7s* decelerate
267 the cycle, partly by directly repressing the expression of *nhr-23*.
268
269 **NHR-23 promotes oscillatory expression of primary *let-7* and its paralogs.**
270 Based on the findings of the longitudinal studies described above, we hypothesized that
271 NHR-23 may directly activate transcription of *let-7*. Consistent with this hypothesis, a binding peak
272 for NHR-23 was reported within ~300 bp upstream of primary *let-7* by the ModENCODE
273 Consortium (Figure 3A) (Celniker et al., 2009). Nuclear hormone receptors usually bind DNA
274 response elements as homotypic or heterotypic dimers (Evans and Mangelsdorf, 2014). NHR-23
275 and its mammalian counterpart RORα are among the few that bind the consensus sequence 5′-
276 (A/G)GGTCA-3′ as monomers to activate transcription of target genes (Giguere et al., 1994;
277 Kouns et al., 2011). We identified 3 occurrences of this sequence, called the ROR response
278 element (RORE), within the reported NHR-23 binding peak (Figure 3A). Additionally, the 300 bp
279 region containing the ROREs is contained within a previously characterized enhancer element
280 required for *let-7* transcription (Johnson et al, 2003, Kai et al, 2013).

281 To validate NHR-23 binding upstream of *let-7* during L3 and L4, we appended the coding
282 sequence for a 3xFLAG affinity tag to the endogenous *nhr-23* gene using the CRISPR-Cas9
283 system (Paix et al., 2015) and performed chromatin immunoprecipitation coupled with gene-
284 specific, quantitative polymerase chain reactions (ChIP-qPCR). The signal flanking RORE3 was
285 enriched 4-fold during the L3 stage and 21-fold during the L4 stage in QK159[*nhr-23::3xflag*]
286 samples as compared with wild-type (N2) samples. In contrast, signal from the promoter of *col-*
287 *19*, which is not targeted by NHR-23, was not detectably enriched in either strain (Figure 3B, C).
288 Together, the data show that NHR-23 binds one or more ROREs in the promoter of *let-7* during
289 two sequential larval stages. Using the same combination of bioinformatic and biochemical
290 approaches, we also found that NHR-23 occupies the promoters of three *let-7* sisters (*mir-48*,
291 *mir-241* and *mir-84*) in both L3 and L4 larvae (Supplemental Figure 1A–D) (Johnson et al., 2003).
292 We next asked whether *nhr-23* promotes the temporally reiterated expression from the
293 promoter of *let-7*. To address this question, we measured and compared the abundance of
294 nuclear-localized GFP expressed from the *let-7* promoter (Kai et al., 2013) in stage-specific *nhr-23*
295 knockdowns and age-matched control animals via quantitative fluorescence microscopy
296 (Supplemental Figure 2A, B). In preliminary studies, we tracked the cycling signal associated with
297 this particular *let-7p::nls-gfp* fusion gene and detected peaks early in the third and fourth molts.
298 Accordingly, nuclei in the lateral epidermis were imaged within the first hour of the L3/L4 and
299 L4/adult molts. The signal intensity in hyp7 nuclei was 2.3 ± 1.3-fold (mean ± sd) lower in
300 *nhr-23(RNAi)* than control animals. Levels of GFP detected in seam nuclei were more variable
301 during the L3-to-L4 molt than the L4-to-Adult molt, possibly due to continuation of the cell cycle.
302 Even so, the mean signal intensity in the seam was consistently lower in *nhr-23* knockdowns than
303 control animals (Supplemental Figure 2A, B).
304 To determine the extent to which *nhr-23* promotes the reiterated expression of
305 endogenous *let-7*, we used TaqMan RT-qPCR to detect primary (pri-) *let-7* and mature *let-7* in
306 successive samples of *nhr-23* knockdowns and mock-treated, wild-type animals developing from
307 L2s into L4s or L3s into young adults (Figure 3D–G). Attenuation of the RNAi of *nhr-23* enabled
308 the collection of hundreds of *nhr-23(RNAi)* animals late in larval development, as <40% of
309 *nhr-23(RNAi)* animals exhibited molting defects by the endpoint. Under these conditions, peak
310 levels of *nhr-23* transcripts were 4.1-fold lower in *nhr-23(RNAi)* than wild-type animals (data not
311 shown). Levels of pri-*let-7* in control samples peaked in L3 and once again in L4 (Figure 3D and
312 3F). In contrast, transcript levels of pri-*let-7* detected in *nhr-23* knockdowns were 1.5-fold lower
313 at L3 (30h) and 3-fold lower at L4 (42h) than the peak value detected in age-matched, control
314 larvae (Figure 3D and 3F). Levels of mature *let-7* stagnated in *nhr-23(RNAi)* knockdowns but rose

315 continuously in control samples collected across the L3-to-L4 and larval-to-adult transitions
316 (Figure 3E and 3G). In both L3 and L4 stages, molting-defective larvae were first observed as
317 levels of *let-7* plateaued, consistent with the attribution of the phenotype to knockdown of *nhr-23*.
318 The levels of the other members of the *let-7* family, *mir-48, mir-84* and *mir-241*, were similarly
319 reduced in *nhr-23(RNAi)* larvae developing across the L3 stage, as compared with age-matched
320 control larvae (Supplemental Figure 2C, D). Collectively, these findings strongly suggest that
321 NHR-23 directly and repeatedly activates the transcription of primary *let-7* family of microRNAs.
322

323 **Scrambling the ROREs reduces NHR-23 binding at *let-7* promoters and phenocopies *let-7***
324 ***loss-of-function (lf)* mutants.**

325 To test the physiological relevance of the three consensus ROREs in the promoter of *let-*
326 *7*, we used CRISPR/Cas9 mediated gene editing to scramble the ROREs in pairs (Figure 4A).
327 The GC content of the scrambled region was the same in mutant and wild-type animals. Mutant
328 strains were outcrossed multiple times and then subjected to molecular assays and phenotypic
329 analyses. For technical reasons, we were only able to generate *let-7(scRORE1,2)* and *let-*
330 *7(scRORE1,3)* strains.

331 To determine the extent to which the ROREs were necessary for NHR-23 occupancy at
332 the promoter of *let-7*, we performed ChIP-qPCR in *let-7(xk41-scRORE1,2)*, *let-7(xk39-*
333 *scRORE1,3)* and wild-type animals during the L4 stage. The level of enrichment of the wild-type
334 *let-7* promoter in the *nhr-23::3xflag* samples was 25-fold higher, relative to control animals. In
335 contrast, the enrichment was only ~5-fold higher in both *let-7(scRORE1,2)* and *let-7(scRORE1,3)*
336 mutants relative to the control animals (Figure 4B, Supplemental Figure 1E). The level of
337 enrichment of the *let-7* promoter in *let-7(scRORE1,2)* and *let-7(scRORE1,3)* mutants was still
338 above background, suggesting that the remaining RORE not scrambled in each of the *let-*
339 *7(scRORE)* mutants may contribute to some binding by NHR-23.

340 Next, we queried the levels of primary and mature *let-7* transcripts in *let-7(scRORE1,2),*
341 *let-7(scRORE1,3)* and wild-type animals immediately following the L2/L3 molt (Figure 4C, D). At
342 the peak of expression (22 h), the levels of *pri-let-7* in *let-7(scRORE1,2)* and *let-7(scRORE1,3)*
343 animals were decreased by 2.4-fold and 1.7-fold, respectively, relative to wild type (Figure 4C).
344 Correspondingly, the levels of mature *let-7* at the same time points were reduced by 2.7-fold and
345 2.5-fold in the *let-7(scRORE1,2)* and *let-7(scRORE1,3)* animals, respectively, relative to wild type
346 animals (Figure 4D). However, no significant difference was detected in the levels of mature *let-*
347 *7* at the L4 stage in *let-7(scRORE1,2)* and *let-7(scRORE1,3)* animals compared to wild type

348 animals (data not shown). Thus, reduced binding of NHR-23 is accompanied by reduced
349 transcription and slower accumulation of *let-7* in these strains.
350 To characterize heterochronic phenotypes associated with scrambling the ROREs, we
351 scored the number of seam cell nuclei in the *let-7(scRORE1,2)* and *let-7(scRORE1,3)* mutants
352 and wild-type animals. At least two independent isolates of each scrambled mutant were
353 analyzed. As positive controls, we included two *let-7* hypomorphs, *let-7(n2853)* and *let-7(mg279)*,
354 since these mutants have higher numbers of seam cells than wild type animals (Chan and Slack,
355 2009; Reinhart et al., 2000). Seam cell nuclei were identified and scored in adult animals based
356 on the fluorescent reporter gene *Pscm::gfp*, which was crossed into each strain prior to scoring.
357 All lines of the *let-7(scRORE1,2)* and *let-7(scRORE1,3)* strains exhibited significantly increased
358 number of seam cells relative to wild-type adults (Figure 4E). The extent of seam cell hyperplasia
359 detected in the *let-7(scRORE)* mutants was comparable to *let-7(mg279),* but less severe than
360 *let-7(n2853)* (Figure 4E).
361 To examine how the ROREs, and by extension, NHR-23-mediated activation of *let-7*,
362 affect the biorhythm of molting, we conducted longitudinal behavioral studies on
363 *let-7(scRORE1,2)*, *let-7(scRORE1,3)* and wild-type animals developing from the L3-to-L4 molt
364 until young adulthood (Figure 4F). All four mutant strains (i.e., two independent alleles of
365 *let-7(scRORE1,2)* and *let-7(scRORE1,3)*) were found to enter into and emerge from the L4-to-
366 adult molt significantly earlier than wild type, similar to previous findings with *let-7(lf)* mutants.
367 Therefore, scrambling the ROREs is sufficient to increase the speed of development, consistent
368 with our model that NHR-23-mediated activation of the *let-7s* normally slows the pace of molting.
369 Thus, reduced occupancy of the *let-7* promoter by NHR-23, reduced levels of primary *let-7*
370 transcripts, seam cell hyperplasia and quicker pace of the molting cycle are all associated with
371 the *let-7(scRORE1,2)* and *let-7(scRORE1,3)* mutants. It is likely that the kinetics of accumulation
372 of mature *let-7* strongly affects development of the seam and the pace of molting, consistent with
373 prior reports on the time sensitive nature of *let-7* function (Reinhart et al., 2000).
374
375 **The *nhr-23* 3′ UTR contains a functional *let-7* consensus site.**
376 To determine if NHR-23 and *let-7* constitute a feedback loop, we next asked whether the
377 *let-7* family of microRNAs downregulates *nhr-23* transcript abundance in developing larvae. We
378 identified a single element in the 868-bp 3′ UTR of *nhr-23* (Mangone et al., 2010) that perfectly
379 complements the 5′ seed sequence of *let-7* and partially complements the remainder of the
380 microRNA. Hereafter, this element is called the *let-7* consensus site (LCS). Three other

381 sequences in the 3′ UTR of *nhr-23* partially complement the *let-7s* with mismatches to the seed
382 (Figure 5A and Supplemental Table 2).
383 To assess the significance of the LCS, we designed and utilized a set of bicistronic
384 reporters for post-transcriptional *cis*-regulatory elements, each housed in a distinct
385 extrachromosomal array and unique transgenic strain (Figure 5B). Briefly, the coding sequence
386 of tandem (td) Tomato was fused with the 3′ UTR of *nhr-23*, whereas the coding sequence of GFP
387 was fused with the 3′ UTR of *unc-54*, which is not targeted by the *let-7s.* An SL2 trans-spliced
388 leader sequence bridged the two fusion genes. The promoter of *dpy-7* drove expression of the
389 operon in the hypodermis. The readout was the ratiometric signal of TdTomato to GFP detected
390 in the lateral epidermis (Supplemental Figure 3). This approach controlled for potential differences
391 in gene expression associated with particular arrays or mosaic animals rather than the test 3′
392 UTR.
393 Figure 4C shows the merged and individual signals detected in transgenic animals in the
394 L4-to-adult molt, at which time both *let-7* and *dpy-7* are highly expressed. The ratiometric signal
395 for the *nhr-23* 3′ UTR reporter was ~6 fold lower than the negative control *unc-54* 3′ UTR reporter
396 (Figure 5D). Similarly, the ratiometric signal for the positive control *lin-41* 3′ UTR reporter was 3-
397 fold lower than the negative control. It is unlikely that the 3′ UTR fused to TdTomato affects the
398 efficiency of trans-splicing or causes nonsense-mediated decay of the polycistronic pre-mRNA,
399 because the absolute intensities of GFP of all three constructs were equivalent.
400 We next systematically deleted each of the four predicted *let-7* binding sites in the *nhr-23*
401 3′ UTR and compared their reporter signals with the signal detected from the wild-type reporter
402 for *nhr-23* 3′ UTR. Excision of the LCS led to a two-fold increase in the ratio of tdTomato/GFP
403 signals, relative to the average ratio associated with the reporter for the full-length 3′ UTR of
404 *nhr-23* (Figure 5E). In contrast, deletions of the other predicted *let-7* binding sites (Δ26–42, Δ227–
405 249, and Δ623–646) in the *nhr-23* 3′ UTR reporters did not increase the ratio of the tdTomato/GFP
406 signals, suggesting that the LCS is the only bona fide *let-7* binding site tested in the *nhr-23* 3′
407 UTR. Consistent with this result, a highly-sensitive, high-throughput approach to catalog targets
408 of microRNAs identified the 3′ UTR of *nhr-23* among cellular transcripts associated with ALG-1,
409 the primary Argonaute of the worm microRNA RISC complex (Broughton et al., 2016; Grishok et
410 al., 2001). Thus, *let-7* represses *nhr-23* by directly binding the LCS in its 3′ UTR.
411
412 **Both the LCS and *let-7s* contribute to dampening the expression of *nhr-23.***
413 We next deleted the endogenous LCS of *nhr-23* by CRISPR/CAS9 (Paix *et al.*, 2015) to
414 generate the *nhr-23(aaa20-ΔLCS)* strain. We then detected and compared temporal waves in the

415 abundance of *nhr-23* transcripts among wild-type animals and both *nhr-23(aaa20-ΔLCS)* and
416 *let-7(n2853)* mutants developing from late L2s into young adults by TaqMan RT-qPCR. To stage
417 each strain, we inspected and scored the behavior of ~100 worms as active or quiescent at each
418 timepoint prior to collection of the sample. Lethargi, and by extension the molts, were identified
419 *post-hoc* based on these measurements. Wild-type larvae developed more slowly than gain-of-
420 function *nhr-23(aaa20-ΔLCS)* or loss-of-function *let-7(n2853)* mutants in this particular
421 experiment. However, we captured oscillatory expression of *nhr-23* across the target stages
422 among the time samples of each strain (Figure 6A and Supplemental Figure 4A). Additionally, we
423 used the program Metacycle (Wu et al., 2016) to calculate the amplitude and phase of the
424 expression curves of *nhr-23* and performed manual calculations to determine the rates of
425 accumulation and decay of *nhr-23* transcripts (Figure 6A′). Peak levels of *nhr-23* were typically
426 detected one-third to one-half of the way through the L2, L3 and L4 stages in wild-type time
427 samples. However, the peak values of sequential waves dropped by a regular increment of ~1.5-
428 fold from one life stage to the next, an indication of dampening (Figure 6A′, Supplemental Table
429 3).

430 Three metrics of the expression curves for *nhr-23*, amplitude, peak value and rising slope,
431 were consistently higher both in *nhr-23(aaa20-ΔLCS)* mutants and *let-7(n2853)* mutants, as
432 compared with wild-type animals, across both the L3 and L4 stages in two independent biological
433 replicates (Figure 6A, A′, Supplemental Figure 4A, A′, Supplemental Table 3). For instance, the
434 peaks in *nhr-23* transcript levels that were detected early in L3 and L4 were ~1.6-fold higher in
435 *nhr-23(aaa20-ΔLCS)* samples than in wild-type samples, despite the dampening (Figure 6A,
436 Supplemental Table 3). Similarly, the amplitude, peak value, and slope of *nhr-23* curves in
437 *let-7(n2853)* mutants were also both significantly higher relative to wild type during the L3 and L4
438 stages. The phases of the *nhr-23* waveforms differed among the three cohorts but were not
439 consistently earlier in either mutant relative to wild-type animals, across both life stages and
440 biological replicates (Supplemental Table 3). Interestingly, an extra pulse of *nhr-23* expression
441 was detected in both *nhr-23*(*aaa20-ΔLCS)* and *let-7(n2853)* time samples collected after the
442 fourth molt, suggesting the potential for a supernumerary molt (see arrows, Figure 6A).

443 We used a similar approach to determine the extent to which the *let-7s* repress the
444 expression of *nhr-23* during the L2 stage. We compared the abundance of *nhr-23* transcripts in
445 regular time samples of *nhr-23(aaa20-ΔLCS)* single mutants, *mir-48 mir-241(nDf51);*
446 *mir-84(n4037)* triple mutants, and wild-type larvae developing from late L1s into early L3s
447 (Supplemental Figure 4B–B′). The L2 stage expression curves detected in both mutants were at
448 least 3-fold steeper and peaked at higher levels than the those detected in wild-type larvae.

449 In complementary studies, we tracked the abundance of NHR-23 protein expression in
450 epidermal nuclei as indicated by the signal associated with the NHR-23::GFP fusion protein.
451 Protein levels also cycled from the L2 through the L4 stage. For example, the signal peaked 2 h
452 after emergence in the L4 stage but was not detected 3 h later (Supplemental Figure 5A, B). Both
453 the extent and kinetics of protein increase and decrease corresponded well with the expression
454 curves for *nhr-23* transcripts detected in wild-type larvae. We next asked if the *let-7s* regulate the
455 abundance of NHR-23 proteins by comparing the abundance of the NHR-23::GFP fusion protein
456 in the *let-7(mg279); mir-84(tm1304)* double mutant and wild-type animals (Supplemental Figure
457 5C). GFP was detected in the epidermal nuclei of the *let-7(mg279); mir-84(tm1304)* mutant
458 molting from L4s to adults but was not readily detected in wild-type molting animals. The signal
459 from NHR-23::GFP became bright in the *let-7(mg279); mir-84(tm1304)* mutant that had emerged
460 as adults but remained dim in wild-type adults. Interestingly, the corresponding 3.4-fold increase
461 in fluorescence intensity matched the 3.4-fold increase in abundance of *nhr-23* transcripts
462 detected in *let-7(n2853)* versus wild-type samples collected at a comparable timepoint. Of note,
463 the native 3′ UTR of *nhr-23* was fused to *nhr-23::gfp* in the genetic reagent used in our study,
464 whereas the ectopic 3′ UTR of *unc-54*, which is not a target of the *let-7s*, was fused to *nhr-23::gfp*
465 in a distinct reagent used in previous research (Hayes et al., 2006; Kostrouchova et al., 1998).
466 Thus, the current study is the first to report that the *let-7s* likely directly repress *nhr-23* through
467 association with the LCS in the *nhr-23* 3′ UTR to prevent the accumulation of *nhr-23* transcripts
468 and proteins in wild-type adults.
469 To study how the LCS, and by extension, *let-7*-mediated repression of *nhr-23*, affects the
470 biorhythm of molting, we tracked cohorts of *nhr-23(aaa20-ΔLCS)* larvae across both the L3 and
471 L4 stages (Figure 6B, C). As a complementary approach, we also tracked larvae that expressed
472 multiple copies of *nhr-23* from an integrated, tandem array across the same life stages (Celniker
473 *et al.*, 2009). The majority of *nhr-23(aaa20-ΔLCS)* L3 larvae entered lethargus and emerged as
474 L4 larvae before most wild-type L3 larvae began to molt. The wake-to-wake interval of the
475 *nhr-23(aaa20-ΔLCS)* L3-stage cohort was 1.5 ± 0.9 h shorter than that of wild-type L3s. Likewise,
476 the majority of *wgIs43[nhr-23^{++}]* larvae, which overexpress *nhr-23*, entered lethargus and
477 emerged in the next life stage faster than age-matched, wild-type animals (Figure 6B, C). The
478 wake-to-wake interval was 6.9 ± 0.6 h for the *wgIs43[nhr-23^{++}]* cohort developing from L3 to L4,
479 compared with 7.8 ± 0.6 h for the wild-type cohort ($p \leq 0.01$). Combining *wgIs43[nhr-23^{++}]* with *let-*
480 *7(n2853)* led to larval lethality and prohibited a similar analysis. Thus, both de-repression and
481 increased dosage of *nhr-23* were associated with advanced lethargus and faster cycles, similar
482 to our earlier findings with *let-7(lf)* mutants.

483 Together, these findings show that the endogenous LCS in the *nhr-23* 3' UTR is indeed a *cis*-
484 regulatory repressive element, strongly suggesting that *let-7* and its paralogs bind this functional
485 LCS and negatively regulate the expression of *nhr-23* transcripts and proteins, while larvae transit
486 the molts and emerge in the subsequent life stage. Therefore, these data are consistent with a
487 model whereby NHR-23 and the *let-7s* form a transcriptional-post transcriptional feedback loop
488 that regulates the duration of the molt. Immediately following the molt, NHR-23 activates
489 transcription of the *let-7*s early during the larval stage. The post transcriptional repression of
490 *nhr-23* by the *let-7s* keeps the levels of *nhr-23* below a particular threshold, preventing early entry
491 into the next molt.
492
493 **Forced expression of *nhr-23* is sufficient to trigger supernumerary molts.**
494 As described above, there was no detectable dampening of *nhr-23* transcript levels in
495 *let-7(n2853)* mutants, whereas the phenomenon was obvious in wild-type animals (Figure 6A,
496 Supplemental Figure 4A). Mutations in *let-7* were originally characterized as retarded
497 heterochronic mutants that underwent supernumerary molts (Hayes *et al.*, 2006; Reinhart *et al.*,
498 2000). Considering this, we hypothesized that *let-7*-dependent dampening of the oscillatory
499 expression of *nhr-23* effectively counts down the number of molts and ultimately extinguishes the
500 molting cycle.
501 To test this idea, we tracked and compared instances of molting-associated behaviors and
502 animal viability between wild-type adults and age-matched gain-of-function (*gf*) mutants where
503 *nhr-23* is overexpressed: *nhr-23(aaa20-ΔLCS)* (Figure 6A, Supplemental Figure 4A) and
504 *wgIs43[nhr-23^{++}]* (Celniker et al, 2009). At first, we inspected partially synchronized populations
505 at regular timepoints 2–5 days after the emergence of adults. Behavioral quiescence, defined by
506 a lack of detectable pharyngeal pumping or locomotion, was more common among both
507 *nhr-23(aaa20-ΔLCS)* and *wgIs43[nhr-23^{++}]* adults than wild-type animals across this interval.
508 Moreover, the percentage of quiescent *nhr-23(gf)* adults peaked and significantly exceeded the
509 percentage of quiescent wild-type adults during 3 to 4 successive time samples (Figure 7A). We
510 next asked whether quiescent *nhr-23(aaa20-ΔLCS)* and *wgIs43[nhr-23^{++}]* adults observed at
511 those particular timepoints were in fact undergoing lethargi associated with supernumerary molts
512 rather than transient, satiety-induced quiescence (You et al., 2008). To distinguish between these
513 two possibilities, we singled quiescent adults into 3 respective cohorts per genotype and tracked
514 the animals within each cohort for an additional 12 h (Figure 7B). In parallel, we singled and
515 tracked quiescent wild-type adults. The overwhelming majority of singled *nhr-23(gf)* adults were
516 quiescent for several hours and then attempted to ecdyse, a sequence of events indicative of a

517 supernumerary molt. Most animals shed entire cuticles or parts thereof, but nonetheless died
518 (Supplemental Movie 2, 3). The *nhr-23(aaa20-ΔLCS)* adult shown in Supplemental Movie 3 is
519 one such example. The animal was quiescent for 6 h, then exhibited intermittent twitches of the
520 grinder, a behavior that accompanies ecdysis, and ultimately bagged, likely because unshed
521 cuticle occluded the vulva. In contrast, all quiescent wild-type adults regained activity and only
522 one animal died during the period of observation (Figure 7B, Supplemental Movie 1). By the
523 abovementioned criteria, 97% (n = 34) of singled *nhr-23(aaa20-ΔLCS)* adults and 91% (n = 33)
524 of singled *wgIs43[nhr-23^{++}]* adults underwent supernumerary molts whereas none (n = 11) of the
525 wild-type adults did so ($P < 0.0001$, chi-square test). Figure 7C shows one example each of an
526 *nhr-23(aaa20-ΔLCS)* and a *wgIs43[nhr-23^{++}]* adult that underwent aberrant molts and became
527 trapped in partly shed cuticles. Both animals had eggs in the uterus. However, the
528 *nhr-23(aaa20-ΔLCS)* animal had an old cuticle attached to its tail. Also, alae were visible on both
529 the lateral surface of the extant cuticle and the partly shed cuticle, implying that the epidermis had
530 terminally differentiated prior to the attempted molt. These results show that forced expression of
531 *nhr-23* is sufficient to initiate a supernumerary molt but not sufficient to properly complete the
532 molt. Taken together, these data suggest that artificially increasing the abundance of NHR-23
533 relative to the *let-7s* drives additional iterations of the molting cycle.
534
535 **Dynamic levels of *nhr-23* and the *let-7s* shape expression curves of many effectors of the**
536 **molting cycle.**
537 NHR-23 and *let-7* may act as core components of a molecular-genetic oscillator that
538 regulates the onset and duration of the molts. Other biological clocks generate and sustain orderly
539 waves in the expression of both core clock components and groups of "clock-controlled genes
540 (CCGs)" that encode coordinated effectors of the biorhythm. Consistent with this model, genes
541 that are depleted in *nhr-23* knockdowns are strongly enriched for oscillating genes (Tsiairis et al,
542 2021). From this perspective, we considered how the negative feedback loop between *nhr-23* and
543 the *let-7s* might affect the expression of genes that oscillate in phase with different events linked
544 to the molting cycle. To test this idea, we chose two oscillatory genes linked to molting: 1) *fbn-1*,
545 which encodes a component of the sheath that encloses and protects animals during each molt
546 (Katz et al., 2021); and 2) *mlt-10*, which encodes a component of the cuticle (Frand et al., 2005;
547 Meli et al., 2010). We then queried the expression levels of each of the above transcripts in
548 *nhr-23(RNAi)*, *nhr-23(aaa20-ΔLCS)* and *let-7(n2853)* mutants and control animals collected at
549 regular intervals from late L2 through young adulthood using RT-qPCR (Figure 8A–D). As

550 described earlier, the amplitude and phase of each waveform were determined using Metacycle,
551 while the slope of each waveform was calculated manually.

552 As expected, peak levels of *fbn-1* were detected early in the L3 and L4 stages in control
553 animals (Figure 8 A, B). Knockdown of *nhr-23* during both stages reduced the amplitude of *fbn-1*
554 by 4–5-fold (Figure 8A). However, the slope and phase of the *fbn-1* waveform were virtually
555 identical in both *nhr-23(RNAi)* and mock-treated larvae (Supplemental Table 3). In contrast, both
556 LCS deletion and *let-7* mutations increased the amplitude and peak level of *fbn-1* transcripts by
557 ~1.5-fold in L4-stage animals as compared with age-matched controls (Figure 8B, Supplemental
558 Table 3). The slope of the *fbn-1* expression curves was 2-fold higher in *nhr-23(aaa20-ΔLCS)*
559 mutants and 3-fold higher in *let-7(n2853)* mutants than wild type (Supplemental Table 3). Notably,
560 the phase of *fbn-1* expression was ~1 h earlier in both *nhr-23(aaa20-ΔLCS)* and *let-7(n2853)*
561 mutants relative to wild type (Supplemental Table 3). This is consistent with the observation that
562 *nhr-23(aaa20-ΔLCS)* and *let-7(n2853)* mutants molt earlier than wild-type animals. Similar
563 findings were observed in a second, independent trial with *nhr-23(aaa20-ΔLCS)*, *let-7(n2853)* and
564 wild-type animals (Supplemental Figure 6A).

565 Peak levels of *mlt-10* transcripts were detected late in each larval stage, right before
566 animals enter the molt (Figure 8C). In L4-stage *nhr-23(RNAi)* larvae, the peak level of *mlt-10* was
567 reduced by 2-fold, relative to control animals, even though the amplitude and phase remained
568 similar in both backgrounds. Additionally, knockdown of *nhr-23* reduced the slope of the *mlt-10*
569 expression curve to 0.1, compared with 0.4 in control animals, suggesting that *nhr-23* likely affects
570 the rate of accumulation of *mlt-10* transcripts (Supplemental Table 3). In *nhr-23(aaa20-ΔLCS)*
571 and *let-7(n2853)* mutants, both the amplitude and peak value of *mlt-10* expression were about
572 ~2-fold higher than wild type. Consistent with earlier findings on *fbn-1*, the slope of the *mlt-10*
573 expression curve was ~4-fold higher and the phase was ~1 h earlier than wild type. Supplemental
574 Figure 6B shows similar results that were obtained in an additional independent experiment. Thus,
575 the cyclical expression profiles of *fbn-1* and *nhr-23* are altered in *nhr-23* knockdowns, and in
576 *nhr-23(gf)* and *let-7(lf)* mutants. As we describe below, both genes have *cis*-regulatory elements
577 for NHR-23 and the *let-7s* in their promoters and 3′ UTRs, respectively, suggesting direct
578 transcriptional activation by NHR-23 and direct repression by the *let-7s*. The feedback loop likely
579 sculpts the temporal expression profiles of *fbn-1* and *mlt-10*, as well as other genes linked to
580 molting.

581 To determine whether joint regulation by NHR-23 and *let-7s* was a signature of oscillatory
582 genes that are linked to molting, we used a bioinformatics approach. We selected a set of potential
583 target genes of the molting timer based on two criteria: 1) expression of the gene oscillates with

584 a period of 8–10 h across larval development (Hendriks et al., 2014; Kim et al., 2013); and 2)
585 activity of the gene affects one of the many distinct but interdependent steps within the molting
586 cycle. We consider these genes as "clock-controlled genes (CCGs)". Collectively, the 67 selected
587 CCGs encode transcription factors, signaling molecules, enzymes and matrix proteins that are
588 involved in the synthesis and removal of cuticles, and neuropeptides that regulate quiescence
589 and arousal (Supplemental Table 4). Next, we systematically and independently evaluated each
590 CCG as a probable target of NHR-23 or *let-7s* through meta-analyses of published datasets
591 mentioned below and original bioinformatic approaches. A CCG classified as a direct target of
592 NHR-23 met at least two of the following criteria: 1) NHR-23 occupied the 5′ regulatory region of
593 the gene *in vivo*, as annotated in a ChIP-Seq dataset (Celniker *et al.*, 2009); 2) the same
594 regulatory region contained more ROREs than expected by chance; and 3) knock down of *nhr-*
595 *23* resulted in lower transcript levels (Kouns *et al.*, 2011). A CCG classified as a target of the *let-*
596 *7s* met two criteria: 1) ALG-1 bound the 3′ UTR of the respective mRNA *in vivo*, as reported in an
597 ALG-1 iCLIP dataset (Broughton *et al.*, 2016); and 2) the 3′ UTR contained more LCSs than
598 expected by chance.
599 By these rubrics, 57% of CCGs were classified as shared targets of both NHR-23 and the
600 *let-7s* (including *fbn-1* and *mlt-10*); 24% as targets of only NHR-23; 10% as targets of only *let-7s*;
601 and 13% as targets of neither factor (Figure 8E, Supplemental Table 4). Notably, multiple
602 response elements for NHR-23 were identified in the promoters of almost all CCGs classified as
603 *let-7* targets and vice versa, even though NHR-23 or ALG-1 were not enriched at those genomic
604 locations in the abovementioned ChIP-Seq or iCLIP datasets. Therefore, 57% may be an
605 underestimate and more outputs of the molting timer may ultimately be recognized as dual targets
606 of both NHR-23 and the *let-7s*. Only 10% of twenty randomly selected genes that are not known
607 to cycle in expression were classified as shared targets of both NHR-23 and *let-7s,* suggesting
608 that NHR-23 and the *let-7s* together may specifically regulate the expression of oscillatory genes
609 that drive molting. These findings suggest that partly interdependent waves in the abundance of
610 NHR-23 and the *let-7s* sculpt the temporal expression profiles of *fbn-1*, *mlt-10* and possibly many
611 additional effectors of the molting timer.
612
613 **NHR-23 and *let-7s* govern the temporal expression profile of other key clock genes**
614 The bioinformatics analysis described above provided more evidence for regulatory
615 interactions among other key components of the oscillator. Our analysis suggested that NHR-23
616 promotes the expression of both *lin-42/PER* and the *let-7s*, whereas *let-7s* repress the expression
617 of both *lin-42/PER* and *nhr-23* transcripts. Three major isoforms of *lin-42* are recognized

618 regulators of the molting cycle and components of the heterochronic pathway (Edelman et al.,
619 2016; Jeon *et al.*, 1999; Monsalve *et al.*, 2011). We identified three ROREs in the unique promoter
620 of *lin-42a* and three additional ROREs in the shared promoter of *lin-42b* and *lin-42c* (Supplemental
621 Figure 7A). The ROREs in both promoters correspond to sites of NHR-23 enrichment detected
622 by ChIP-Seq and annotated by the modENCODE Consortium (Celniker *et al.*, 2009). Consistent
623 with the data from the modENCODE consortium, NHR-23 ChIP-qPCR analysis during L3 showed
624 that the *lin-42a* promoter was enriched by 5-fold and the *lin-42b* promoter was enriched 7-fold in
625 the *nhr-23::3xflag* samples, relative to background (Figure 9A). To further characterize the extent
626 to which NHR-23 activates the pulsatile expression of *lin-42*, we measured and compared the
627 levels of *lin-42* transcripts across the L4 stage in attenuated *nhr-23* knockdowns and control
628 animals (Figure 9B). As expected, levels of *lin-42* in control samples peaked in L3 and once again
629 in L4. No such peak was detected in *nhr-23(RNAi)* at the L4 stage. The transcript levels of *lin-42*
630 detected in *nhr-23* knockdowns at the L4 stage (42 h) were 2.6-fold lower than the peak value
631 detected in age-matched, control larvae. Likewise, the amplitude and slope of *lin-42* expression
632 were 3-fold and 6-fold lower, respectively, in L4-stage *nhr-23(RNAi)* larvae, relative to age-
633 matched controls. Moreover, we identified a single RORE site 827–833 bp upstream of the start
634 codon of human *PER2*, suggesting that NHR-23/ROR-mediated transcriptional activation of
635 *lin-42/Per* may be conserved in mammals.

636 We identified four LCSs, including one with perfect complementarity to the *let-7* seed
637 region, in the shared 3′ UTR of *lin-42a* and *b*, suggesting that the *let-7s* directly repress both *lin-42*
638 isoforms (Supplemental Figure 7D). Although *lin-42* was previously described as containing sites
639 complementary to the *let-7s*, the specific *cis*-regulatory elements were not well defined (Reinhart
640 *et al.*, 2000). No LCSs were detected in the 3′ UTR of *lin-42c*, which is modeled as a dominant
641 negative (Monsalve *et al.*, 2011). To determine how *let-7* affects the expression of *lin-42*, we
642 measured the levels of *lin-42* transcripts in *let-7(n2853)* and wild-type animals (Figure 9C). We
643 also included samples from *nhr-23(aaa20-ΔLCS)* mutants in the analysis. Both the amplitude and
644 peak level of *lin-42* expression were 1.5-fold higher in *let-7(n2853)* mutants relative to the control.
645 The phase was advanced by ~1 h in *let-7(n2853)* larvae (Supplemental Table 3). Similar results
646 were observed in *nhr-23(aaa20-ΔLCS)* mutants, as well as in a second biological replicate
647 (Supplemental Figure 7C). Going further, we identified two LCSs perfectly complementary to the
648 *let-7* seed in the 3′ UTR of human *Per2* transcripts (Supplemental Figure 7D), suggesting that the
649 regulatory interactions between LIN-42 and the *let-7s* may be conserved in humans.

650 The bioinformatics analysis also provided evidence of potential positive autoregulation of
651 *nhr-23*. We found eight ROREs within the upstream regulatory region of *nhr-23*. Two of these

652 RORE s were occupied by NHR-23 *in vivo*, as indicated by ChIP-Seq data from the modENCODE
653 Consortium (Supplemental Figure 7B). NHR-23 ChIP-qPCR during L3 showed that the promoter
654 of the *nhr-23* gene was enriched in *nhr-23::3xflag* samples, further substantiating the hypothesis
655 of autoregulation. To test whether NHR-23 promotes its own expression, we used a fusion gene
656 wherein the last two and a half exons of *nhr-23* were replaced with *gfp* fused to the 3′ UTR of
657 *unc-54* (Figure 9D). We compared the expression of this fusion gene in the lateral epidermis of
658 *nhr-23* knockdown and control animals during the mid-L4 stage (Figure 9E, F). In this assay, the
659 dsRNAs used to downregulate *nhr-23* expression specifically target the last two and half exons
660 and thus, in theory, should affect expression of only endogenous *nhr-23* and not the
661 *nhr-23::gfp::unc-54* transgenic reporter. Fluorescence signal was easily detectable in the
662 epidermis of control animals, but not in *nhr-23(RNAi)* larvae (Figure 9E). The intensity of GFP
663 detected in hyp7 of *nhr-23(RNAi)* animals was ~2-fold lower than mock-treated animals (Figure
664 9F). The intensity of GFP in the seam was similarly lowered upon knockdown of *nhr-23*. These
665 data suggest that NHR-23 activates its own expression. Together, these data show that the
666 positive autoregulation of *nhr-23*, in combination with the previously characterized NHR-23-*let-7*
667 negative feedback loop, may contribute to a self-sustaining molecular-genetic oscillator. Key
668 components of the molting cycle timer, including *lin-42* and CCGs, may be regulated by both
669 NHR-23 and *let-7s*.
670
671 **Reciprocal regulatory elements may be conserved in mammalian *ROR* and *let-7* genes.**
672 We next asked whether the feedback loop between NHR-23/ROR and the *let-7s* may be
673 conserved between nematodes and vertebrates. Using bioinformatic approaches, we searched
674 for RORE s upstream of the homologs of *let-7* in the fully sequenced and annotated genomes of
675 humans, mice, and zebrafish. We inspected the genomic region 3 kb upstream of the precursor
676 *let-7* microRNA and identified 1 to 5 distinct RORE s in all homologs (Supplemental Figure 8A).
677 Figure 10A depicts the RORE s found upstream of selected homologs of *let-7.* In each example,
678 more RORE s were found than predicted by chance.
679 To determine the extent to which NHR-23/ROR could promote the expression of
680 mammalian homologs of *let-7*, we fused the promoter of *M. musculus let-7a-1* with *gfp* and used
681 fluorescence microscopy to detect and compare the expression of the reporter gene in
682 *nhr-23(RNAi)* and control animals undergoing the L4-to-adult molt (Figure 10B, C). Fluorescence
683 signal of this heterologous reporter in control animals was bright in the pharynx, a tissue where
684 *nhr-23* is normally expressed (Figure 10B; Kostrouchova et al, 1998). In contrast, negligible signal
685 was detected in the pharynx of *nhr-23(RNAi)* animals. Quantitative analyses of the GFP

686 fluorescence signal show that the intensity in *nhr-23(RNAi)* animals was ~3-fold lower, on
687 average, than control animals (Figure 10C). Thus, these findings show that NHR-23 regulates the
688 expression of the promoter of *M. musculus let-7a-1* in *C. elegans*, suggesting that the positive
689 arm of the NHR-23-*let-7* feedback loop may be conserved to mammals.

690 Next, we searched for LCSs in the 3′ UTRs of all 13 homologs of *nhr-23/ROR* annotated
691 in the reference genomes of flies, frogs, zebrafish, chickens, mice and humans (Figure 10D,
692 Supplemental Table 2). We first aligned and compared the nucleotide sequence of the query 3′
693 UTR with the sequences of corresponding ESTs. In two cases – zebrafish RORβ and RORγ –
694 multiple ESTs supported longer 3′ UTRs than those presently annotated on the UCSC Genome
695 Browser (see Key Resources Table). We found 1–3 LCSs perfectly complementary to the seed
696 sequence of *let-7* within 3′ UTRs of 10 of the *nhr-23/ROR* homologs. We also found one or two
697 more LCSs with a single mismatch to the seed sequence of *let-7* in 6 of the corresponding 3′
698 UTRs. For example, we identified one perfectly complementary LCS in the center of the validated
699 3′ UTR of human RORβ, flanked by two more sites with respective single nucleotide mismatches
700 to the seed of *let-7* (Figure 10D). Similar LCSs with at most a single mismatch to the seed
701 sequences of the *let-7s* were found in the 3′ UTRs for each of the remaining four homologs
702 (Supplemental Table 2).

703 To test the significance of the LCSs detected in the mammalian ROR 3′ UTRs, we focused
704 on the 3′ UTRs of *H. sapiens* RORβ and *M. musculus* RORα. Each 3′ UTR has two LCSs that
705 perfectly match the seed region of *let-7*: sequences starting at nt 3576 and 4055 in *H. sapiens*
706 RORβ, and nt 2055 and 2184 in *M. musculus* RORα (Figure 10D). We selected a 590 bp fragment
707 of the *H. sapiens* RORβ 3′ UTR, spanning the two LCSs (Figure 10D, boxed region). Similarly,
708 we chose a 281 bp fragment of the *M. musculus* RORα 3′ UTR also spanning the two LCSs
709 (Figure 10D, boxed region). We fused each fragment, as well as variants thereof that lack both
710 LCSs, to *tdTomato* in the bicistronic reporter system described in Figure 5B. We then used
711 fluorescence microscopy to measure the intensity of tdTomato and GFP signals in the lateral
712 epidermis of animals undergoing the L4-to-adult molt. When the *H. sapiens* RORβ 3′ UTR was
713 fused to *tdTomato*, the intensity of tdTomato signal was barely detectable in the epidermis,
714 whereas the intensity of GFP signal in the same animal was conspicuous (Figure 10E,
715 Supplemental Figure 8B). Deletion of both LCSs from the *H. sapiens* RORβ 3′ UTR increased the
716 intensity of TdTomato signal by ~30-fold relative to the wild-type constructs (Figure 10F). Similar
717 findings were made with the bicistronic reporter constructs that housed the *M. musculus* RORα 3′
718 UTR (Figure 10G, H, Supplemental Figure 8C). These data suggest that *C. elegans let-7* can
719 repress the expression of specific mammalian ROR 3′ UTRs. Taken together, these findings imply

720 that the feedback loop between NHR-23/ROR and *let-7s* may be conserved and may regulate the
721 cyclical expression of target genes in mammalian tissues.
722
723 **DISCUSSION**
724 The principal findings of this study unite two distinct time keeping mechanisms mutually
725 dependent on a transcriptional-post-transcriptional feedback loop between NHR-23 and the *let-*
726 *7s*: the heterochronic genetic pathway that controls the singular switch from larval to adult fates
727 and the genetic oscillator that controls the biorhythm of the molting cycle.
728
729 **NHR-23 transcriptionally activates *let-7* and *let-7* post-transcriptionally represses *nhr-23***
730 **to form a molecular-genetic oscillator.**
731 In *C. elegans*, the primary transcripts of the *let-7* family of microRNAs (*mir-48, mir-84*, *mir-*
732 *241* and *let-7*) oscillate in abundance and peak once in every larval stage (McCulloch and
733 Rougvie, 2014; Van Wynsberghe et al., 2011). This oscillatory gene expression pattern is
734 regulated at the transcriptional level (Kai et al., 2013). A few negative and positive regulators of
735 *let-7* transcription have been identified previously, although none completely account for the
736 oscillatory expression of the primary *let-7s*. The transcription factor HBL-1 negatively regulates
737 the transcription of *let-7* in the hypodermis until the L3 stage (Roush and Slack, 2009). Similarly,
738 the transcription factor LIN-14 restricts the transcription of *mir-48, mir-84* and *mir-241* until the L2-
739 to-L3 transition (Tsialikas et al., 2017). The Period protein homolog LIN-42 binds the promoter of
740 *let-7* and dampens the amplitude of primary *let-7* oscillations to prevent early accumulation of
741 mature *let-7* (McCulloch and Rougvie, 2014; Perales et al., 2014; Van Wynsberghe et al., 2014).
742 LIN-42 also dampens oscillations of primary *mir-48* transcripts and prevents the early
743 accumulation of *mir-48*. However, *lin-42* is not required for the oscillatory expression pattern of
744 the primary *let-7* transcripts (McCulloch and Rougvie, 2014). The transcription factor DAF-12 is
745 involved in a complex regulatory network that couples environmental and developmental signals
746 to regulate *let-7* family transcription. During unfavorable conditions, unliganded DAF-12 represses
747 the expression of the *let-7s.* However, during favorable conditions, and in the presence of its
748 ligand, DAF-12 binds the promoters of *mir-84* and *mir-241* and mildly upregulates transcription
749 (Bethke et al., 2009; Hammell et al., 2009). The GATA transcription factor ELT-1 binds upstream
750 of *let-7* and promotes transcription during the L4 stage. ELT-1 also acts redundantly with DAF-12
751 to positively regulate the levels of *mir-48, mir-84* and *mir-241* (Cohen et al., 2015). However, both
752 *daf-12* and *elt-1* are expressed at nearly constant levels during post embryonic development

753 (Hendriks et al., 2014; Kim et al., 2013) and hence, cannot completely explain the oscillatory
754 expression pattern of the primary transcripts of the *let-7* family.
755 We have shown that NHR-23 binds upstream of *let-7*, *mir-48*, *mir-84* and *mir-241* during
756 L3 and L4 stages (Figure 3B, 3C, Supplemental Figure 1C, 1D) and is required for the
757 transcriptional activation of these microRNAs (Figure 3D-G, Supplemental Figure 2). Importantly,
758 we show that NHR-23 is necessary for the cyclical expression profile of primary *let-7*, *mir-48* and
759 *mir-84*, as the oscillations in the primary transcript levels of these microRNAs are almost
760 undetectable upon knockdown of *nhr-23* (Figure 3D, 3F, Supplemental Figure 2C). We
761 demonstrate that scrambling the RORE sites in the *let-7* promoter results in decreased binding
762 by NHR-23 (Figure 4B, Supplemental Figure 1E), decreased primary *let-7* levels (Figure 4C) and
763 slower accumulation of mature *let-7* (Figure 4D). The increased number of seam cells (Figure 4E)
764 and the quicker pace of development of *let-7(scRORE1,2)* and *let-7(scRORE1,3)* animals (Figure
765 4F) also supports our conclusion that NHR-23 binding at the RORE sites is necessary for
766 physiologically sufficient transcriptional activation of *let-7*.
767 A previous study proposed that the *let-7* family of microRNAs negatively regulated *nhr-23*
768 by an indirect mechanism, independent of the 3′ UTR of *nhr-23* (Hayes et al., 2006). Here, we
769 show that *let-7* directly represses *nhr-23* in a manner dependent on a *let-7* complementary
770 sequence (LCS) in the *nhr-23* 3′ UTR (Figure 5, 6A, 6A′, Supplemental Figure 4A, 4A′). However,
771 our data do not rule out the possibility of additional regulatory pathways that are dependent on
772 *let-7* but independent of the *nhr-23* 3′ UTR. During the adult stage, the level of inappropriately
773 expressed *nhr-23* in *let-7(n2853)* was higher than the level of *nhr-23* in the *nhr-23(aaa20-ΔLCS)*
774 strain, suggesting the involvement of more than one pathway in the repression of *nhr-23* by *let-7*
775 (Figure 6A, Supplemental Figure 4A). During the juvenile-to-adult transition, *let-7* represses the
776 RNA binding protein *lin-41* and this allows the translation of the LIN-41 target, *lin-29* (Reinhart *et*
777 *al.*, 2000; Slack et al., 2000). Mutants of *lin-29* exhibit increased expression of NHR-23 during
778 adulthood, suggesting that LIN-29 represses transcription of *nhr-23* (Harris and Horvitz, 2011).
779 Therefore, the *lin-29*-mediated inhibition may be the 3' UTR independent pathway by which *let-7*
780 represses *nhr-23*.
781 Thus, NHR-23 and *let-7* form a transcriptional-post-transcriptional negative feedback loop.
782 Within a given larval stage, NHR-23 promotes the expression of the *let-7s* and the *let-7s* repress
783 *nhr-23*. The expression levels of *let-7* peak ~1.6 hours after *nhr-23,* resulting in an intrinsic delay
784 between the accumulation of *nhr-23* and that of *let-7* (Figure 3D, 3F, 6A). Across development,
785 the *let-7s* dampen the relative amplitude of *nhr-23* expression from one larval stage to the next
786 (Figure 6A, Supplemental Figure 4A). Furthermore, NHR-23 autoregulates its own expression

787 (Figure 9A, 9D-F). Together, these interconnected feedback loops set up a self-sustained
788 molecular-genetic oscillator that is extinguished in adulthood.
789
790 **Negative feedback between NHR-23 and *let-7s* sets the pace of the molting cycle.**
791 The feedback loop between NHR-23 and the *let-7s* functions in an oscillator-based
792 mechanism to regulate the duration of the molting cycle, in part by driving waves in expression of
793 both key clock components, as well as output/target genes. We have shown that the Period
794 homolog *lin-42* is a transcriptional target of NHR-23 (Figure 9A-C, Supplemental Figure 7C). The
795 *let-7* family also post-transcriptionally represses *lin-42*. (McCulloch and Rougvie, 2014; Perales
796 *et al.*, 2014; Van Wynsberghe *et al.*, 2014). Similarly, other genes necessary for molting, including
797 *fbn-1* and *mlt-10*, are shared targets of NHR-23 and *let-7* (Figure 8, Supplemental Table 4). The
798 transcription factor NHR-25, which is required for molting, may also be a shared target of NHR-23
799 and *let-7* (Supplemental Table 4) (Hayes et al, 2006). We propose that the NHR-23-*let-7* feedback
800 loop acts within the LIN-42/PER-based molting cycle timer, alongside other as-yet unidentified
801 components.
802 Based on our findings, we propose a model to explain how the feedback loop between
803 NHR-23 and the *let-7s* controls the speed of the molting cycle. Early in each larval stage, as
804 animals commit to a forthcoming molt, NHR-23 first reaches a functional concentration at the
805 promoters of genes with relatively higher numbers of ROREs, such as *fbn-1* and *noah-1*, and
806 initiates the gene expression programs leading to the biogenesis of the sheath. The sheath is a
807 temporary exoskeleton that encapsulates molting animals and is thought to protect the body of
808 the worm from imploding while the old cuticle is released and a new one is synthesized (Katz *et*
809 *al.*, 2021). At the same time, NHR-23 also promotes accumulation of the repressor *let-7*. As
810 NHR-23 continues to accumulate, it begins to activate the expression of genes with relatively
811 fewer ROREs such as *mlt-10* and *osm-11*, which respectively encode components of the cuticle
812 and lethargus-promoting peptides (Meli *et al.*, 2010; Singh et al., 2011). In this manner, NHR-23
813 might schedule the start of cuticle biogenesis and onset of lethargus. Then, *let-7*-mediated
814 repression of the same CCGs and *nhr-23* likely signals both the end of cuticle remodeling and
815 lethargus. Repression of *nhr-23* delays accumulation of the protein in the next life stage and the
816 onset of any subsequent molt (Figure 6, Figure 7 and Supplemental Figure 4A). Thus, negative
817 feedback between NHR-23 and the *let-7s* regulates the pace of the molting cycle in part by
818 controlling the rate at which *nhr-23* transcripts accumulate and the amplitude of *nhr-23*
819 expression. This model is consistent with the earlier onset of lethargus and accelerated
820 development observed in both *nhr-23(aaa20-ΔLCS)* and *let-7(n2853)* mutants (Figure 2B and

821 6B). Both mutants have steeper curves and higher amplitude of *nhr-23* expression (Figure 6A and
822 Supplemental Figure 4A). In contrast, delayed and protracted lethargus are observed in
823 *nhr-23(RNAi)* animals (Figure 2B), which have shallower curves and lower amplitude of *nhr-23*
824 expression. Thus, in theory, the intrinsic rates of ascent of *nhr-23* and the *let-7s* transcripts, and
825 the ~1.6 h time difference between the accumulation of NHR-23 and accumulation of the *let-7s*
826 together likely impact the amplitudes of the expression curves of multiple CCGs and, by
827 extension, the temporal organization of critical phases of the molting cycle such as cuticle
828 synthesis, lethargus and ecdysis. To determine whether the pace of the molting cycle is regulated
829 by the amplitude of *nhr-23* expression versus the rate of accumulation of *nhr-23* transcripts will
830 require future experiments wherein the two factors are manipulated independently of one another.
831
832 ***let-7* mediated dampening of *nhr-23* levels sets the number of oscillations.**
833 All nematodes molt four and only four times. This represents striking and specific uniformity
834 across some 25,000 different species, including numerous parasites of humans. In contrast, intra-
835 and interspecies variation in the number of molts both before and after reproductive maturity
836 occurs in animals of other phyla in the Ecdysozoan clade (Aguinaldo et al., 1997). Therein, the
837 total number of molts varies in response to intrinsic and extrinsic factors, including the salinity and
838 temperature of aquatic habitats, the availability of blood meals and other food sources, and the
839 photoperiod (Esperk et al., 2007). The fundamental basis of this seemingly invariant limitation
840 among nematodes is not known, despite the long-standing recognition of supernumerary molts
841 associated with loss-of-function mutations in *let-7* and other heterochronic genes.
842 We propose that the balance between the activity of NHR-23 and the activity of the *let-7*s
843 controls the finite number of molts. In our model, NHR-23 is a positive effector and the *let-7s* are
844 negative regulators of molting. Consistent with this model, both *nhr-23(gf)* and *let-7(lf)* mutants
845 undergo extra molts. As larvae develop from one stage to the next, the amplitude of NHR-23
846 expression gradually declines, while the levels of the *let-7s* gradually increase, culminating in the
847 extinction of the cycle in adulthood. We have shown that *let-7*-mediated repression is at least
848 partially responsible for the dampening of *nhr-23* expression (Figure 7A, Supplemental Figure
849 4A). Gradual reduction of positive autoregulation by NHR-23 through successive larval stages
850 may be a second factor that could contribute to the dampening of *nhr-23* expression.
851
852 **NHR-23 and *let-7* act together with other feedback loops, by a possibly conserved**
853 **mechanism, to regulate developmental timing.**

854 We have shown that NHR-23 and *let-7* are key components of a biological clock that
855 regulates the pace of molting. Previous studies have characterized ~3700 genes that exhibit
856 oscillatory patterns of gene expression coupled to the molting cycle (Hendriks *et al.*, 2014; Kim *et*
857 *al.*, 2013; Meeuse et al., 2020). These ~3700 genes have been proposed to form a massive
858 genetic oscillator that could act as a developmental clock during *C. elegans* development
859 (Meeuse *et al.*, 2020; Tsiairis and Grosshans, 2021). The interdependence of the molting cycle
860 and the proposed developmental clock remain unknown (Tsiairis and Grosshans, 2021). The
861 extent to which the pace of the molting cycle timer sets the pace of the theoretical developmental
862 clock, and vice versa, is unclear. However, given the significant coupling of the molting cycle and
863 the proposed developmental clock, the NHR-23-*let-7* genetic oscillator may contribute to the pace
864 of the *C. elegans* developmental clock.
865 Using transgenic reporters, we showed that the transcriptional activation of *let-7* by
866 NHR-23 and the post-transcriptional inhibition of *nhr-23* by *let-7* may be conserved in the context
867 of mammalian homologs (Figure 10). RORs and mammalian *let-7* both regulate the expression
868 of key clock components in the hepatic circadian clock. Specifically, RORs promote the
869 expression of the clock components *Bmal1* and *Cry1*, as well as clock-controlled genes *Elovl3*
870 and *Cyp8b1*, in both the livers of mice and cultured human liver cell lines (Takeda et al., 2012;
871 Zhang *et al.*, 2017). Liver-specific genetic disruption of only RORγ, or in combination with RORα,
872 alters the levels of serum cholesterol, HDL and LDL, and liver triglycerides relative to wild-type
873 mice (Takeda et al., 2014; Zhang *et al.*, 2017). Thus, our work on the molting cycle timer may
874 have implications for mammalian circadian clocks and related disorders of sleep and metabolism.
875 Our findings are consistent with the emerging concept that microRNA-mediated feedback
876 loops increase the robustness of numerous gene regulatory networks and related outcomes,
877 including cell fate decisions, stress responses, and developmental trajectories. The NHR-23-*let-7*
878 genetic oscillator integrates the molting cycle timer with the heterochronic pathway in *C. elegans*,
879 representing an elegant and possibly conserved mechanism of regulating developmental timing.
880
881
882 **ACKNOWLEDGEMENTS**
883 The American Cancer Society (RSG-12-149-01-DDC to ARF), the National Science Foundation
884 (IOS1258218 to ARF), and the National Institutes of Health (R01 GM129301 awarded to JKK)
885 supported this research. Some strains were provided by the *Caenorhabditis* Genetics Center
886 (CGC), which is funded by the NIH Office of Research Infrastructure Programs (P40 OD010440).

887 **FIGURE LEGENDS**

888

889 **Figure 1**. Animal development requires coordination between reiterated processes and
890 successive transitions in cell fate. **A)** Stages of the molting cycle of *C. elegans*, emphasizing the
891 regular intervals of lethargus (yellow), ecdysis (orange) and physical activity (blue). Upon
892 hatching, the embryo grows and develops through four larval stages that are punctuated by molts.
893 **B)** Successive transitions in the fate of the lateral epidermal stem cells, called seam cells (red
894 nuclei), in developing worms. The microRNAs *mir-48*, *mir-84*, *mir-241* are paralogs of *let-7* that
895 promote transitions in the fate of the seam that are specific to the L2 stage. The microRNA *let-7*
896 promotes fate transitions that are associated with the L3 and L4 stages. The adult stage is
897 characterized by the presence of cuticular structures called alae. **C)** Schematic depicting
898 interactions between ROR/*nhr-23*, *let-7* microRNAs and PER/*lin-42* in *C. elegans.* Arrowheads
899 and bars signify positive and negative regulation, respectively. Question marks distinguish
900 regulatory events evaluated in this study from those previously established.

901

902 **Figure 2.** Opposite and codependent effects of *nhr-23* and *let-7* on molting biorhythms. **A)** Stages
903 of the life cycle (left) and the molting cycle (right) of *C. elegans.* **B)** Actograms depict the behavior,
904 life stage and phenotype of worms observed at 1 h intervals from emergence in L4 onward. Each
905 chart combines records from two independent trials. The records within each column correspond
906 to a single worm. In addition, the molting-defective phenotype is labelled only when first detected.
907 The wake-to-wake interval (W-W) has been indicated. Relevant scoring rubrics are fully defined
908 in the Results and Methods. ****$p \leq 0.0001$; Ordinary One-Way ANOVA with Bonferroni's
909 correction for multiple comparisons. **C)** The same as B, except that the actograms depict animals
910 observed from the emergence in the L3 onward. ****$p \leq 0.0001$, *$p \leq 0.05$; Ordinary One-Way
911 ANOVA with Bonferroni's correction for multiple comparisons. Supplemental Table 1 includes the
912 active, lethargic, and w-w intervals of these eight cohorts and additional cohorts of both *let-7s(-)*
913 mutants and *nhr-23* knockdowns.

914

915 **Figure 3.** NHR-23 promotes transcription of primary *let-7*. **A)** Schematic of the *let-7* locus in *C.*
916 *elegans* (top) and corresponding NHR-23 ChIP peaks (bottom). Top: Magenta labels mature *let-*
917 *7*; black labels *pri-let-7*; dark gray labels upstream DNA present in the *let-7p::gfp* transcriptional
918 reporter (Kai et al, 2013)**;** light gray labels the minimal seam-specific enhancer (MP) (Johnson et
919 al, 2003); brown labels the consensus ROREs **.** TSS indicates the major transcriptional start site
920 for pri-*let-7* (Kai et al, 2013). Dotted line represents the amplicon quantified by ChIP-qPCR.

921 Bottom: The NHR-23 ChIP-seq peaks reported by the modENCODE consortium are indicated.
922 **B-C)** ChIP-qPCR analysis of NHR-23 enrichment at the *let-7* promoter in L3 and L4 stage wild
923 type (untagged NHR-23) and *nhr-23::3xflag* larvae. The promoter of *col-19,* which had no NHR-
924 23 ChIP-seq peak, was used as a negative control. Values represent the mean ± sem of three
925 independent trials, each of which included three technical replicates. Values for the amplicon of
926 interest in QK159 [*nhr-23::3xflag*] and N2 were first normalized to the respective input. The
927 average fold-enrichment in QK159 samples was then normalized to the average fold-enrichment
928 in N2 samples within each trial. **p≤0.01, ***p≤0.001; Two-way ANOVA with Bonferroni's
929 correction for multiple comparisons. **D)** Levels of primary *let-7* transcript determined by TaqMan
930 RT-qPCR in *nhr-23(RNAi)* and mock-treated larvae developing from the late L2 stage until the
931 L3-to-L4 molt. Each value was normalized to *ama-1* transcript levels in the same sample. Values
932 were then normalized to the average of all control time samples. Symbols represent the mean
933 and range from two biological replicates. The x-axis indicates time elapsed (h) on food. The
934 underlying bar depicts developmental stages; gray boxes therein signify lethargi. The times of
935 initial exposure to *nhr-23* siRNAs and the appearance of molting-defective *nhr-23(RNAi)* larvae
936 are indicated. ****p≤0.0001, **p≤0.01; Two-way ANOVA with Bonferroni's correction for multiple
937 comparisons. **E)** Same as D, except the levels of mature *let-7* transcripts, normalized to levels of
938 the snoRNA U18, are shown. ****p≤0.0001, ***p≤0.001; Two-way ANOVA with Bonferroni's
939 correction for multiple comparisons. **F-G)** Same as D and E respectively, except the larvae were
940 collected from the early L3 stage until the L4-to-adult stage. **p≤0.01, *≤0.05; Two-way ANOVA
941 with Bonferroni's correction for multiple comparisons.
942
943 **Figure 4.** Scrambling the ROREs in the *let-7* promoter reduces NHR-23 occupancy and
944 phenocopies *let-7(lf)* mutants. **A)** The RORE sites upstream of the endogenous pri-*let-7* were
945 scrambled in pairs using CRISPR/Cas9 mediated genome editing. The dotted line represents the
946 amplicon quantified by ChIP-qPCR. **B)** ChIP-qPCR analysis of NHR-23 binding to the *let-7*
947 promoter in *nhr-23::3xflag; let-7(xk41-scRORE1,2)* and *nhr-23::3xflag; let-7(xk39-scRORE1,3)*.
948 The promoter of *col-19,* which had no NHR-23 ChIP-seq peak, was used as a negative control
949 One biological replicate of ChIP-qPCR from L4 animals is shown. The bar graph represents the
950 mean of the 2 technical replicates. The error bars represent mean +/- standard deviation. Values
951 for the amplicon of interest were first normalized to the respective input. The average fold-
952 enrichment for each genotype was then normalized to the average fold-enrichment in N2 samples.
953 n.s. not significant, *p<0.05; Two tailed Student's unpaired t-test. A second biological replicate is
954 shown in Supplemental Figure 1E. **C)** Levels of primary *let-7* transcript determined by RT-qPCR

955 in *let-7(xk41-scRORE1,2)* and *let-7(xk39-scRORE1,3)* immediately after the L2/L3 molt. Three
956 biological replicates, with 2 technical replicates each are shown. The bar graph represents the
957 mean of the 6 values first normalized to the levels of *eft-2* and then normalized to the value of the
958 N2 sample at 20 h. The error bars represent mean +/- standard deviation. *p≤0.05, **p≤0.01,
959 ***p<0.001; Two tailed Student's paired t-test. **D)** Same as C, except levels of mature *let-7*
960 determined using Taqman RT-qPCR were first normalized to U18 snoRNA and then normalized
961 to the value of the N2 sample at 20h. *p≤0.05, **p≤0.01, ***p<0.001; two tailed Student's paired
962 t-test. **E)** Number of seam cell nuclei in *let-7(RORE-1,2)* and *let-7(RORE-1,3)* at 25°C. *let-*
963 *7(n2853)* and *let-7(mg279)* were scored as controls. All scoring was done in the background of
964 JR672 (*Pscm::GFP).* Mean ± standard deviation has been shown. (n≥100) ***p<0.001; One-way
965 ANOVA. **F)** Left: Actograms depict the behavior and life stage of single wild type or mutant
966 animals observed at regular 1 h intervals, as described in Figure 2B. Here, high activity (H) refers
967 to continuous pharyngeal pumping, whereas low activity (L) refers to intermittent pharyngeal
968 pumping at the time of observation. Right: Table with wake-to-wake intervals for multiple
969 independent isolates. ****p≤0.0001, ***p≤0.001, **p≤0.01; Mann-Whitney Test.
970
971 **Figure 5.** The 3′ UTR of *nhr-23* contains a functional *let-7* consensus site (LCS). **A)** Predicted
972 base-pairing between the LCS in the *nhr-23* 3′ UTR and mature *let-7.* Schematic also shows three
973 other predicted *let-7* binding sites. Stop codon is shown as a black box. **B)** Design of bicistronic
974 reporters for 3′ UTR-mediated gene regulation. **C)** Rows of representative fluorescence images
975 show merged and individual signals from tdTomato and GFP co-expressed in the lateral
976 epidermis of the same worm. Labels indicate the 3′ UTR fused to tdTomato in the corresponding
977 reporter. Arrowheads point to hyp-7 nuclei. Scale bar = 10 µm. All images were captured with an
978 exposure time of 10 milliseconds. **D)** Quantitation of the ratiometric signal (tdTomato/GFP)
979 associated with each 3′ UTR reporter detected. Each symbol represents the average value of
980 three ROIs per worm. N indicates the cumulative sample size from two independent experiments.
981 Bars signify the mean ± sd for the cumulative sample. ****p≤0.0001, ***p≤0.001, Ordinary One-
982 Way ANOVA with Tukey's correction for multiple comparisons. **E)** As above, except that
983 ratiometric values were normalized to same-day controls. The full-length *nhr-23* construct is
984 depicted in blue; deletion constructs in brown.
985
986 **Figure 6.** Steeper waveforms of *nhr-23* expression and an increased pace of development are
987 both associated with deletion of the LCS from the 3′ UTR of *nhr-23* and genetic inactivation of
988 *let-7*. **A)** Levels of *nhr-23* transcripts detected by TaqMan RT-qPCR in regular time samples of

989 wild-type, *nhr-23*(*aaa20-ΔLCS)* and *let-7(n2853)* animals collected from late L2 through early
990 adulthood. Rectangles beneath the x-axis signify lethargi (shaded by genotype, as per the
991 legend); white rectangles signify intervals of physical activity. Values for *nhr-23* were first
992 normalized to *ama-1* transcripts within each same time sample. The resulting values were further
993 normalized to the mean of all wild-type time samples, represented by the dashed y-axis gridline.
994 Dots and error bars represent the mean and range from three technical replicates. As the rates
995 of development of the three genotypes differ from one another, the waveforms for the wild-type
996 samples were shifted to the left by 4 h in both charts, to align the mutant and wild-type samples
997 by developmental stage. The *p* values shown are for comparisons between wild-type and mutant
998 values at the indicated time points. ****p≤0.0001, ***p≤0.001, **p≤0.01, Two-Way ANOVA with
999 Tukey's correction for multiple comparisons. Supplemental Figure 4 shows the results of an
1000 independent biological replicate. Arrows point to the supernumerary peaks in *nhr-23* transcript
1001 levels detected in both *nhr-23(aaa20-ΔLCS)* and *let-7(n2853)* animals. Wild-type animals were
1002 sampled 24–50 h after release from L1 diapause; both mutant animals, 22–48 h. **A')** Metrics used
1003 to compare the sequential waves of *nhr-23* expression associated with each of the indicated
1004 genotypes. The amplitude of the waveforms was calculated using Metacycle. The rising slope
1005 refers to the rate at which transcript levels ascend from the trough detected before or during the
1006 preceding molt to the peak detected within the specified stage. **B-C)** Actograms depict the
1007 behavior and life stage of single animals observed at regular 1 h intervals, as described in Figure
1008 2. In this case, high or low activity refers to continuous or sporadic pharyngeal pumping observed
1009 during the time sample. As previously described, Supplemental Table 1 has the active, lethargic,
1010 and w-w intervals of the cohorts in these studies. ****p≤0.0001, **p≤0.01, Ordinary One-Way
1011 ANOVA with Bonferroni's correction for multiple comparisons.
1012
1013 **Figure 7.** Both derepression and overexpression of *nhr-23* trigger additional molts in
1014 reproductively mature animals. **A)** The percentage of wild-type, *nhr-23*(*aaa20-ΔLCS)*,
1015 and *wgIs43[nhr-23++]* adults that appeared quiescent at regular timepoints 54–120 h after
1016 release from diapause and cultivation with food. Values represent the mean ± standard deviation
1017 from 2 independent trials, with cumulative sample sizes of 300 to 400 animals per timepoint. The
1018 values for the wild-type cohort were repeated in both graphs for ease of comparison. Significant
1019 peaks in the prevalence of quiescent animals are marked by asterisks. The corresponding values
1020 significantly exceeded the values for age-matched, wild-type animals (p<0.0001, chi-square test,
1021 $\chi 2$ ranged from 39 to 223). **B)** Actograms depict the behavior and fate of quiescent adults singled
1022 at each timepoint marked by an arrow and then observed at regular 2 h intervals. Records within

1023 each row correspond to a single worm. The behavior of a worm at a particular timepoint was
1024 scored as active, lethargic, or ecdysing as described in the Methods section. Aberrant molts and
1025 death were also recorded (see Methods). **C)** DIC micrographs show examples of adults that
1026 attempted to molt. Arrows point to former cuticles dislodged from the tail or head; arrowheads, to
1027 alae on both the passing and emergent cuticles. The letter "e" denotes fertilized embryos within
1028 the uterus. Scale bars = 10 μm.
1029
1030 **Figure 8.** Most genes regulated by the molting clock are shared targets of both NHR-23 and
1031 *let-7s.* **A)** Levels of *fbn-1* transcripts detected by TaqMan RT-qPCR in regular time samples of
1032 mock-treated and *nhr-23(RNAi)* animals collected from the late L2 through young adulthood. The
1033 data were collected from distinct experiments: one set, which comprised two independent trials,
1034 covered the late L2 stage until the L3-to-L4 molt; and the other set, which also comprised two
1035 independent trials, covered the late L3 stage until the L4-to-adult molt. Rectangles beneath the x-
1036 axis signify lethargus; white rectangles signify intervals of physical activity. Values for *fbn-1* were
1037 first normalized to *ama-1* transcripts within each same time sample. The resulting values were
1038 further normalized to the mean of all wild-type time samples, represented by the dashed y-axis
1039 gridline. Dots and error bars represent the mean and range from two biological replicates. The
1040 table beneath the chart lists the amplitude and rising slope for the waveforms for the L4 stage,
1041 calculated as described earlier. ****$p \leq 0.0001$, *$p < 0.05$, Two-way ANOVA with Bonferroni's
1042 correction for multiple comparisons. **B)** Same as A, except that the levels of *fbn-1* transcripts were
1043 measured in wild-type, *nhr-23*(*aaa20-ΔLCS)* and *let-7(n2853)* animals collected from late L2
1044 through early adulthood. Additionally, the rectangles beneath the x-axis that depict the molts are
1045 shaded by genotype, as per the legend. ****$p \leq 0.0001$, Two-way ANOVA with Bonferroni's
1046 correction for multiple comparisons. Wild-type animals were sampled 24–50 h after release from
1047 L1 diapause; both mutant animals, 22–48 h. **C-D)** Same as B and C, respectively, except the
1048 levels of *mlt-10* transcripts were measured using Taqman RT-qPCR. ****$p \leq 0.0001$, **$p < 0.01$,
1049 Two-way ANOVA with Bonferroni's correction for multiple comparisons. **E)** Venn diagram
1050 summarizes the classification of 67 clock-controlled genes (CCGs) as direct targets of NHR-23,
1051 *let-7s*, both or neither based on original bioinformatic approaches and meta-analyses of published
1052 ChIP-Seq, comparative microarray, and ALG-1-iCLIP data sets (Broughton *et al.*, 2016).
1053 Supplemental Table 4 provides the detailed information used to classify each gene of interest.
1054 Relevant scoring rubrics are fully described in the results and methods. The flowchart beneath
1055 the Venn diagram shows examples of prospective components of the molting timer and effectors
1056 of specific subroutines of the molting cycle that emerged as dual targets from the meta-analysis.

1057

1058 **Figure 9.** NHR-23 and *let-7s* govern the temporal expression profile of other key clock genes**. A)**
1059 ChIP-qPCR for NHR-23 enrichment at *lin-42* and *nhr-23* promoters in N2 (untagged NHR-23) or
1060 *nhr-23::3xflag* L3 stage larvae. Values represent the mean ± sem of three independent trials, each
1061 of which included two technical replicates. Values for the amplicon of interest in each sample was
1062 first normalized to the respective input and then the average values for QK159 [*nhr-23::3xflag*]
1063 were normalized to the average value of the amplicon in N2 within each trial. ****p≤0.0001,
1064 **p≤0.01; Two-way ANOVA with Bonferroni's correction for multiple comparisons. **B)** Levels of
1065 *lin-42* transcripts detected by TaqMan RT-qPCR in regular time samples of mock-treated and
1066 *nhr-23(RNAi)* animals collected from the late L2 through young adulthood, as described in Figure
1067 8A. ***p≤0.001, *p<0.05; Two-way ANOVA with Bonferroni's correction for multiple comparisons.
1068 **C)** Levels of *lin-42* transcripts detected by TaqMan RT-qPCR in regular time samples of wild-type,
1069 *nhr-23*(*aaa20-ΔLCS)* and *let-7(n2853)* animals collected from late L2 through early adulthood, as
1070 described in Figure 8B. ****p≤0.0001, ***p≤0.001; Two-way ANOVA with Bonferroni's correction
1071 for multiple comparisons. **D)** Schematic of the *nhr-23* genomic locus and the *nhr-23::gfp* fusion
1072 gene that was used to determine the extent to which NHR-23 regulates the expression of itself.
1073 The light teal rectangle depicts the region 2.5 kb upstream of the start codon of *nhr-23* Isoform A,
1074 the dark teal rectangles depict exons in *nhr-23* and the light grey rectangle represents the *nhr-23*
1075 3′ UTR. The last two and half exons of *nhr-23* were replaced by the coding sequence for *gfp*, as
1076 shown by a green rectangle. The 3′ UTR of *nhr-23* was replaced by the *unc-54* 3′ UTR, which is
1077 depicted in dark grey. The ROREs are shown as brown boxes. The dotted line represents the
1078 region complementary to the dsRNA used to knockdown endogenous *nhr-23*. While the dotted
1079 line is shown spanning the introns, the dsRNA only targets the exonic regions. **E)** Fluorescence
1080 and DIC micrographs show the signal from GFP detected in the lateral epidermis of mid-L4 stage
1081 animals that express the *nhr-23::gfp::unc-54* reporter. Micrographs on the left show a
1082 representative mock-treated animal and those on the right show a representative *nhr-23(RNAi)*
1083 animal. **F)** Related signal intensities in E were measured and are depicted. Therein, circles
1084 represent the average of three separate nuclei within the same worm, and error bars indicate the
1085 mean and standard deviation. Scale bar = 15 μm and exposure time = 25 ms. ****p≤0.0001,
1086 ***p≤0.001; One-way ANOVA with Bonferroni's correction for multiple comparisons.
1087

1088 **Figure 10.** Reciprocal regulatory elements may be conserved in mammalian *ROR* and *let-7*
1089 genes. **A)** Each schematic depicts the 3 kb region upstream of selected homologs of *let-7*. Brown
1090 boxes show the multiple ROREs identified upstream of mature *let-7* (magenta) in the annotated

1091 genomes of the indicated species and are numbered relative to the first nucleotide of the mature
1092 microRNA. Black arrows are aesthetic landmarks for probable, but not experimentally verified,
1093 transcriptional start sites. **B-C)** A transgenic strain containing the 3 kb fragment upstream of *M.*
1094 *musculus let-7* fused to the coding sequence for *gfp* was used to determine the extent to which
1095 *C. elegans nhr-23* regulates the expression of *M. musculus let-7*. Fluorescence and DIC
1096 micrographs show expression of the *M. musculus let-7a-1* promoter in the pharynx of mock-
1097 treated and *nhr-23(RNAi)* animals undergoing the L4-to-adult molt. Quantification of fluorescence
1098 intensity is shown in the graph in C. Each dot represents the mean of three ROIs measured within
1099 the pharynx and error bars depict the mean and standard deviation in measurements across the
1100 entire sample. The yellow asterisk represents the GFP signal in the neurons attributed to the
1101 *ttx-3::gfp* coinjection marker. Scale bar = 15 μm; Exposure time = 200 milliseconds. **p≤0.01;
1102 One-way ANOVA with Bonferroni's correction for multiple comparisons. **D)** Schematic shows the
1103 LCSs (gold), 3′ UTR (blue), and stop codons (black) of six annotated homologs of *nhr-23/ROR*.
1104 Gradients and bold labels distinguish sites perfectly complementary to the seed of *let-7s*. The
1105 dotted boxes indicate regions tested in Figures E-H. Each 3′ UTR was retrieved from the UCSC
1106 genome browser; verified by comparison with curated ESTs; and LCSs identified using
1107 RNAhybrid. Supplemental Table 2 provides additional information about the prospective duplexes
1108 between each of these LCSs and *let-7.* Accession numbers for the related ESTs and genomic
1109 sequences are included in the Key Resources Table. **E-H)** Representative images and
1110 quantitation of the ratiometric signal (tdTomato/GFP) associated with fragments of the 3′ UTRs of
1111 *H. sapiens RORβ* and *M. musculus RORα* and variants thereof that lack both LCSs. Each symbol
1112 represents the average value of three ROIs per worm. N indicates the total sample size from two
1113 independent experiments. Bars signify the mean ± sd for the sample. ****p≤0.0001; Ordinary One-
1114 Way ANOVA with Bonferroni's correction for multiple comparisons. Representative images from
1115 multiple independent isolates are shown in Supplemental Figure 8.

1116 **METHOD DETAILS**

1117

1118 **Working with *C. elegans***

1119 Unique strains of the model nematode *Caenorhabditis elegans* (*C. elegans*) generated by
1120 and applied to this research are described in the Key Resources Table. *C. elegans* were
1121 cultivated, preserved, observed, and transformed using standard methods (Stiernagle, 2006).
1122 Strains were cultivated at 25°C unless otherwise specified. Newly-hatched worms were
1123 developmentally synchronized by passage through starvation-induced, L1-stage diapause.
1124 Briefly, eggs were isolated by lysis of gravid hermaphrodites in sodium hypochlorite, suspended
1125 in M9 buffer supplemented with 5 µg/mL cholesterol, and incubated for 16 to 24 h with rotational
1126 aeration. Hatchlings were then plated on solid nematode growth medium (NGM) seeded with
1127 *Escherichia coli* (*E. coli*) strain OP50-1, HT115(DE3) or HB101, as indicated. One to two hundred
1128 hatchlings were routinely plated on 6 cm NGM plates; ten to fifteen thousand hatchlings, on 10
1129 cm NGM plates seeded with 10-fold concentrated bacteria; twenty five thousand hatchlings on
1130 15cm NGM plates seeded with 10-fold concentrated bacteria.

1131

1132 **Bacterial-mediated RNA-interference (RNAi)**

1133 Relevant clones of *E. coli* HT115(DE3) were cultured, plated on solid NGM supplemented
1134 with 8 mM isopropyl β-D-1-thiogalactopyranoside (IPTG, Laguna Scientific), and incubated for 16
1135 to 24 h at 25° C, allowing for IPTG-induced expression of dsRNAs. Worms used as controls were
1136 fed bacteria transformed with the empty vector pPD129.36 (a gift from Andy Fire, Stanford
1137 University). Alternatively, worms were fed bacteria transformed with a derivative of the same
1138 vector with an inserted *nhr-23* sequence. The latter clone matched I-3F11 (Source BioScience)
1139 but was isolated directly from the Ahringer *C. elegans* Genome RNAi library (Kamath and
1140 Ahringer, 2003). Because the insert corresponds to three constitutive exons at the 3′ end of the
1141 *nhr-23*, the dsRNA made by this clone targets all 6 isoforms of *nhr-23* annotated in WS273.

1142 To knockdown *nhr-23* during a specific larval stage and circumvent predominant arrest
1143 during a preceding molt, hatchlings were fed control bacteria for a certain interval as elaborated
1144 below, harvested, washed thrice in M9 buffer, and then divided into two samples. Next, larvae in
1145 the test sample were fed bacteria that expressed *nhr-23* dsRNAs; larvae in the control sample
1146 were once again fed bacteria that expressed only short, dsRNAs dissimilar from any worm gene
1147 (Kamath and Ahringer, 2003). Hatchlings destined to become test subjects in longitudinal studies
1148 of newly-emerged L2s, L3s, and L4s were initially fed control bacteria for 0, 6, and 14 h,
1149 respectively. To further attenuate the efficacy of RNAi, as needed to collect large time samples of

1150 synchronized L2s, L3s and L4s for RT-qPCR experiments, hatchlings were initially fed control
1151 bacteria for 16 h and then split into test and control samples, as above. For L3s, L4s and young
1152 adults, as in Figure 3F and 3G, hatchlings were initially fed control bacteria for 24 h and then split
1153 into test and control samples, as above.
1154
1155 **Longitudinal studies of molting-associated biorhythms**
1156 This section provides additional information about the collection, analysis, and presentation
1157 of data in Figure 2, Figure 4, Figure 6 and Supplemental Table 1. Cohorts of larvae molting to the
1158 stage of interest were isolated from synchronized populations; singled in 12-well NGM-RNAi
1159 plates; and observed for 5 to 60 s at regular 1 h intervals, using a Zeiss M^2BioDiscovery
1160 microscope. L4s and older worms were observed at 300-fold magnification; L3s and younger
1161 worms, at 600-fold magnification. At each time sample, each subject was classified as active or
1162 lethargic based on the observation of defined target behaviors. Molting-defective (Mlt) and
1163 ruptured through the vulva (Rup) worms were identified by conventional criteria (Reinhart *et al.*,
1164 2000).
1165 The longitudinal studies represented in Figure 2 included videotaping the head of the worm
1166 using a Sony HDR-XR500V or Nikon D500 camera attached to the microscope. Later, the number
1167 of pharyngeal contractions (pumps) in a 15 s recorded interval was counted while the film was
1168 viewed at 4-fold reduced speed using iMovie version 10.11.2. Pumping rates (Hz) determined by
1169 three independent counts of selected films fell within 95% of the mean, validating this method.
1170 High, medium and low levels of activity were then graded *post-hoc* on a one-way standard scale
1171 defined by the standard deviations and mean pumping rate of all age-matched, wild-type time
1172 samples. As an example, wild-type young adults pumped at 3.9 ± 1.1 Hz (mean ± sd). The activity
1173 levels of nearly all worms that reawakened from lethargi associated with the L4/A molt were
1174 therefore graded as high, medium, or low if the worm pumped at greater than, or equal to, 2.8 Hz;
1175 between 2.8 and 1.7 Hz; or less than 1.7 Hz, respectively. A reasonable exception to this system
1176 was made if sinusoidal locomotion was obvious but no pharyngeal pumps were captured on video.
1177 In this scenario, the worm was scored as active at a low level. This exception applied to only 8
1178 out of 56 time samples of *nhr-23* single knockdowns and 14 out of 84 time samples of *nhr-*
1179 *23(RNAi) let-7(n2853)* double mutants. Among animals that reawakened from lethargi associated
1180 with the L3/L4 molt, the same exception applied to 20 out of 120 time samples of *nhr-23* single
1181 knockdowns and 20 out of 180 time samples of *nhr-23(RNAi) let-7(n2853)* double mutants. The
1182 longitudinal studies represented in Figure 3 and Figure 6 did not involve video-recordings.
1183 Instead, high versus low levels of activity were assigned based on the direct observation of

1184 continuous versus sporadic pharyngeal pumps during the time sample.
1185
1186 **Detection and characterization of supernumerary lethargi and molts**
1187 To score quiescence among populations of young adults, synchronized hatchlings were
1188 released from starvation-induced diapause by plating on 10-fold concentrated lawns of *E. coli*
1189 OP50-1 at a density of 200-400 worms per 10 cm NGM plate. For each strain of interest, six
1190 distinct clutches were plated at 12 h intervals, facilitating the later evaluation of time samples
1191 covering a 72-h interval. As described, worms were observed by light microscopy and scored as
1192 quiescent or active at regular 3 h intervals, 54 to 120 h post-release from diapause. For related
1193 longitudinal studies, quiescent adults were selected and singled in 12-well NGM plates seeded
1194 with thin lawns of bacteria. Each cohort of animals was then either observed at regular 2 h
1195 intervals (Figure 7), or video-recorded for 15-30 s, at regular 2 h intervals, with a Nikon D500
1196 camera. All the previously described scoring rubrics were applied. In addition, ecdysis was
1197 recognized by the execution of one or more of the following idiosyncratic movements: rotation on
1198 the long axis (flipping), bilateral contraction and relaxation on the long axis, and elevation plus
1199 semi-circular rotation of the head. Aberrant molts were scored based on the observation of
1200 puckered sections of cuticle along the body, or the adherence of partly shed cuticle fragments to
1201 the body. If a particular animal had passed through lethargus, then the following behaviors were
1202 also considered evidence of an aberrant molt: pharyngeal spasms, incomplete pumps wherein
1203 the grinder failed to close, and incomplete flips that resulted in twists or kinks along the body.
1204 Detection of a shed cuticle, or parts thereof, on the culture plate was recorded separately. The
1205 latter categories were not mutually exclusive. An inactive or decrepit worm unresponsive to
1206 adverse stimuli was pronounced dead. Absence of a supernumerary molt was inferred if the
1207 animal was active and superficially normal at the endpoint.
1208
1209 **Construction of fusion genes and transgenic strains**
1210 The sequences of all oligonucleotides used in this study are specified in Supplemental
1211 Table 5. All DNA nucleotides were synthesized by and purchased from Integrated DNA
1212 Technologies (IDT). The bicistronic reporters used to detect regulatory elements within 3′ UTRs
1213 were constructed by Gibson Assembly (NEB) and standard methods. Phusion High-Fidelity DNA
1214 Polymerase (NEB) was used to amplify DNA molecules. The resulting plasmids contained the
1215 pBR322 backbone of Fire Lab vectors; the *dpy-7* promoter, which corresponds to nucleotides
1216 7,537,914-7,538,219 of *C. elegans* Chr. X (NC_003284); the synthetic intron embedded in primer
1217 HM01; the coding sequence for *tandem (td) tomato*, which was isolated from Addgene plasmid

1218 #30530 (a gift from Gerhart Ryffel); one of the test 3′ UTRs described below; and an
1219 *SL2::gfp::unc-54* 3′ UTR cassette. The gene-specific 3′ UTRs from *C. elegans* comprised
1220 nucleotides amplified from Chr. I (NC_003279) as follows: *nhr-23*, 7,220,953-7,221,820; *unc-54*,
1221 14,855,909-14,856,180; *lin-41*, 9,334,850-9,335,964. Deletions within the *nhr-23* 3′ UTR reporter
1222 (cloned in pHR017) were created using a Q5 Site-Directed Mutagenesis Kit (NEB) and verified
1223 by Sanger Sequencing (Genewiz Inc.). Additionally, a 565-bp fragment of the 3′ UTR of *H. sapiens*
1224 *RORβ* (chr9:74689171-74689705; GRCh38/hg38), a 256-bp fragment of the 3′ UTR of *M.*
1225 *musculus RORα* (chr9:69380941-69381196 GRCm39/mm39), as well as derivatives lacking both
1226 LCSs, were ordered as gBlocks Gene Fragments from IDT and fused to *tdTomato*. To generate
1227 distinct extrachromosomal arrays harboring each bicistronic reporter, mixtures of the
1228 corresponding plasmid (1 ng/µl), the co-transformation marker *ttx-3::gfp* (40 ng/µl), and filler DNA
1229 pRS316 (59 ng/µl) were microinjected into the gonads of wild-type hermaphrodites. Transgenic
1230 progeny and unique descendent strains were isolated by standard methods.
1231 A transcriptional reporter for *M. musculus Mirlet7a-1* was generated by using fusion PCR
1232 to combine the 3000-bp region upstream of the mature *let-7-a-1* miRNA (chr13:48538273-
1233 48541272; GRCm38/mm10) with *gfp* (pPD95.75). The resulting PCR product was first cloned into
1234 the topo vector pCR-Blunt-II-Topo (ThermoFisher Scientific) to generate pRA46. The strain
1235 ARF431 was generated by co-injecting pRA46 (1 ng/µl,), *ttx-3::gfp* (40 ng/µl, and pRS316 (59
1236 ng/µl) into wild-type hermaphrodites.
1237 The strain ARF422 was made by first crossing *wgIs43* hermaphrodites with *let-7(mg279)*
1238 *mir-84(tm1304)* males. After singling F2's from the crosses, we screened for *wgIs43* homozygotes
1239 among the F3 generation. Only the strains that were homozygous for *wgIs43* were selected and
1240 screened for *let-7(mg279); mir-84(tm1304)* homozygotes. The transgene *wgIs43* was obtained
1241 from OP43 and *let-7(mg279); mir-84(tm1304)* was obtained from ARF249.
1242 The strain ARF432 was generated by injecting construct 4271 (Kostrouchova et al, 1998)
1243 at a concentration of 5 ng/µl, together with the co-injection marker *ttx-3::gfp* (40 ng/ ng/µl), and
1244 pRS316 (45 ng/µl) into wild-type hermaphrodites. Transgenic lines were isolated by standard
1245 methods.
1246
1247 **CRISPR/Cas9-mediated editing of *C. elegans* genes**
1248 The CRISPR/Cas9 system was used essentially as described (Paix *et al.*, 2015) to delete
1249 the endogenous LCS from the 3′ UTR of *nhr-23*, generating the allele *nhr-23(aaa20)*. Briefly, wild-
1250 type hermaphrodites were microinjected with a mixture containing the following: *nhr-23* crRNA
1251 (400ng/µL), tracrRNA (1µg/µL), *dpy-10* crRNA (160 ng/µL, GE Dharmacon), *dpy-10* ssODN

1252 (13.75 ng/μL, IDT), and CAS9 protein (500 ng/μL, PNA Bio) in HEPES buffer pH 7.5
1253 (Sigma-Aldrich) supplemented with 0.025 μM KCL (Sigma-Aldrich). Injected hermaphrodites
1254 (P0s) were singled and screened for Dumpy (Dpy) or Roller (Rol) offspring (F1s), both phenotypes
1255 associated with mutations in *dpy-10*. One hundred F1s were singled from a selected P0.
1256 Genotyping the F1s and their descendants (F2s) identified two strains homozygous for identical
1257 chromosomal deletions of precisely the 21 nucleotides comprising the LCS. One *nhr-23(aaa20-*
1258 *ΔLCS)* strain was backcrossed to N2 thrice prior to phenotypic analysis. No edits in the *dpy-10*
1259 gene were found in the backcrossed strain (ARF414).

1260 To construct *xk22*, wild-type hermaphrodites were injected with *nhr-23* crRNA oHG202
1261 (40μM, IDT Alt-R CRISPR crRNA), *nhr-23::3xflag* repair template (120ng/μL, IDT Ultramer DNA
1262 oligo), *dpy-10* crRNA (5.6 μM, IDT Alt-R CRISPR crRNA), *dpy-10* repair template (12 ng/μL, IDT
1263 Ultramer DNA oligo), tracrRNA (40 μM, IDT Alt-R CRISPR-Cas9 tracrRNA) and Cas9 (15.5 μM,
1264 stock at 40 μM in 20 mM HEPES-KOH pH 7.5, 150 mM KCl, 10% glycerol, 1 mM DTT from
1265 Berkeley QB3 MacroLab). All reagents were diluted in IDT duplex buffer. The crRNA and repair
1266 template both target the C-terminus of NHR-23, which is common to all predicted isoforms.
1267 Injected hermaphrodites were singled and F1 offspring were screened for the same phenotypes
1268 described above. One hundred and twenty F1s were singled from plates that had a high
1269 penetrance of Dpy and Rol phenotypes. Genotyping the F1s identified 3 lines that had *3xflag*
1270 inserted precisely before the stop codon of the *nhr-23* gene. One *nhr-23(xk22)* line was
1271 backcrossed to N2 five times to generate QK159. No edits in the *dpy-10* gene were found in
1272 QK159.

1273 To construct the *let-7(scRORE1,2)* and *let-7(scRORE1,3)* strains, the ROREs were
1274 serially scrambled. *let-7(scRORE1)* was first made by injecting wild type hermaphrodites with
1275 crRNA oHG287(40μM, IDT Alt-R CRISPR crRNA), repair template oHG293(120ng/μL, IDT
1276 Ultramer DNA oligo), and other components as described above. Injected hermaphrodites were
1277 singled and F1 offspring were screened for the same phenotypes described above. Genotyping
1278 the F1s identified several lines that had RORE1 scrambled in the *let-7* promoter. The *dpy-10*
1279 mutation was outcrossed from 1 line. To construct *let-7(scRORE1,2)*, this line was then injected
1280 with crRNA oHG282(40μM, IDT Alt-R CRISPR crRNA), repair template oHG367(120ng/μL, IDT
1281 Ultramer DNA oligo), and other components as described above. Injected hermaphrodites were
1282 singled and F1 offspring were screened for the same phenotypes described above. Genotyping
1283 the F1s identified 3 lines that had RORE1 and RORE2 scrambled in the *let-7* promoter. These
1284 lines were backcrossed to N2 three times to generate QK201, Q202 and QK203. To construct *let-*
1285 *7(scRORE1,3)*, *let-7(scRORE1)* was injected with crRNA oHG278(40μM, IDT Alt-R CRISPR

1286 crRNA), repair template oHG291(120ng/μL, IDT Ultramer DNA oligo), and other components as
1287 described above. Injected hermaphrodites were singled and F1 offspring were screened for the
1288 same phenotypes described above. Genotyping the F1s identified 2 lines that had RORE1 and
1289 RORE3 scrambled in the *let-7* promoter. These lines were backcrossed to N2 three times to
1290 generate QK198 and QK199.
1291
1292 **Quantitative fluorescence microscopy**
1293 *C. elegans* were anesthetized with 2.5% NaN_3 (v/v) in M9 buffer, mounted on 2% agarose
1294 pads, and observed using a Zeiss Axioplan compound microscope with an attached Hamamatsu
1295 Orca ER CCD camera. The image acquisition and analysis software package Volocity 6.3 (Perkin
1296 Elmer) was used to control the microscope and digital camera and also to measure average
1297 fluorescence intensities within selected regions of interest (ROIs). In particular experiments,
1298 transgenic animals were staged partly by DIC microscopy and imaged during the L3/L4 or
1299 L4/Adult molts. Molting animals were identified by occlusion of the buccal cavity (Monsalve *et al.*,
1300 2011). Stereotypical rearrangements of vulva precursor cells (VPCs) demarcated early versus
1301 late sub-stages of the L3-to-L4 molt. The presence of a lumen in the incipient vulva demarcated
1302 early versus late sub-stages of the L4/Adult molt (Gupta et al., 2012; Van Buskirk and Sternberg,
1303 2007).
1304 To measure GFP signals associated with the both the *C. elegans let-7p::nls-gfp*
1305 transcriptional reporter (Kai *et al.*, 2013) and the *M. musculus let-7p::gfp* reporter, worms were
1306 imaged at 400X total magnification. For the *C. elegans let-7* transcriptional reporter, both DIC and
1307 fluorescence images of the lateral epidermis were acquired – the latter with an exposure time of
1308 25 ms. Three nuclei in hyp7 and three in the seam were traced from the DIC image of each worm.
1309 The average fluorescence intensity within each nucleus was then measured and corrected for
1310 background signal. The average values for both hyp7 and seam nuclei (per worm) were used in
1311 further statistical analysis. For the *M. musculus let-7* transcriptional reporter, the pharynx was
1312 imaged in both the DIC and fluorescence channels. An exposure time of 200 ms was used to
1313 capture the GFP signal. Three ROIs in the pharynx were traced from the DIC image of each worm.
1314 As stated above, the average fluorescence intensity within each traced ROI was measured,
1315 corrected for background signal and used in further statistical analysis.
1316 Signals associated with tdTomato and GFP expressed from bicistronic reporters for
1317 regulatory elements within 3′ UTRs were measured using similar approaches. In this case, three
1318 distinct ROIs with areas of 40–70 μm^2 were manually selected per worm; each ROI included
1319 approximately equal areas of the nucleus and cytoplasm. In addition, multiple images of tdTomato

1320 and GFP were automatically captured over a range of exposure times. The average fluorescence
1321 intensity of each ROI was measured and plotted versus the exposure time. Values within the
1322 linear range of the assay were then used to determine the ratiometric signal (tdTomato/GFP) for
1323 each ROI. The average ratiometric value of all three ROIs per worm was used for subsequent
1324 statistical analysis. Notably, the morphology of the vulva was abnormal in a subset (≤ 10%) of
1325 animals that expressed any bicistronic reporter. Because the phenotype precluded staging by the
1326 abovementioned criteria, this subset of animals was excluded from the analysis.
1327 Measurement and analysis of the GFP signal from the NHR-23::GFP reporter was done
1328 exactly as described for the *C. elegans let-7::nls-gfp* reporter above, except that an exposure time
1329 of 200 ms was used to capture the fluorescence signal.
1330
1331 **Chromatin immunoprecipitation coupled with quantitative PCR (ChIP-qPCR)**
1332 Animals grown at 25°C were collected as a ~500μL packed pellet in M9. The animals were
1333 nutated for 30min at room temperature in 12mL of 2.6% (v/v) formaldehyde in autoclaved DI water
1334 for live crosslinking. To quench the reaction, 600 μL of 2.5 M glycine was added and the worms
1335 incubated on the nutator for another 5 min. The samples were then washed thrice in water and
1336 flash-frozen. Frozen pellets were ground twice, for 1 min each, in a Retsch MM400 CryoMill at 30
1337 Hz in liquid nitrogen-chilled stainless steel cryomill chambers, producing a frozen powder of
1338 partially lysed worms. The powder was resuspended and further lysed in 2 mL of RIPA buffer (1x
1339 PBS, 1% (v/v) NP40, 0.5% sodium deoxycholate, and 0.1% SDS), supplemented with the HALT
1340 Protease and Phosphatase Inhibitor Cocktail (ThermoFisher Scientific), for 10 min at 4° C. To
1341 shear the chromatin, samples were sonicated in a Bioruptor Pico (Diagenode) for 3 min (30 s
1342 ON/30 s OFF cycles), three times, at 4° C. A 20 μL aliquot of the sample was treated with
1343 Proteinase K for 10 min and then cleaned by phenol chloroform extraction, as described below.
1344 The concentration of the aliquot was determined using a Qubit Fluorometer 3.0 (Invitrogen).
1345 Based on the initial concentration of the aliquot, the chromatin sample was diluted to 20-30 ng/μL.
1346 To check the extent of shearing, the same aliquot was run on an agarose gel. The sample was
1347 processed and analyzed further provided the DNA smear centered at 200 bp. Of the total amount
1348 of chromatin that remained, 10% was used as the input sample – i.e. stored at 4° C – and 90%
1349 was subject to immunoprecipitation. Every 10 μg of chromatin was incubated with 2 μg of mouse
1350 M2 anti-FLAG monoclonal antibodies (Sigma-Aldrich) overnight at 4° C on a nutator. Next,
1351 samples were incubated with 1.5 mg of affinity-purified sheep anti-mouse IgG antibodies
1352 covalently attached to superparamagnetic Dynabeads M-280 (Invitrogen) for 2 h, at 4° C.

1353 Thereafter, complexes bound to the beads were separated thrice from the supernatant and
1354 washed in 800 µL LiCl buffer (100 mM Tris-HCL pH 7.5, 500 mM LiCl, 1% (v/v) NP40, and 1%
1355 sodium deoxycholate). The resulting immunoprecipitates were de-crosslinked by incubation with
1356 80 µg of Proteinase K in 400 µL of worm lysis buffer (100 mM Tris-HCL pH 7.5, 100 mM NaCl, 50
1357 mM EDTA, and 1% SDS) at 65° C for 4 h—the input samples also underwent the same treatment
1358 in parallel. Residual proteins were removed from both IP and Input samples by phenol-chloroform
1359 extraction. Briefly, 400 µL of phenol-chloroform-isoamyl alcohol pH 8.0 (Sigma-Aldrich) was
1360 added to each sample. The sample was vortexed vigorously and centrifuged at 15,000 x g for 5
1361 min at 4° C. The top layer was transferred to a new tube and DNA was precipitated by incubating
1362 with 1 mL of 0.3 M ammonium acetate (Sigma-Aldrich) in ethanol for 1 h at 30° C. The resulting
1363 DNA pellet was washed twice in 100% ethanol and re-suspended in Tris-EDTA, pH 8.0. Prior to
1364 use as a template for qPCR, the entire DNA sample was treated with RNase A for 1 h at 37° C.
1365 Quantitative PCR for promoter regions of interest was performed with Absolute Blue SYBR
1366 Green (Thermo Scientific) using a CFX96 Real Time System Thermocycler (BioRad) as per the
1367 manufacturers' instructions, with custom primers described in Supplementary Table 5. The Ct
1368 value for each IP sample was first normalized to the Ct value for the respective input sample. The
1369 log 2 transformed fold-change values for samples derived from QK159[*nhr-23::3xflag*] were then
1370 normalized to the respective N2 sample. Three biological replicates, each with two technical
1371 replicates, were completed for each amplicon of interest, as specified in corresponding figure
1372 legends. Pairwise statistical comparisons of the fold enrichment of a given amplicon in samples
1373 from QK159[*nhr-23::3xflag*] versus N2 were made by Two-way ANOVA with Bonferroni's
1374 correction for multiple comparisons.
1375 For L3 ChIP-qPCR samples, hypochlorite prepped embryos were directly plated on HB101
1376 and animals were collected after 29 hours at 25°C as a semisynchronous population. For L4 ChIP-
1377 qPCR samples in Figure 3C and Supplementary Figure 1D, hypochlorite prepped embryos were
1378 nutated in M9 buffer for 24 hours. L1 diapause worms were plated on HB101 and collected after
1379 32 hours at 25°C as a synchronous population of mid-L4 worms. For L4 ChIP-qPCR samples in
1380 Figure 4B, hypochlorite prepped embryos were directly plated on HB101 and collected after 35
1381 hours at 25°C as a semi-synchronous population.
1382
1383 **Isolation of RNA**
1384 RNA was extracted from developmentally synchronized *C. elegans* as described
1385 (McCulloch and Rougvie, 2014). Samples of ~1,500 worms were collected at regular 2 h intervals.
1386 Because the strains seemed to develop at different rates, light microscopy was used to count the

1387 fraction of pumping (active) versus non-pumping (lethargic) animals in each sample prior to
1388 collection (n = 50-100). Lethargic phases were empirically identified *post hoc* by troughs in the
1389 proportion of pumping animals. Related graphs in Figure 6A, Figure 8B, Figure 8C and
1390 Supplemental Figure 4 include 14 time samples encompassing three lethargic and two active
1391 phases per strain. Pellets containing worms (~100 µl) were re-suspended in 4 volumes of TRIzol
1392 (ThermoFisher Scientific) and 1 volume of glass beads 400-625 µm in diameter (Sigma). The
1393 suspensions were vortexed, flash frozen, and thawed thrice. Samples were then mixed with 0.17
1394 volumes of 24:1 chloroform: isoamyl alcohol (OmniPur) and centrifuged. The aqueous layer was
1395 collected, mixed with an equal volume of 5:1 acid phenol: chloroform (ThermoFisher Scientific),
1396 and centrifuged again. After collection of the top layer, RNA was extracted by precipitation with
1397 ice-cold isopropanol (Sigma) and GlycoBlue (ThermoFisher Scientific). The concentration of RNA
1398 in each time sample was measured using a NanoDrop 2000 (ThermoFisher Scientific).
1399 Thereafter, 5 µg of total RNA per sample was treated with 2U of TURBO DNase (ThermoFisher
1400 Scientific) for 1 h.
1401
1402 **Quantitative RT-PCR**
1403 The sequences of gene-specific RT primers and identifiers for TaqMan assays used in this
1404 research are provided in Supplemental Table 5. To quantify levels of primary *let-7* and *ama-1*
1405 transcripts in the abovementioned extracts, we processed 50ng of RNA using a High-Capacity
1406 cDNA Reverse Transcription Kit (ThermoFisher Scientific). Reaction mixtures of 15 µL included
1407 random primers, dNTPs, RNaseOUT, and reverse transcriptase, per the manufacturer's
1408 guidelines. To quantify levels of mature *let-7* and the U18 small nucleolar (sno) RNA, we
1409 processed RNA with the same kit but used gene-specific rather than random primers. Three
1410 volumes of nuclease-free water were added to completed RT reactions. Next, we set-up TaqMan
1411 assays (ThermoFisher Scientific) in 96-well plates, in triplicate. Per the manufacturer's
1412 instructions, each reaction included TaqMan Universal PCR Master Mix, no AmpErase UNG,
1413 gene-specific primers, and 1.3 µL of the preceding RT product in a volume of 20 µL. Reactions
1414 ran on a Stratagene MX3000P (Agilent Genomics). To measure levels of protein-coding
1415 transcripts, 1µg of RNA was reverse transcribed using the enzyme Transcriptor (Roche). Each
1416 reaction mixture (20 µL) also included hexadeoxynucleotide primers (Promega), dNTPs and
1417 RNasin (Promega). Four volumes of nuclease-free water were added to completed RT reactions.
1418 TaqMan assays were performed as described using 2 µL of the RT product as template in a
1419 volume of 10 µL.
1420 The amount of template used in each TaqMan assay gave Ct values in the linear range of

1421 21 to 36. In nearly all cases, technical replicates gave Ct values within 95% of the mean and the
1422 mean Ct value was used in subsequent analyses. Separate TaqMan reactions using templates
1423 made in the absence of reverse transcriptase produced no detectable PCR products, confirming
1424 the amplification of RNA rather than genomic DNA. As described, the levels of transcripts of
1425 interest were normalized to the levels of *ama-1* mRNAs or U18 snoRNAs within each sample,
1426 which were quantified in parallel TaqMan assays. For studies of gene expression over several
1427 developmental stages, the normalized values for each time sample were further standardized to
1428 the mean of all time samples derived from mock-treated or wild-type animals.
1429
1430 **RNA extraction and RT-qPCR for *let-7(scRORE)* mutants**
1431 Hypochlorite prepped embryos were synchronized and plated on HB101. Development was
1432 tracked by monitoring pharyngeal pumping as described before. Samples of ~8000 worms were
1433 collected every 2 hours, starting at 18 hours after plating at 25°C in TRIzol (ThermoFisher
1434 Scientific). Following 3 freeze-thaw cycles, 1-bromo-3-chloropropane was added and the RNA in
1435 the resulting aqueous phase was precipitated by incubating with isopropanol for 2 hours at -30°C.
1436 Samples were then spun at 21,000g for 30 minutes at 4°C to pellet the RNA. The pellet was
1437 washed with 75% ethanol thrice and then resuspended in water.
1438 cDNA synthesis for primary *let-7* was done using SuperScript III Reverse Transcriptase
1439 (Invitrogen). 250ng of RNA was used for cDNA synthesis in the Eppendorf Mastercycler Pro
1440 S6325. Quantitative PCR for *pri-let-7* and *eft-2* were performed with Absolute Blue SYBR Green
1441 (Thermo Scientific) on the CFX63 Real Time System Thermocyclers (Biorad) using custom
1442 primers as listed in Supplemental Table 5. The cycle numbers for *pri-let-7* were normalized to
1443 respective cycle numbers for *eft-2*. 2 biological replicates with 2 technical replicates were done.
1444 The values were all normalized to the average of the 4 readings for the N2 sample. Two-tailed
1445 Student's t-test was done to evaluate p-values. RT-qPCR for *mlt-10* was used to validate the age
1446 matched synchronous populations across the genotypes.
1447 TaqMan synthesis for mature *let-7* was done using probes synthesized by Applied
1448 Biosystems. 100ng of RNA was used for TaqMan Synthesis using High capacity cDNA Reverse
1449 Transcription Kit (ThermoFisher Scientific). Quantitative PCR for *let-7* and *U18* were performed
1450 using TaqMan Universal Master Mix, No AmpErase UNG (ThermoFisher Scientific) on the CFX63
1451 Real Time System Thermocyclers (Biorad). The cycle numbers for *let-7* were normalized to
1452 respective cycle numbers for U18. 2 biological replicates with 2 technical replicates were done.
1453 The values were all normalized to the average of the 4 readings for the N2 sample. Two-tailed
1454 Student's t-test was done to evaluate p-values.

1455

1456 **Counting seam cell nuclei**

1457 Hypochlorite prepped embryos were nutated and hatched over 24 hours in M9 buffer. L1
1458 diapause worms were plated on HB101 at 25°C. Animals were scored between 40 and 44 hours
1459 after plating. Worms were immobilized in 50 mg/mL levamisole on a 2% agarose pad on a slide.
1460 The number of Pscm::GFP expressing cells in each worm were counted under the Zeiss Axio
1461 Zoom V16 Fluorescence Stereo Scope.

1462

1463 **MetaCycle analysis of gene expression curves**

1464 The MetaCycle 1.2.0 package was used to calculate the amplitude and phase of expression
1465 of the genes listed in Figure 6, Figure 8, Figure 9, Supplemental Figure 4, Supplemental Figure
1466 6, Supplemental Figure 7 and Supplemental Table 3. The normalized levels of transcripts of each
1467 gene, derived from the analysis described above were provided to MetaCycle. For each gene,
1468 the expression curves recorded from the L2-L3 molt until the L3-L4 molt, were considered as
1469 corresponding to the L3 stage. Similarly, expression curves recorded from the L3-L4 molt until
1470 the L4-A molt were considered as corresponding to the L4 stage. Gene expression curves
1471 recorded in the L3 stage were analyzed separately from those recorded during the L4 stage.
1472 Additionally, expected periods of 8 h and 10 h were used for analysis of the L3 and L4 stage data,
1473 respectively.

1474

1475 **Identification of conserved *cis*-regulatory elements in homologous genes**

1476 DNA sequences corresponding to the upstream regulatory region, first intron and 3′ UTR
1477 for each nematode gene of interest were retrieved from WormBase (WS) v.264 and saved as
1478 SnapGene v.4 (GSL Biotech) files. The upstream sequences extracted from WS included all
1479 nucleotides between the transcriptional start site of the gene of interest and the nearest protein-
1480 coding gene. Particular sequences were extended or shortened based on gene models, ESTs
1481 and transcriptional start sites archived in WS264. If the gene of interest lacked an annotated
1482 3′UTR, then we initially retrieved 1 kb of sequence downstream of the stop codon. Particular 3′
1483 UTR sequences were revised based on ESTs and poly-AAA sites that are archived in WS264 but
1484 not yet incorporated in current gene models.

1485 Both the upstream regulatory regions of vertebrate homologs of *let-7* and the 3′ UTRs of
1486 vertebrate homologs of *nhr-23*/*RORs* were retrieved from the UCSC genome browser. Three
1487 human genes, two mouse genes, and six zebrafish genes encode mature miRNAs identical in
1488 sequence to *C. elegans let-7*. We extracted 3 kb of sequence upstream of each *let-7* homolog,

1489 except in the case of *H. sapiens let-7a-3*, wherein the promoter has been experimentally delimited
1490 to 1 kb of upstream sequence (Wang et al., 2012). For a given gene, the longest 3′ UTR was
1491 selected if multiple 3′ UTRs existed. The 3′ UTR sequences were individually and systematically
1492 validated by comparison with EST; only those genes with annotated 3′ UTRs supported by ESTs
1493 were included in further analyses.
1494
1495 **Finding clock-controlled genes regulated by NHR-23 and *let-7s***
1496 Genes were determined to be "involved in molting" based on the literature. For example,
1497 if mutations in a particular gene caused a molting defective phenotype, the gene was considered
1498 to be involved in molting (Frand *et al.*, 2005). Similarly, if inactivation of the gene had an effect on
1499 lethargus, the gene was also considered to be involved in the molting cycle. Genes were
1500 annotated as "oscillatory" based on published RNA-Seq studies (Hendriks *et al.*, 2014; Kim *et al.*,
1501 2013); therein, genes whose expression at 8-10 h intervals was significantly correlated ($P<0.05$)
1502 were considered to be cycling in expression.
1503 To identify ROR response elements that might function as transcriptional enhancers of
1504 miRNAs or protein-coding genes of interest, we searched the upstream regulatory sequences
1505 and/or first introns for instances of the consensus response element 5′-(A/G)GGTCA-3′ on both
1506 the coding and anti-coding strands of DNA. Figures 1A, 8A and Supplemental Figure 1A depict
1507 the results of these computational searches. To accurately calculate the probability of an RORE
1508 occurring by chance, we first used the k-mer counting software program DSK (Rizk G. et al, 2013)
1509 to find that the reference genome of *C. elegans*, which comprises 100.2 mega bases, includes
1510 41,203 distinct instances of the consensus RORE. For non-nematodes, the expected frequency
1511 was the chance of either six-nucleotide sequence appearing in a longer oligonucleotide; this
1512 frequency is approximately one per 1 kb.
1513 Regions of *C. elegans* chromosomal DNA occupied by NHR-23 *in vivo* were identified on
1514 the modEncode *C. elegans* Genome Browser (v. 2.48). The two relevant datasets archived
1515 therein were ChIP-Seq of strain OP43 cultivated at 20° C and harvested during the L2 or L3 stage.
1516 Most genomic regions where NHR-23 was significantly enriched were detected in the dataset
1517 collected from L3 stage larvae, however, we do not discriminate between the two stages in our
1518 analysis. The upstream regulatory sequences and/or first intron for each gene of interest were
1519 viewed in this browser. Regions of significant enrichment ("peaks") were identified by Z-scores ≥
1520 2 (Celniker *et al.*, 2009). Sequences extracted and aligned with the upstream regulatory regions
1521 and/or first intron as above, adjusting for differences in the related chromosomal coordinates
1522 between WS220 and WS264.

1523 Evidence of direct or indirect regulation of transcript levels by NHR-23 – i.e expression of
1524 the gene was at least 1.2-fold reduced in *nhr-23(RNAi)* versus control larvae – was either detected
1525 by Affymetrix microarrays (Kouns *et al.*, 2011), or shown in prior publications (*lin-42a/b, nas-36*).
1526 Targets of NHR-23 followed 2 out of the 3 following criteria: 1) The upstream regulatory
1527 region and/or first intron contained Chip-Seq NHR-23 peaks (Celniker *et al.*, 2009); 2) the same
1528 region contained more ROREs than predicted by chance alone; and 3) Expression was 1.2-fold
1529 lower in *nhr-23* knockdowns than mock-treated larvae.
1530 The software RNAhybrid (Rehmsmeier et al., 2004) was used to detect sequences
1531 partially complementary to the 21-nt. mature *let-7* in the 3′ UTRs of annotated homologs of *nhr-23*
1532 in the genomes of *H. sapiens*, *M. musculus*, *D. rerio* and *C. briggsae*. Mature *C. elegans let-7*,
1533 which is identical to human *let-7*a, was used as the query sequence. No more than 1 mismatched
1534 nucleotide within the *let-7* seed sequence was tolerated for the prediction of LCSs in this report.
1535 Targets of *let-7* fulfilled both of the following criteria: 1) LCSs, with up to one mismatch in
1536 the seed region, were detected in the 3′ UTR more often than, or equal to, the number predicted
1537 by chance alone (Rehmsmeier *et al.*, 2004); and 2) ALG-1 co-IP the 3′ UTR, on the coding strand
1538 of the gene by iCLIP-Seq (Broughton *et al.*, 2016).
1539
1540 **Quantification and statistical analyses**
1541 The software package Volocity 6.3 (Perkin Elmer) was used to both acquire fluorescence
1542 micrographs and measure the signal intensity of selected ROIs. The software package GraphPad
1543 Prism v6.0h was used for all statistical tests except for those done on data from ChIP-qPCR
1544 experiments. Statistical tests for the ChIP-qPCR experiments were done using R Studio version
1545 1.1.463 and R version 3.5.2. The software package MetaCycle 1.2.0 was used to calculate the
1546 amplitude and phase of expression for the cycling genes. Samples sizes for all experiments,
1547 statistical analyses, and outcomes thereof are included within each figure and its legend.

1548 **SUPPLEMENTAL MATERIAL LEGENDS**

1549

1550 **Supplemental Figure 1.** NHR-23 interacts with ROREs upstream of *let-7* and its paralogs**.**
1551 **A-B)** Three analogous schematics show the alignment of ROREs identified in verified or predicted
1552 upstream regulatory regions (gray shading) of *mir-48*, *mir-241* and *mir-84* with NHR-23 occupancy
1553 of the respective chromosomal regions (brown shading) as captured in mid-L3s by ChIP-Seq by
1554 the modENCODE consortium (Celniker *et al.*, 2009). Beige shading with a teal liner indicates
1555 regions of significant enrichment. Magenta labels mature microRNA; dark gray labels upstream
1556 DNA**.** Coordinates refer to *C. elegans* Chr. V (NC_003283.11) and Chr. X (NC_003284.9) as
1557 indicated. Dotted lines mark the location of qPCR primers used in C and D. **C)** Detection and
1558 quantitation of the indicated 100 bp fragments upstream of *mir-48*, *mir-241* and *mir-84* by ChIP-
1559 qPCR in L3 stage larvae, as described in Figure 3B. Error bars represent the mean ± sem from
1560 six distinct samples: two technical replicates per three biological replicates. ****p≤0.0001, Two-
1561 way ANOVA with Bonferroni's correction for multiple comparisons. For a particular gene-specific
1562 amplicon, the value for each QK159 or N2 sample was first normalized to the respective input.
1563 The average fold-enrichment in QK159 samples was then normalized to the average fold-
1564 enrichment in N2 samples. **D)** Same as C, except L4 stage larvae were used in the analysis.
1565 ****p≤0.0001, *** p≤0.001, ** p≤0.01, Two-way ANOVA with Bonferroni's correction for multiple
1566 comparisons. **E**) Second biological replicate of ChIP-qPCR for NHR-23 enrichment at the *let-7*
1567 promoter in *nhr-23::3xflag; let-7(xk41-RORE-1,2)* and *nhr-23::3xflag; let-7(xk39-RORE-1,3)* L4
1568 animals. The bar graph represents the mean of the 2 technical replicates. The error bars represent
1569 mean +/- standard deviation. Values for the amplicon of interest was first normalized to the
1570 respective input. The average fold-enrichment for each genotype was then normalized to the
1571 average fold-enrichment in N2 samples. n.s. not significant, *p<0.05; Two tailed Student's t-test

1572

1573 **Supplemental Figure 2.** NHR-23 regulates the expression of the *let-7* family during the L3 stage.
1574 **A-B)** Representative pairs of fluorescence images and respective overlays (GFP/DIC) show
1575 nuclear-localized GFP expressed from the promoter of *let-7* in the lateral epidermis. Arrows point
1576 to nuclei in hyp7 syncytia; arrowheads, seam nuclei. Scale bars = 20 µm. Adjacent scatter plots
1577 show aggregated values from two independent trials. Bars signify the mean and sd. ****p≤0.0001,
1578 **p≤0.01, Ordinary One-Way ANOVA with Bonferroni's correction for multiple comparisons. C)
1579 Levels of primary *mir-48*, primary *mir-241*, or primary *mir-84*, determined by TaqMan qRT-PCR
1580 in *nhr-23(RNAi)* and mock-treated larvae developing from the late L2 stage until the L3-to-L4 molt.
1581 As described for Figure 3D, each value was normalized to *ama-1* transcript levels in the same

1582 sample. Values were then normalized to the average of all control time samples. Symbols
1583 represent the mean and range from two biological replicates. The x-axis indicates time elapsed
1584 (h) on food. The underlying bar depicts developmental stages; gray boxes therein signify
1585 observed intervals of behavioral quiescence. The times of initial exposure to *nhr-23* siRNAs and
1586 the appearance of molting-defective *nhr-23(RNAi)* larvae are indicated. **p≤0.01; Two-way
1587 ANOVA with Bonferroni's correction for multiple comparisons. **D)** Same as above, for levels of
1588 mature *mir-48*, mature *mir-241*, or mature *mir-84*, each normalized to U18. ****p≤0.0001, *p<0.05;
1589 Two-way ANOVA with Bonferroni's correction for multiple comparisons. N2 was used for this
1590 analysis.
1591
1592 **Supplemental Figure 3.** Molecular mechanisms relevant to the design and performance of
1593 bicistronic reporters for *cis*-regulatory elements in 3′ UTRs of interest.
1594 Schematic depicts the following series of anticipated events: 1) transcription of the bicistronic
1595 reporter under control of the *dpy-7* promoter; 2) trans-splicing of the resulting pre-mRNA, which
1596 generates distinct *tdTomato::test 3′ UTR* and *gfp::unc54 3′ UTR* mRNAs; and 3) standalone
1597 translation of the latter messages into fluorescent proteins.
1598
1599 **Supplemental Figure 4.** Both the functional LCS in the 3′ UTR of *nhr*-23 and *let-7*-family miRNAs
1600 limit the abundance of *nhr-23* transcripts across larval development. **A)** An independent replicate
1601 of the experiment described in Figure 6A. Briefly, the values represent normalized levels of *nhr-23*
1602 transcripts detected in regular 2 h time samples of wild-type, *nhr-23(aaa20-ΔLCS)* and
1603 *let-7(n2853)* larvae and newly emerged adults. As previously described, wild-type samples were
1604 shifted to the left by 2 h to account for the apparent difference in the pace of development of this
1605 cohort relative to the mutant cohorts. Also, *p* values are for comparisons between wild-type and
1606 mutant values at the indicated time points. ****p≤0.0001, Two-Way ANOVA with Tukey's
1607 correction for multiple comparisons. The samples in this trial were collected after hatchlings were
1608 cultivated on food for 24-50 h. **A′)** Metrics used to compare sequential waves of *nhr-23*
1609 expression, also as described in Figure 5. **B)** Normalized *nhr-23* transcript levels detected in wild-
1610 type larvae, *nhr-23(aaa20-ΔLCS)* single mutants, and *mir-48(Δ) mir-241(Δ); mir-84(n4037)* triple
1611 mutants sampled across the L2 stage. In this chart, time samples for *nhr-23(aaa20-ΔLCS)* were
1612 shifted to the left by 2 h because the pace of development of this strain differed from the others
1613 used in this experiment. ****p≤0.0001, Two-Way ANOVA with Tukey's correction for multiple
1614 comparisons. Both wild-type and *let-7s* triple mutant larvae were collected after cultivation with

1615 food for 14–26 h; *nhr-23(aaa20-ΔLCS)* larvae, after 16–28 h. **B′)** Charts show the amplitude and
1616 rising slope of the *nhr-23* curve during the L2 stage, calculated as described earlier.
1617
1618 **Supplemental Figure 5**. The abundance of NHR-23 cycles across larval development and is
1619 elevated in *let-7(lf)* mutants relative to wild type. **A)** Representative images show NHR-23::GFP
1620 fusion proteins detected in the lateral epidermis of OP43 [*wgIs43[nhr-23::gfp]*] larvae at the
1621 indicated stages. Fluorescence images were all captured with an exposure time of 300
1622 milliseconds. In the image of an early L4, the arrowhead points to a nucleus in the seam; the
1623 arrow, to a nucleus in hyp7. Scale bars = 10 µm. **B)** Quantification of the NHR-23::GFP signal
1624 detected in cohorts of larvae collected at regular 1 h intervals across the entirety of the L4 stage.
1625 Gray and white rectangles drawn above the x-axis approximate phases of lethargus and activity,
1626 respectively. Values represent the mean ± sd derived from samples of 6-10 worms per timepoint.
1627 Within each worm, signals detected in 3 hyp7 nuclei and 3 seam nuclei were measured and the
1628 average value applied to further analysis. **C)** Pairs of fluorescence and merged GFP/DIC
1629 micrographs show NHR-23::GFP fusion proteins detected in the lateral epidermis of
1630 *wgIs43[nhr-23::gfp^{++}]* and *wgIs43; let-7(mg279) mir-84(tm1304)* animals at the indicated stages.
1631 Arrowheads point to nuclei in the syncytial hypodermis. The arrow points to a seam (s) nucleus.
1632 The letter g underscores signal detected in several germline nuclei. Scale bar = 10 µm.
1633
1634 **Supplemental Figure 6.** The genes *fbn-1* and *mlt-10* are shared targets of NHR-23 and *let-7s*.
1635 **A)** An independent replicate of the experiment described in Figure 8B. The values represent
1636 levels of *fbn-1* transcripts, normalized to *ama-1*, detected in regular 2 h time samples of wild-
1637 type, *nhr-23(aaa20-ΔLCS)* and *let-7(n2853)* larvae and newly emerged adults. These particular
1638 samples were collected after hatchlings were cultivated on food for 24-50 h. The accompanying
1639 table shows metrics that were calculated as described earlier. **B)** Same as A, except the levels
1640 of *mlt-10* transcripts are shown. ****p≤0.0001, **p≤0.01; *p≤0.05. Two-way ANOVA with
1641 Bonferroni's correction for multiple comparisons.
1642
1643 **Supplemental Figure 7.** NHR-23 and *let-7s* govern the temporal expression profile of other key
1644 clock genes**. A)** Schematics showing the alignment of the major isoforms of *lin-42* with NHR-23
1645 occupancy of the respective chromosomal regions (brown shading) as captured in mid-L3s by
1646 ChIP-Seq, analyzed and contributed by the modENCODE consortium (Celniker *et al.*, 2009).
1647 Beige shading with a teal liner indicates regions of significant enrichment in the NHR-23 ChIP-
1648 seq. Purple rectangles depict coding sequences in the exons; grey rectangles depict UTRs in the

1649 exons; dotted line represents the putative promoter regions; brown rectangles depict ROREs; red
1650 rectangles depict the position of the ChIP-qPCR amplicons from Figure 9A. Coordinates refer to
1651 reverse complement of *C. elegans* Chr II (NC_003280.10) **B)** Schematic similar to A, except
1652 depicting isoforms of *nhr-23*. Coordinates refer to reverse complement of *C. elegans* Chr I
1653 (NC_003279.8) as indicated. **C)** Levels of *lin-42* transcripts detected by TaqMan RT-qPCR in
1654 regular time samples of wild type wild-type, *nhr-23*(*aaa20-ΔLCS)* and *let-7(n2853)* animals
1655 collected from late L2 through early adulthood, as described in Figure 9C. ****p≤0.0001; Two-way
1656 ANOVA with Bonferroni's correction for multiple comparisons. **D)** Schematic depicting LCSs
1657 (gold) in the 3′ UTR (blue) of *C. elegans lin-42a/b* and *H. sapiens PER2*. Gradients and bold labels
1658 distinguish sites perfectly complementary to the seed of *let-7s*. Each 3′ UTR was retrieved from
1659 the UCSC genome browser; verified by comparison with curated ESTs; and LCSs identified using
1660 RNAhybrid.
1661
1662 **Supplemental Figure 8.** Reciprocal regulatory elements may be conserved in mammalian RORs
1663 and *let-7*. **A)** The 3 kb region upstream of selected homologs of *let-7*. Brown boxes label ROREs;
1664 magenta labels mature *let-7.* ROREs are numbered relative to the first nucleotide of the mature
1665 microRNA. Black arrows are landmarks for probable, but not experimentally verified,
1666 transcriptional start sites. **B-C).** Similar to Figure 10E, 10G, representative images show the
1667 tdTomato and GFP signal associated with fragments of the 3′ UTRs of **B)** *H. sapiens RORβ* and
1668 **C)** *M. musculus RORα* and variants thereof that lack both LCSs.
1669
1670 **Supplemental Table 1.** Metrics of the molting biorhythm associated with specific genotypes. The
1671 active, lethargic, and wake-to-wake intervals are defined in the text. The values derived from
1672 longitudinal studies of stage-specific cohorts of singled, isogenic worms. The top row of each
1673 section corresponds to the same-day cohort of singled, wild-type worms. Dashes (–) beneath
1674 'RNAi' indicate continuous cultivation of the worms on *E. coli* HT115(DE3). "N" is the cumulative
1675 sample size from two independent trials. All *p* values were generated by pairwise comparisons
1676 between individual metrics tabulated for a specific cohort of test subjects and also for the same-
1677 day, age-matched cohort of control subjects: ****p≤0.0001, ***p≤0.001, *p≤0.05; Ordinary One-
1678 Way ANOVA with Bonferroni's correction for multiple comparisons. Entries in the top row of each
1679 subsection correspond to six distinct cohorts of control subjects. By order of first appearance in
1680 the table, the strains tested were N2, QK509 [*let-7(n2853)*], GR1395, GR1436, ARF249, QK201,
1681 QK203, QK198, QK199, OP43, ARF414 and VT1066. Notably, both QK509 [*let-7(n2853)*] and
1682 the ancestral strain MT7626 [*let-7(n2853)*] developed at an accelerated pace: 71% of QK059

1683 hatchlings and 79% of MT7626 hatchlings transited the larval stages and emerged as young
1684 adults within 42 h of cultivation with food, as compared with 12% of N2 hatchlings (N=100,
1685 p≤0.0001, chi-square test).
1686
1687 **Supplemental Table 2.** LCSs found in selected nematode and vertebrate homologs of *ROR*.
1688 Entries correspond to sites shown in Figure 10D. The number of nt. between the 3′ end of each
1689 LCS and the stop codon is specified. The thermostability of every RNA duplex between a
1690 prospective LCS and mature *let-7*, as predicted by RNAhybrid, was lower than the predicted
1691 thermostability (-29 kcal/mol) of duplexes between the functional LCS in the 3′ UTR of *lin-41* and
1692 *let-7* (Rehmsmeier *et al.*, 2004). The 3′ UTRs were supported by ESTs archived in
1693 WBcel235/ce11, WBPS9, GRCh38/hg38, GRCm38/mm10, and GRCz10/danRer10.
1694
1695 **Supplemental Table 3.** Metrics of the expression curves of core clock components and clock-
1696 controlled genes in the indicated genetic backgrounds. As described in the section on Method
1697 Details, Metacycle was used to calculate the amplitude and phase of expression of the
1698 waveforms. The peak values and the slope of rise and decay were obtained by manual
1699 calculation.
1700
1701 **Supplemental Table 4.** Evaluation and classification of clock-controlled genes as direct targets
1702 of NHR-23, *let-7*s, neither or both. The bioinformatic approaches and criteria for assignment of
1703 queries to categories are described in the Method Details. The name and WormBase accession
1704 number of each gene is listed. The shorthand "# Obs./# Exp." stands for the number of observed
1705 DNA or RNA response elements divided by the number of elements predicted by chance alone.
1706 The "⬇" symbol denotes down-regulation of the query transcript in *nhr-23(RNAi)* animals as
1707 compared with wild-type controls. The "+" symbol in column 12 denotes association of the 3′ UTR
1708 with ALG-1 *in vivo*. The symbol "〰" indicates that expression of the gene oscillates across larval
1709 development. Relevant datasets are identified in the text, Method Details and Key Resources
1710 Table.
1711
1712 **Supplemental Table 5.** Oligonucleotides used in this study. The unique identifier for each DNA
1713 or RNA molecules appears in the first column. Suppliers of specific oligonucleotides are identified
1714 in the Method Details. For those primers used to construct a particular bicistronic reporter for
1715 *cis*-regulatory elements in a 3′ UTR of interest, the resulting plasmid and corresponding

1716 extrachromosomal array are identified in the “application” column. All seven reporters and
1717 respective transgenic strains of *C. elegans* are further described in The Key Resources Table.
1718
1719 **Supplemental Movie 1.** Behavior and fate of a quiescent wild-type adult. Movie shows the
1720 behavior and fate of a wild-type adult, video recorded for 15 s every 2 h, that was quiescent at
1721 the initial time point of observation. The wild-type adult was still alive 8 h after the initial incidence
1722 of behavioral quiescence.
1723
1724 **Supplemental Movie 2.** Behavior and fate of a quiescent *nhr-23(aaa20-ΔLCS)* adult. As above,
1725 video recordings were done for 15 s at 2 h intervals from the initial detection of quiescence.
1726 Quiescence was detected at every time sample, and bits of loose cuticle were found along the
1727 head and at the vulva. The animal ultimately bagged.
1728
1729 **Supplemental Movie 3.** Behavior and fate of a quiescent *wgIs43[nhr-23^{++}]* adult. Video recording
1730 was done as described for Supplemental Movies 1 and 2. The animal was quiescent at the first
1731 three time samples. At 8 h after the initial detection of quiescence, the grinder of the animal was
1732 observed to twitch several times, a behavior that normally accompanies ecdysis. At the 10 h time
1733 point, the animal resumed pumping, albeit at a visibly lower rate than wild-type adults. At this time,
1734 loose cuticle could also be detected at the tail. The animal eventually bagged.

1735 **REFERENCES**

1736

1737 Abbott, A.L., Alvarez-Saavedra, E., Miska, E.A., Lau, N.C., Bartel, D.P., Horvitz, H.R.,
1738 and Ambros, V. (2005). The let-7 MicroRNA family members mir-48, mir-84, and mir-241
1739 function together to regulate developmental timing in Caenorhabditis elegans. Dev Cell
1740 *9*, 403-414. 10.1016/j.devcel.2005.07.009.
1741 Aguinaldo, A.M., Turbeville, J.M., Linford, L.S., Rivera, M.C., Garey, J.R., Raff, R.A., and
1742 Lake, J.A. (1997). Evidence for a clade of nematodes, arthropods and other moulting
1743 animals. Nature *387*, 489-493. 10.1038/387489a0.
1744 Alvarez-Saavedra, M., Antoun, G., Yanagiya, A., Oliva-Hernandez, R., Cornejo-Palma,
1745 D., Perez-Iratxeta, C., Sonenberg, N., and Cheng, H.Y. (2011). miRNA-132 orchestrates
1746 chromatin remodeling and translational control of the circadian clock. Hum Mol Genet *20*,
1747 731-751. 10.1093/hmg/ddq519.
1748 Ambros, V., and Ruvkun, G. (2018). Recent Molecular Genetic Explorations of
1749 Caenorhabditis elegans MicroRNAs. Genetics *209*, 651-673.
1750 10.1534/genetics.118.300291.
1751 Banerjee, D., Kwok, A., Lin, S.Y., and Slack, F.J. (2005). Developmental timing in C.
1752 elegans is regulated by kin-20 and tim-1, homologs of core circadian clock genes. Dev
1753 Cell *8*, 287-295. 10.1016/j.devcel.2004.12.006.
1754 Bessho, Y., Hirata, H., Masamizu, Y., and Kageyama, R. (2003). Periodic repression by
1755 the bHLH factor Hes7 is an essential mechanism for the somite segmentation clock.
1756 Genes Dev *17*, 1451-1456. 10.1101/gad.1092303.
1757 Bethke, A., Fielenbach, N., Wang, Z., Mangelsdorf, D.J., and Antebi, A. (2009). Nuclear
1758 hormone receptor regulation of microRNAs controls developmental progression. Science
1759 *324*, 95-98. 10.1126/science.1164899.
1760 Bracht, J., Hunter, S., Eachus, R., Weeks, P., and Pasquinelli, A.E. (2004). Trans-splicing
1761 and polyadenylation of let-7 microRNA primary transcripts. RNA *10*, 1586-1594.
1762 10.1261/rna.7122604.
1763 Broughton, J.P., Lovci, M.T., Huang, J.L., Yeo, G.W., and Pasquinelli, A.E. (2016). Pairing
1764 beyond the Seed Supports MicroRNA Targeting Specificity. Mol Cell *64*, 320-333.
1765 10.1016/j.molcel.2016.09.004.
1766 Celniker, S.E., Dillon, L.A., Gerstein, M.B., Gunsalus, K.C., Henikoff, S., Karpen, G.H.,
1767 Kellis, M., Lai, E.C., Lieb, J.D., MacAlpine, D.M., et al. (2009). Unlocking the secrets of
1768 the genome. Nature *459*, 927-930. 10.1038/459927a.
1769 Chen, R., D'Alessandro, M., and Lee, C. (2013). miRNAs are required for generating a
1770 time delay critical for the circadian oscillator. Curr Biol *23*, 1959-1968.
1771 10.1016/j.cub.2013.08.005.
1772 Cohen, M.L., Kim, S., Morita, K., Kim, S.H., and Han, M. (2015). The GATA factor elt-1
1773 regulates C. elegans developmental timing by promoting expression of the let-7 family
1774 microRNAs. PLoS Genet *11*, e1005099. 10.1371/journal.pgen.1005099.
1775 Cook, D.N., Kang, H.S., and Jetten, A.M. (2015). Retinoic Acid-Related Orphan
1776 Receptors (RORs): Regulatory Functions in Immunity, Development, Circadian Rhythm,
1777 and Metabolism. Nucl Receptor Res *2*. 10.11131/2015/101185.
1778 Diaz-Cuadros, M., Pourquie, O., and El-Sherif, E. (2021). Patterning with clocks and
1779 genetic cascades: Segmentation and regionalization of vertebrate versus insect body
1780 plans. PLoS Genet *17*, e1009812. 10.1371/journal.pgen.1009812.

1781 Du, N.H., Arpat, A.B., De Matos, M., and Gatfield, D. (2014). MicroRNAs shape circadian
1782 hepatic gene expression on a transcriptome-wide scale. Elife *3*, e02510.
1783 10.7554/eLife.02510.
1784 Ecsedi, M., Rausch, M., and Grosshans, H. (2015). The let-7 microRNA directs vulval
1785 development through a single target. Dev Cell *32*, 335-344.
1786 10.1016/j.devcel.2014.12.018.
1787 Edelman, T.L., McCulloch, K.A., Barr, A., Frokjaer-Jensen, C., Jorgensen, E.M., and
1788 Rougvie, A.E. (2016). Analysis of a lin-42/Period Null Allele Implicates All Three Isoforms
1789 in Regulation of Caenorhabditis elegans Molting and Developmental Timing. G3
1790 (Bethesda). 10.1534/g3.116.034165.
1791 Esperk, T., Tammaru, T., and Nylin, S. (2007). Intraspecific variability in number of larval
1792 instars in insects. J Econ Entomol *100*, 627-645. 10.1603/0022-
1793 0493(2007)100[627:ivinol]2.0.co;2.
1794 Evans, R.M., and Mangelsdorf, D.J. (2014). Nuclear Receptors, RXR, and the Big Bang.
1795 Cell *157*, 255-266. 10.1016/j.cell.2014.03.012.
1796 Frand, A.R., Russel, S., and Ruvkun, G. (2005). Functional genomic analysis of C.
1797 elegans molting. PLoS Biol *3*, e312. 10.1371/journal.pbio.0030312.
1798 Galagali, H., and Kim, J.K. (2020). The multifaceted roles of microRNAs in differentiation.
1799 Curr Opin Cell Biol *67*, 118-140. 10.1016/j.ceb.2020.08.015.
1800 Giguere, V., Tini, M., Flock, G., Ong, E., Evans, R.M., and Otulakowski, G. (1994).
1801 Isoform-specific amino-terminal domains dictate DNA-binding properties of ROR alpha, a
1802 novel family of orphan hormone nuclear receptors. Genes Dev *8*, 538-553.
1803 Grishok, A., Pasquinelli, A.E., Conte, D., Li, N., Parrish, S., Ha, I., Baillie, D.L., Fire, A.,
1804 Ruvkun, G., and Mello, C.C. (2001). Genes and mechanisms related to RNA interference
1805 regulate expression of the small temporal RNAs that control C. elegans developmental
1806 timing. Cell *106*, 23-34. 10.1016/s0092-8674(01)00431-7.
1807 Gupta, B.P., Hanna-Rose, W., and Sternberg, P.W. (2012). Morphogenesis of the vulva
1808 and the vulval-uterine connection. WormBook, 1-20. 10.1895/wormbook.1.152.1.
1809 Hammell, C.M., Karp, X., and Ambros, V. (2009). A feedback circuit involving let-7-family
1810 miRNAs and DAF-12 integrates environmental signals and developmental timing in
1811 Caenorhabditis elegans. Proc Natl Acad Sci U S A *106*, 18668-18673.
1812 10.1073/pnas.0908131106.
1813 Harris, D.T., and Horvitz, H.R. (2011). MAB-10/NAB acts with LIN-29/EGR to regulate
1814 terminal differentiation and the transition from larva to adult in C. elegans. Development
1815 *138*, 4051-4062. 10.1242/dev.065417.
1816 Hayes, G.D., Frand, A.R., and Ruvkun, G. (2006). The mir-84 and let-7 paralogous
1817 microRNA genes of Caenorhabditis elegans direct the cessation of molting via the
1818 conserved nuclear hormone receptors NHR-23 and NHR-25. Development *133*, 4631-
1819 4641. 10.1242/dev.02655.
1820 Hayes, G.D., and Ruvkun, G. (2006). Misexpression of the Caenorhabditis elegans
1821 miRNA let-7 is sufficient to drive developmental programs. Cold Spring Harb Symp Quant
1822 Biol *71*, 21-27. 10.1101/sqb.2006.71.018.
1823 Hendriks, G.J., Gaidatzis, D., Aeschimann, F., and Grosshans, H. (2014). Extensive
1824 oscillatory gene expression during C. elegans larval development. Mol Cell *53*, 380-392.
1825 10.1016/j.molcel.2013.12.013.

Iwanir, S., Tramm, N., Nagy, S., Wright, C., Ish, D., and Biron, D. (2013). The microarchitecture of C. elegans behavior during lethargus: homeostatic bout dynamics, a typical body posture, and regulation by a central neuron. Sleep *36*, 385-395. 10.5665/sleep.2456.

Jeon, M., Gardner, H.F., Miller, E.A., Deshler, J., and Rougvie, A.E. (1999). Similarity of the C. elegans developmental timing protein LIN-42 to circadian rhythm proteins. Science *286*, 1141-1146.

Johnson, M.H., and Day, M.L. (2000). Egg timers: how is developmental time measured in the early vertebrate embryo? Bioessays *22*, 57-63. 10.1002/(SICI)1521-1878(200001)22:1<57::AID-BIES10>3.0.CO;2-L.

Johnson, S.M., Lin, S.Y., and Slack, F.J. (2003). The time of appearance of the C. elegans let-7 microRNA is transcriptionally controlled utilizing a temporal regulatory element in its promoter. Dev Biol *259*, 364-379.

Kadener, S., Menet, J.S., Sugino, K., Horwich, M.D., Weissbein, U., Nawathean, P., Vagin, V.V., Zamore, P.D., Nelson, S.B., and Rosbash, M. (2009). A role for microRNAs in the Drosophila circadian clock. Genes Dev *23*, 2179-2191. 10.1101/gad.1819509.

Kai, Z.S., Finnegan, E.F., Huang, S., and Pasquinelli, A.E. (2013). Multiple cis-elements and trans-acting factors regulate dynamic spatio-temporal transcription of let-7 in Caenorhabditis elegans. Dev Biol *374*, 223-233. 10.1016/j.ydbio.2012.11.021.

Kamath, R.S., and Ahringer, J. (2003). Genome-wide RNAi screening in Caenorhabditis elegans. Methods *30*, 313-321.

Katz, S.S., Barker, T.J., Maul-Newby, H.M., Sparacio, A.P., Nguyen, K.C.Q., Maybrun, C.L., Belfi, A., Cohen, J.D., Hall, D.H., Sundaram, M.V., and Frand, A.R. (2021). A transient apical extracellular matrix relays cytoskeletal patterns to shape permanent acellular ridges on the surface of adult C. elegans. bioRxiv, 2021.2012.2028.474392. 10.1101/2021.12.28.474392.

Kim, D., Grun, D., and van Oudenaarden, A. (2013). Dampening of expression oscillations by synchronous regulation of a microRNA and its target. Nat Genet *45*, 1337-1344. 10.1038/ng.2763.

Kostrouchova, M., Krause, M., Kostrouch, Z., and Rall, J.E. (1998). CHR3: a Caenorhabditis elegans orphan nuclear hormone receptor required for proper epidermal development and molting. Development *125*, 1617-1626.

Kouns, N.A., Nakielna, J., Behensky, F., Krause, M.W., Kostrouch, Z., and Kostrouchova, M. (2011). NHR-23 dependent collagen and hedgehog-related genes required for molting. Biochem Biophys Res Commun *413*, 515-520. 10.1016/j.bbrc.2011.08.124.

Mangone, M., Manoharan, A.P., Thierry-Mieg, D., Thierry-Mieg, J., Han, T., Mackowiak, S.D., Mis, E., Zegar, C., Gutwein, M.R., Khivansara, V., et al. (2010). The landscape of C. elegans 3'UTRs. Science *329*, 432-435. 10.1126/science.1191244.

McCulloch, K.A., and Rougvie, A.E. (2014). Caenorhabditis elegans period homolog lin-42 regulates the timing of heterochronic miRNA expression. Proc Natl Acad Sci U S A *111*, 15450-15455. 10.1073/pnas.1414856111.

Meeuse, M.W., Hauser, Y.P., Morales Moya, L.J., Hendriks, G.J., Eglinger, J., Bogaarts, G., Tsiairis, C., and Grosshans, H. (2020). Developmental function and state transitions of a gene expression oscillator in Caenorhabditis elegans. Mol Syst Biol *16*, e9975. 10.15252/msb.209975.

1871 Meli, V.S., Osuna, B., Ruvkun, G., and Frand, A.R. (2010). MLT-10 defines a family of
1872 DUF644 and proline-rich repeat proteins involved in the molting cycle of Caenorhabditis
1873 elegans. Mol Biol Cell *21*, 1648-1661. 10.1091/mbc.E08-07-0708.
1874 Monsalve, G.C., Van Buskirk, C., and Frand, A.R. (2011). LIN-42/PERIOD controls
1875 cyclical and developmental progression of C. elegans molts. Curr Biol *21*, 2033-2045.
1876 10.1016/j.cub.2011.10.054.
1877 Novak, B., and Tyson, J.J. (2008). Design principles of biochemical oscillators. Nat Rev
1878 Mol Cell Biol *9*, 981-991. 10.1038/nrm2530.
1879 Oyama, Y., Bartman, C.M., Gile, J., and Eckle, T. (2017). Circadian MicroRNAs in
1880 Cardioprotection. Curr Pharm Des *23*, 3723-3730.
1881 10.2174/1381612823666170707165319.
1882 Paix, A., Folkmann, A., Rasoloson, D., and Seydoux, G. (2015). High Efficiency,
1883 Homology-Directed Genome Editing in Caenorhabditis elegans Using CRISPR-Cas9
1884 Ribonucleoprotein Complexes. Genetics *201*, 47-54. 10.1534/genetics.115.179382.
1885 Partch, C.L., Green, C.B., and Takahashi, J.S. (2014). Molecular architecture of the
1886 mammalian circadian clock. Trends Cell Biol *24*, 90-99. 10.1016/j.tcb.2013.07.002.
1887 Patke, A., Murphy, P.J., Onat, O.E., Krieger, A.C., Ozcelik, T., Campbell, S.S., and
1888 Young, M.W. (2017). Mutation of the Human Circadian Clock Gene CRY1 in Familial
1889 Delayed Sleep Phase Disorder. Cell *169*, 203-215 e213. 10.1016/j.cell.2017.03.027.
1890 Perales, R., King, D.M., Aguirre-Chen, C., and Hammell, C.M. (2014). LIN-42, the
1891 Caenorhabditis elegans PERIOD homolog, negatively regulates microRNA transcription.
1892 PLoS Genet *10*, e1004486. 10.1371/journal.pgen.1004486.
1893 Puram, R.V., Kowalczyk, M.S., de Boer, C.G., Schneider, R.K., Miller, P.G., McConkey,
1894 M., Tothova, Z., Tejero, H., Heckl, D., Jaras, M., et al. (2016). Core Circadian Clock
1895 Genes Regulate Leukemia Stem Cells in AML. Cell *165*, 303-316.
1896 10.1016/j.cell.2016.03.015.
1897 Raizen, D.M., Zimmerman, J.E., Maycock, M.H., Ta, U.D., You, Y.J., Sundaram, M.V.,
1898 and Pack, A.I. (2008). Lethargus is a Caenorhabditis elegans sleep-like state. Nature *451*,
1899 569-572. 10.1038/nature06535.
1900 Rehmsmeier, M., Steffen, P., Hochsmann, M., and Giegerich, R. (2004). Fast and
1901 effective prediction of microRNA/target duplexes. RNA *10*, 1507-1517.
1902 10.1261/rna.5248604.
1903 Reinhart, B.J., Slack, F.J., Basson, M., Pasquinelli, A.E., Bettinger, J.C., Rougvie, A.E.,
1904 Horvitz, H.R., and Ruvkun, G. (2000). The 21-nucleotide let-7 RNA regulates
1905 developmental timing in Caenorhabditis elegans. Nature *403*, 901-906.
1906 10.1038/35002607.
1907 Rensing, L., Meyer-Grahle, U., and Ruoff, P. (2001). Biological timing and the clock
1908 metaphor: oscillatory and hourglass mechanisms. Chronobiol Int *18*, 329-369.
1909 10.1081/cbi-100103961.
1910 Roenneberg, T., and Merrow, M. (2016). The Circadian Clock and Human Health. Curr
1911 Biol *26*, R432-443. 10.1016/j.cub.2016.04.011.
1912 Roush, S.F., and Slack, F.J. (2009). Transcription of the C. elegans let-7 microRNA is
1913 temporally regulated by one of its targets, hbl-1. Dev Biol *334*, 523-534.
1914 10.1016/j.ydbio.2009.07.012.
1915 Singh, K., Chao, M.Y., Somers, G.A., Komatsu, H., Corkins, M.E., Larkins-Ford, J.,
1916 Tucey, T., Dionne, H.M., Walsh, M.B., Beaumont, E.K., et al. (2011). C. elegans Notch

1917 signaling regulates adult chemosensory response and larval molting quiescence. Curr
1918 Biol *21*, 825-834. 10.1016/j.cub.2011.04.010.
1919 Singh, R.N., and Sulston, J.E. (1978). Some observations on moulting in Caenorhabditis
1920 elegans. Nematologica *24*, 63-71.
1921 Slack, F.J., Basson, M., Liu, Z., Ambros, V., Horvitz, H.R., and Ruvkun, G. (2000). The
1922 lin-41 RBCC gene acts in the C. elegans heterochronic pathway between the let-7
1923 regulatory RNA and the LIN-29 transcription factor. Mol Cell *5*, 659-669.
1924 Stiernagle, T. (2006). Maintenance of C. elegans. WormBook, 1-11.
1925 10.1895/wormbook.1.101.1.
1926 Takahashi, J.S. (2016). Molecular Architecture of the Circadian Clock in Mammals. In A
1927 Time for Metabolism and Hormones, P. Sassone-Corsi, and Y. Christen, eds. pp. 13-24.
1928 10.1007/978-3-319-27069-2_2.
1929 Takahashi, J.S. (2017). Transcriptional architecture of the mammalian circadian clock.
1930 Nat Rev Genet *18*, 164-179. 10.1038/nrg.2016.150.
1931 Takeda, Y., Jothi, R., Birault, V., and Jetten, A.M. (2012). RORgamma directly regulates
1932 the circadian expression of clock genes and downstream targets in vivo. Nucleic Acids
1933 Res *40*, 8519-8535. 10.1093/nar/gks630.
1934 Takeda, Y., Kang, H.S., Freudenberg, J., DeGraff, L.M., Jothi, R., and Jetten, A.M.
1935 (2014). Retinoic acid-related orphan receptor gamma (RORgamma): a novel participant
1936 in the diurnal regulation of hepatic gluconeogenesis and insulin sensitivity. PLoS Genet
1937 *10*, e1004331. 10.1371/journal.pgen.1004331.
1938 Tsiairis, C., and Grosshans, H. (2021). Gene expression oscillations in C. elegans
1939 underlie a new developmental clock. Curr Top Dev Biol *144*, 19-43.
1940 10.1016/bs.ctdb.2020.11.001.
1941 Tsialikas, J., Romens, M.A., Abbott, A., and Moss, E.G. (2017). Stage-Specific Timing of
1942 the microRNA Regulation of lin-28 by the Heterochronic Gene lin-14 in Caenorhabditis
1943 elegans. Genetics *205*, 251-262. 10.1534/genetics.116.195040.
1944 Uriu, K. (2016). Genetic oscillators in development. Dev Growth Differ *58*, 16-30.
1945 10.1111/dgd.12262.
1946 Vadla, B., Kemper, K., Alaimo, J., Heine, C., and Moss, E.G. (2012). lin-28 controls the
1947 succession of cell fate choices via two distinct activities. PLoS Genet *8*, e1002588.
1948 10.1371/journal.pgen.1002588.
1949 Van Buskirk, C., and Sternberg, P.W. (2007). Epidermal growth factor signaling induces
1950 behavioral quiescence in Caenorhabditis elegans. Nat Neurosci *10*, 1300-1307.
1951 10.1038/nn1981.
1952 Van Wynsberghe, P.M., Finnegan, E.F., Stark, T., Angelus, E.P., Homan, K.E., Yeo,
1953 G.W., and Pasquinelli, A.E. (2014). The Period protein homolog LIN-42 negatively
1954 regulates microRNA biogenesis in C. elegans. Dev Biol *390*, 126-135.
1955 10.1016/j.ydbio.2014.03.017.
1956 Van Wynsberghe, P.M., Kai, Z.S., Massirer, K.B., Burton, V.H., Yeo, G.W., and
1957 Pasquinelli, A.E. (2011). LIN-28 co-transcriptionally binds primary let-7 to regulate miRNA
1958 maturation in Caenorhabditis elegans. Nat Struct Mol Biol *18*, 302-308.
1959 10.1038/nsmb.1986.
1960 Wang, D.J., Legesse-Miller, A., Johnson, E.L., and Coller, H.A. (2012). Regulation of the
1961 let-7a-3 promoter by NF-kappaB. PLoS One *7*, e31240. 10.1371/journal.pone.0031240.

Wu, G., Anafi, R.C., Hughes, M.E., Kornacker, K., and Hogenesch, J.B. (2016). MetaCycle: an integrated R package to evaluate periodicity in large scale data. Bioinformatics *32*, 3351-3353. 10.1093/bioinformatics/btw405.

Yoo, S.H., Kojima, S., Shimomura, K., Koike, N., Buhr, E.D., Furukawa, T., Ko, C.H., Gloston, G., Ayoub, C., Nohara, K., et al. (2017). Period2 3'-UTR and microRNA-24 regulate circadian rhythms by repressing PERIOD2 protein accumulation. Proc Natl Acad Sci U S A *114*, E8855-E8864. 10.1073/pnas.1706611114.

You, Y.J., Kim, J., Raizen, D.M., and Avery, L. (2008). Insulin, cGMP, and TGF-beta signals regulate food intake and quiescence in C. elegans: a model for satiety. Cell Metab *7*, 249-257. 10.1016/j.cmet.2008.01.005.

Zhang, Y., Papazyan, R., Damle, M., Fang, B., Jager, J., Feng, D., Peed, L.C., Guan, D., Sun, Z., and Lazar, M.A. (2017). The hepatic circadian clock fine-tunes the lipogenic response to feeding through RORalpha/gamma. Genes Dev. 10.1101/gad.302323.117.

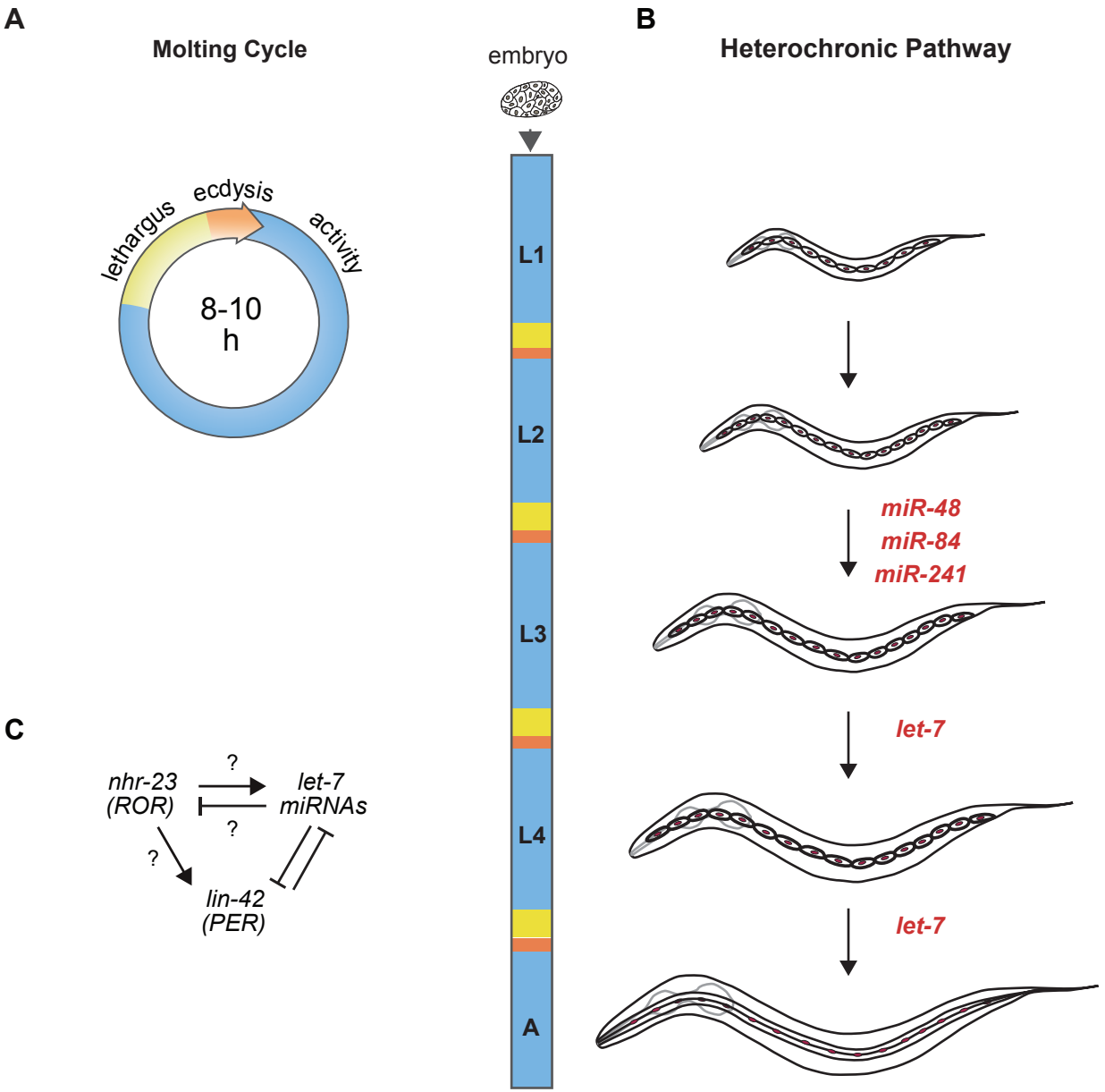
A
Molting Cycle
ecdysis
lethargus
activity
8-10
h
embryo
L1
L2
L3
L4
A
B
Heterochronic Pathway
miR-48
miR-84
miR-241
let-7
let-7
C
nhr-23
(ROR)
?
let-7
miRNAs
?
?
lin-42
(PER)

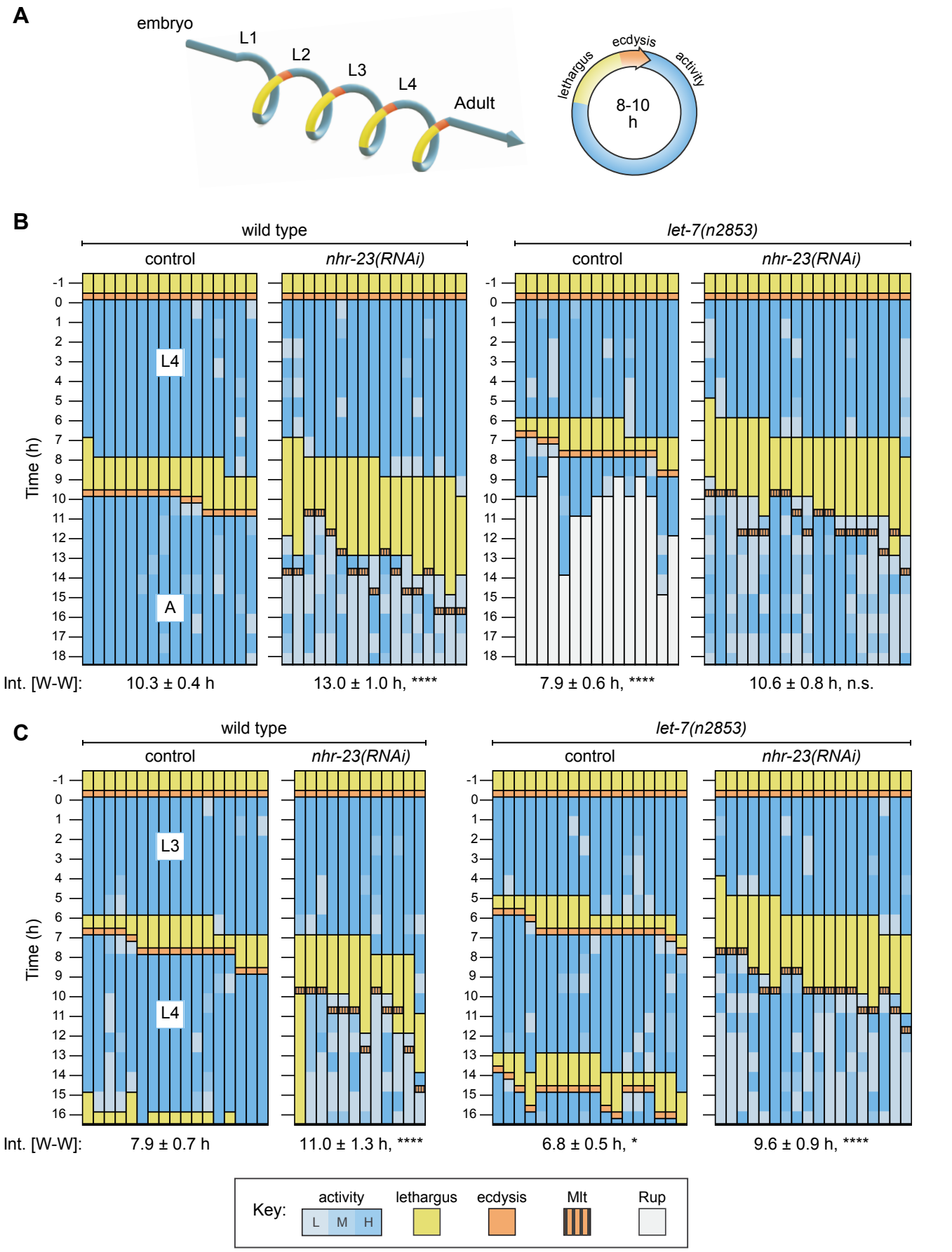
A
embryo
L1
L2
L3
L4
Adult
ecdysis
lethargus
activity
8-10 h
B
wild type
let-7(n2853)
control
nhr-23(RNAi)
control
nhr-23(RNAi)
Time (h)
L4
A
Int. [W-W]:
10.3 ± 0.4 h
13.0 ± 1.0 h, ****
7.9 ± 0.6 h, ****
10.6 ± 0.8 h, n.s.
C
wild type
let-7(n2853)
control
nhr-23(RNAi)
control
nhr-23(RNAi)
Time (h)
L3
L4
Int. [W-W]:
7.9 ± 0.7 h
11.0 ± 1.3 h, ****
6.8 ± 0.5 h, *
9.6 ± 0.9 h, ****
Key:
activity
L M H
lethargus
ecdysis
Mlt
Rup

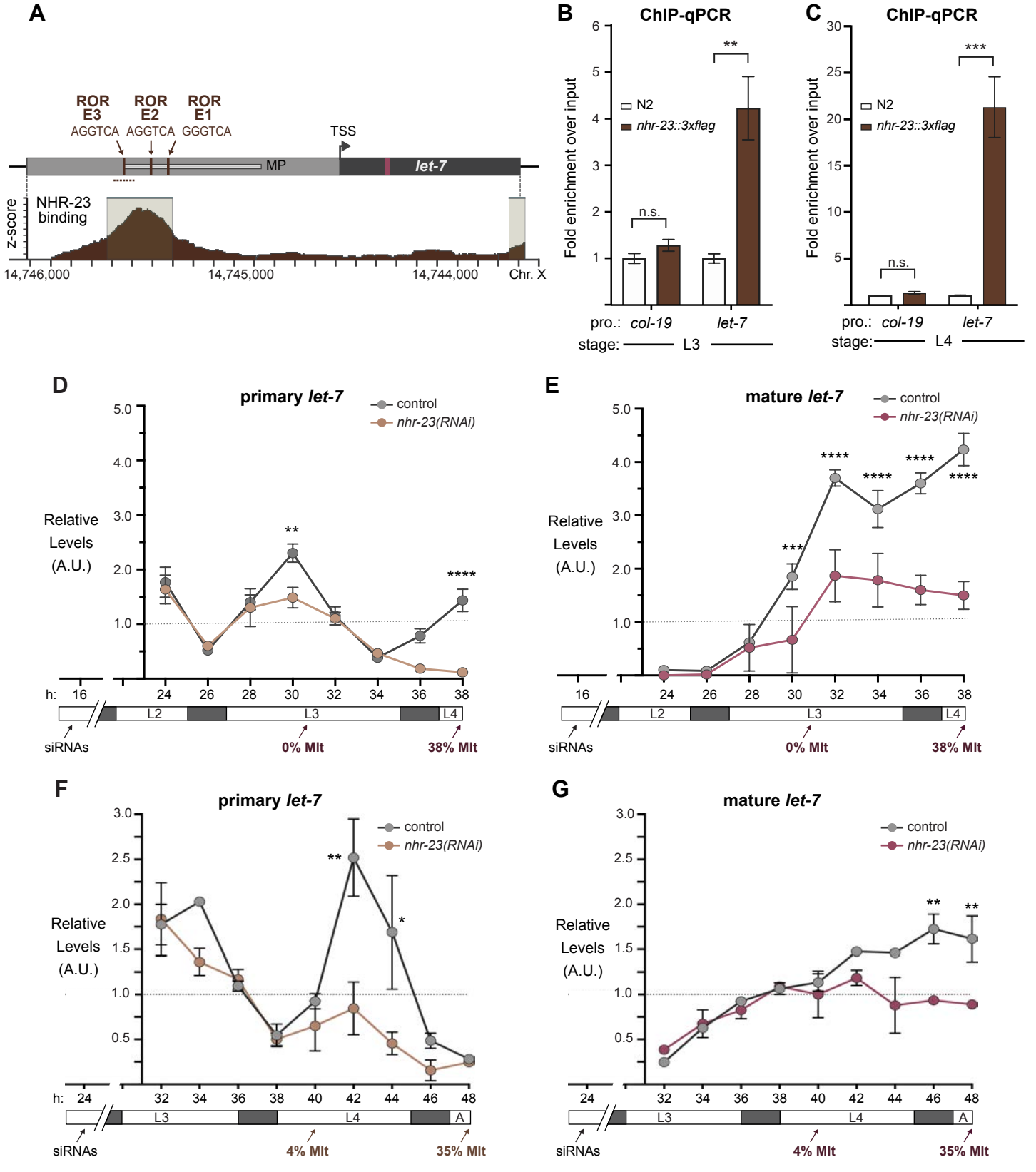
A
ROR E3
AGGTCA
ROR E2
AGGTCA
ROR E1
GGGTCA
TSS
MP
let-7
NHR-23 binding
z-score
14,746,000
14,745,000
14,744,000
Chr. X
B
ChIP-qPCR
Fold enrichment over input
N2
nhr-23::3xflag
n.s.
**
pro.: col-19
let-7
stage: L3
C
ChIP-qPCR
Fold enrichment over input
N2
nhr-23::3xflag
n.s.
***
pro.: col-19
let-7
stage: L4
D
primary let-7
control
nhr-23(RNAi)
Relative Levels (A.U.)
h:
L2
L3
L4
siRNAs
0% MIt
38% MIt
E
mature let-7
control
nhr-23(RNAi)
Relative Levels (A.U.)
L2
L3
L4
siRNAs
0% MIt
38% MIt
F
primary let-7
control
nhr-23(RNAi)
Relative Levels (A.U.)
h:
L3
L4
A
siRNAs
4% MIt
35% MIt
G
mature let-7
control
nhr-23(RNAi)
Relative Levels (A.U.)
L3
L4
A
siRNAs
4% MIt
35% MIt

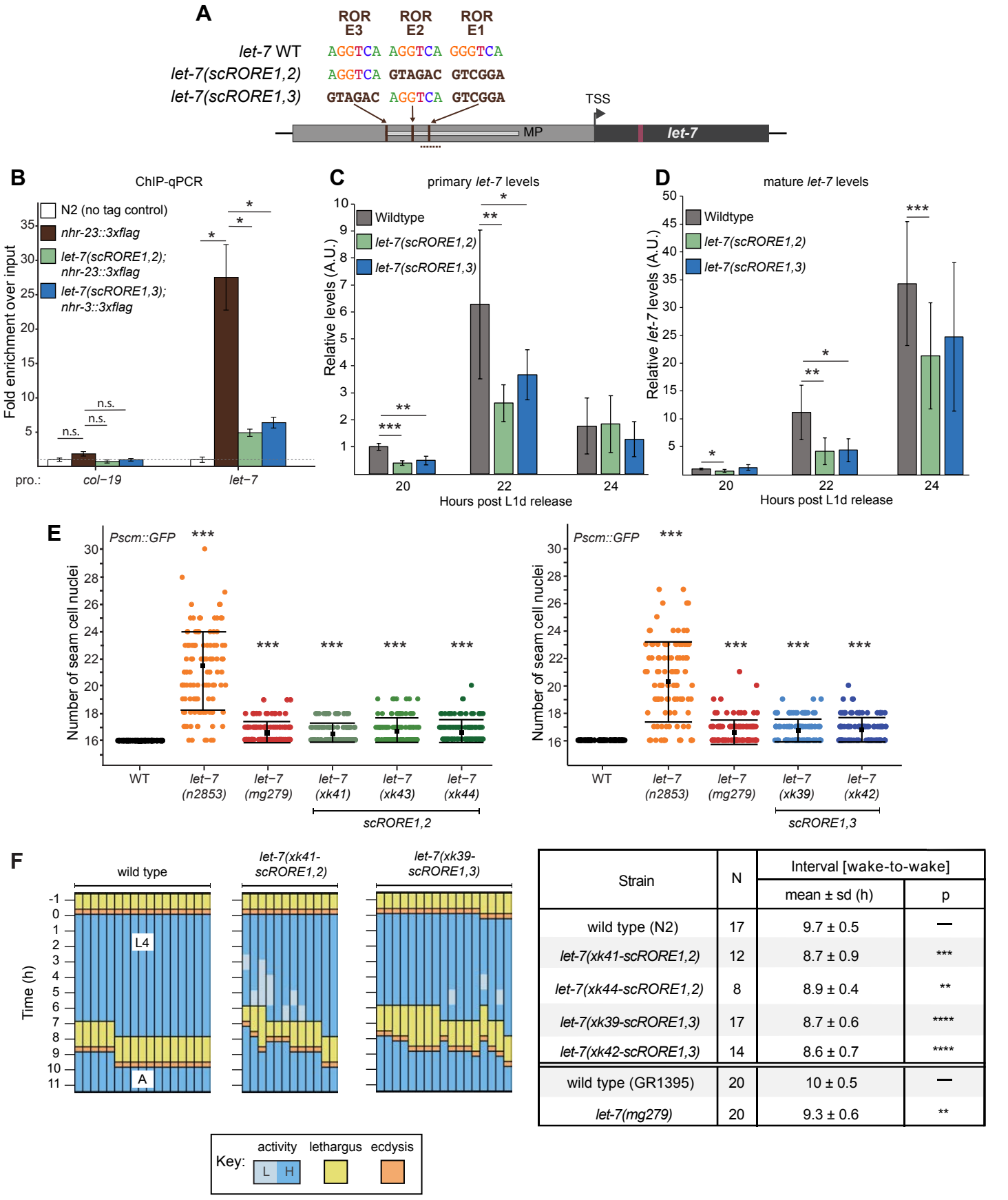

Strain	N	Interval [wake-to-wake]	
		mean ± sd (h)	p
wild type (N2)	17	9.7 ± 0.5	—
let-7(xk41-scRORE1,2)	12	8.7 ± 0.9	***
let-7(xk44-scRORE1,2)	8	8.9 ± 0.4	**
let-7(xk39-scRORE1,3)	17	8.7 ± 0.6	****
let-7(xk42-scRORE1,3)	14	8.6 ± 0.7	****
wild type (GR1395)	20	10 ± 0.5	—
let-7(mg279)	20	9.3 ± 0.6	**

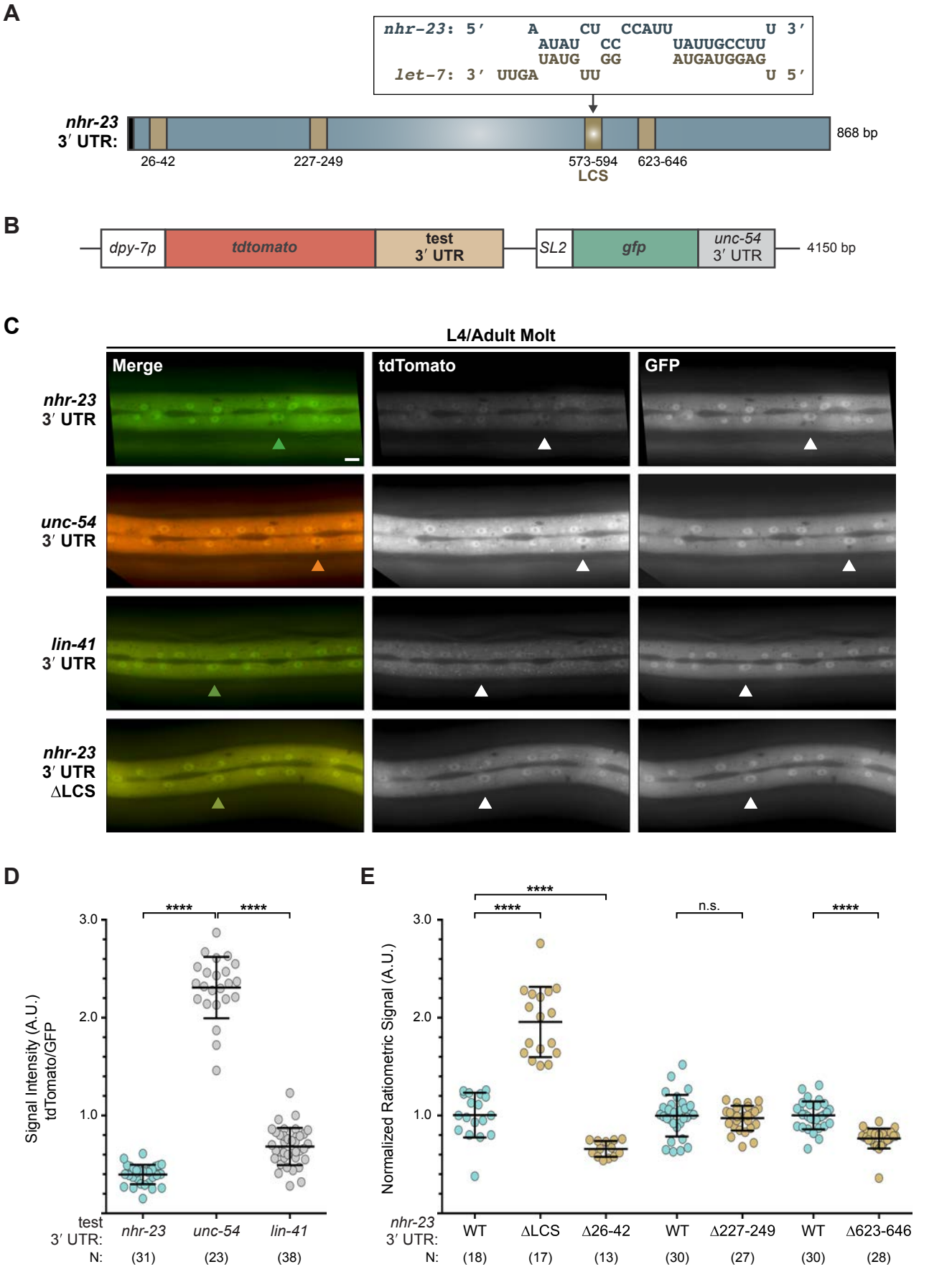
A
nhr-23: 5′ A CU CCAUU U 3′
AUAU CC UAUUGCCUU
UAUG GG AUGAUGGAG
let-7: 3′ UUGA UU U 5′
nhr-23 3′ UTR:
868 bp
26-42
227-249
573-594
623-646
LCS
B
dpy-7p
tdtomato
test 3′ UTR
SL2
gfp
unc-54 3′ UTR
4150 bp
C
L4/Adult Molt
Merge
tdTomato
GFP
nhr-23 3′ UTR
unc-54 3′ UTR
lin-41 3′ UTR
nhr-23 3′ UTR ΔLCS
D
Signal Intensity (A.U.) tdTomato/GFP
3.0
2.0
1.0
****
****
test 3′ UTR:
nhr-23
unc-54
lin-41
N:
(31)
(23)
(38)
E
Normalized Ratiometric Signal (A.U.)
3.0
2.0
1.0
****
****
n.s.
****
nhr-23 3′ UTR:
WT
ΔLCS
Δ26-42
WT
Δ227-249
WT
Δ623-646
N:
(18)
(17)
(13)
(30)
(27)
(30)
(28)

A

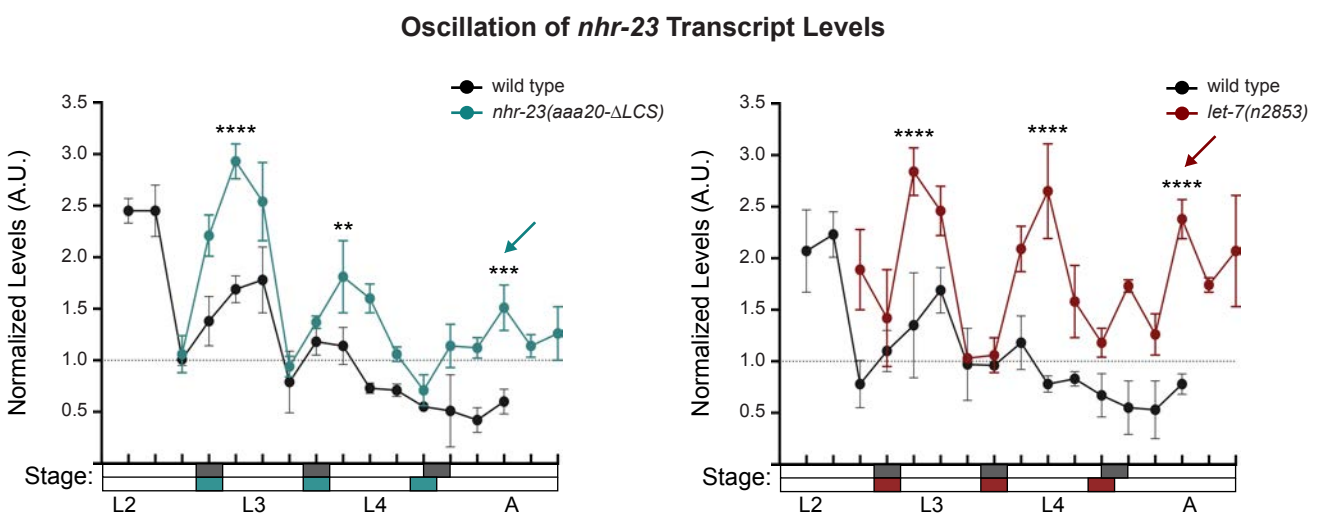

A′

Stage	L3				L4			
Genotype	wild type	*nhr-23(aaa20)*	wild type	*let-7(n2853)*	wild type	*nhr-23(aaa20)*	wild type	*let-7(n2853)*
Amplitude	0.4	1.1	0.5	0.9	0.3	0.4	0.1	0.8
Rising Slope	0.19	0.46	0.15	0.71	0.19	0.21	0.11	0.26

B

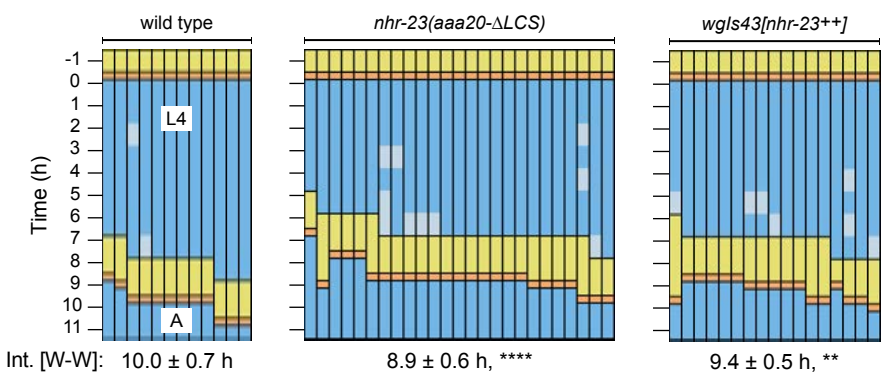

C

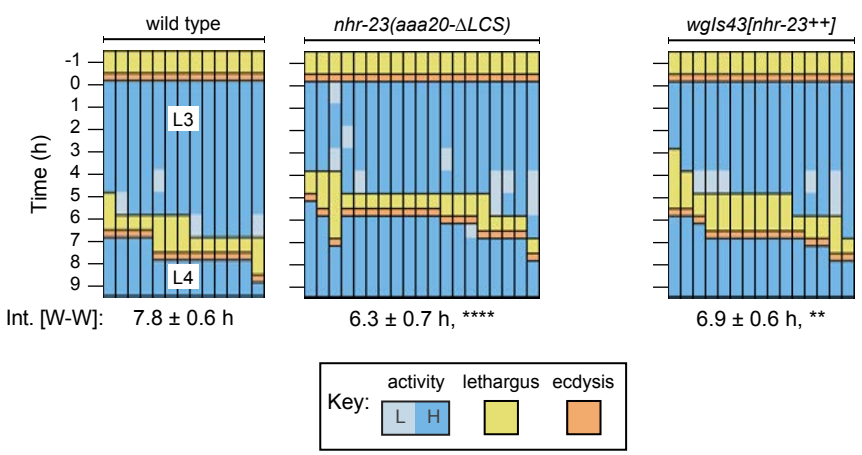

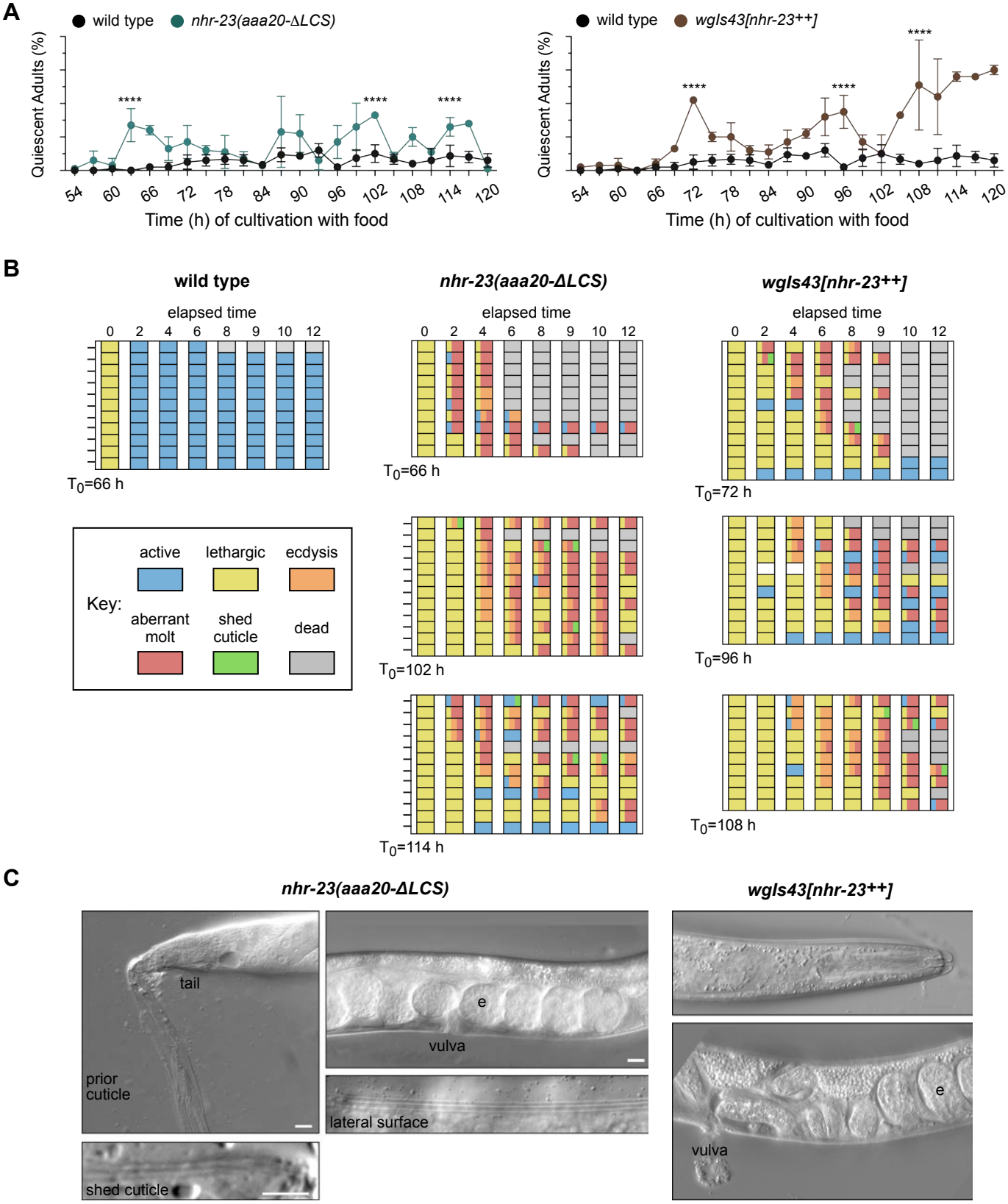
A
wild type
nhr-23(aaa20-ΔLCS)
Quiescent Adults (%)
****
Time (h) of cultivation with food
wild type
wgIs43[nhr-23++]
B
wild type
nhr-23(aaa20-ΔLCS)
wgIs43[nhr-23++]
elapsed time
0 2 4 6 8 9 10 12
T0=66 h
T0=72 h
T0=102 h
T0=96 h
T0=114 h
T0=108 h
Key:
active
lethargic
ecdysis
aberrant molt
shed cuticle
dead
C
nhr-23(aaa20-ΔLCS)
wgIs43[nhr-23++]
tail
prior cuticle
e
vulva
lateral surface
shed cuticle

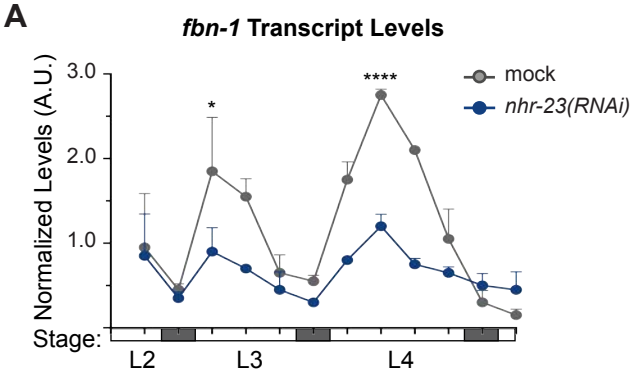

Stage	L3		L4	
RNAi	mock	nhr-23(RNAi)	mock	nhr-23(RNAi)
Amplitude	0.7	0.2	1.0	0.2
Rising Slope	0.68	0.14	0.40	0.30

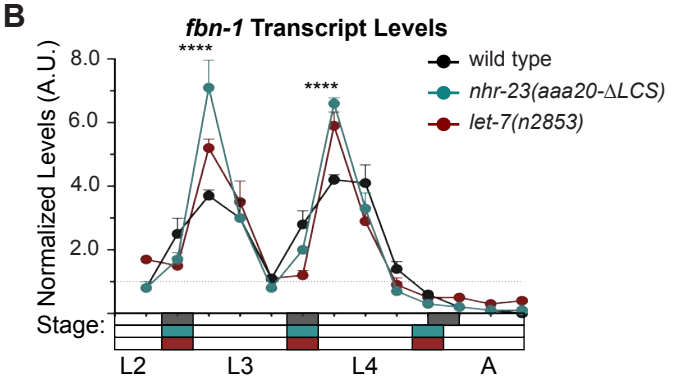

Stage	L3			L4		
Genotype	wild type	nhr-23(aaa20)	let-7(n2853)	wild type	nhr-23(aaa20)	let-7(n2853)
Amplitude	1.4	3.0	2.1	1.2	1.7	1.9
Rising Slope	0.73	1.56	1.85	0.78	1.45	2.35

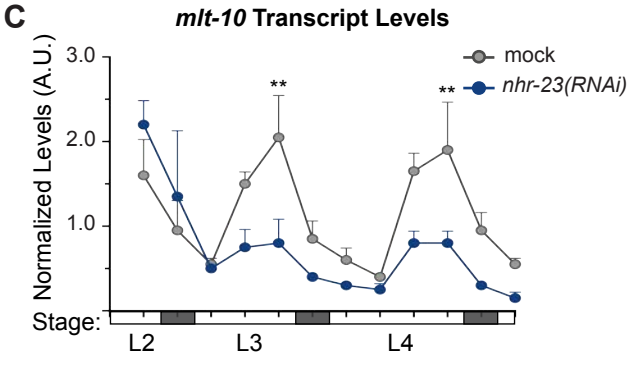

Stage	L3		L4	
RNAi	mock	nhr-23(RNAi)	mock	nhr-23(RNAi)
Amplitude	0.7	0.5	0.7	0.5
Rising Slope	0.36	0.08	0.40	0.10

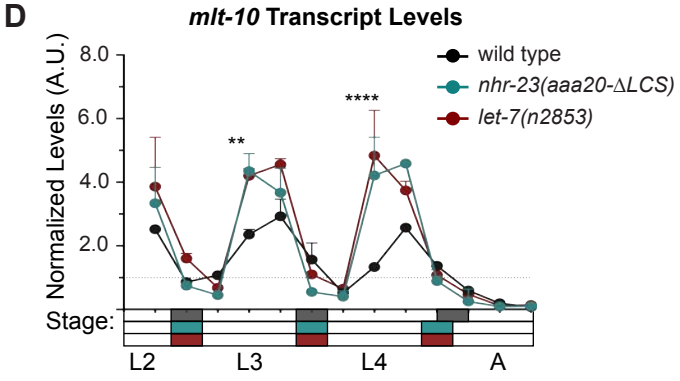

Stage	L3			L4		
Genotype	wild type	nhr-23(aaa20)	let-7(n2853)	wild type	nhr-23(aaa20)	let-7(n2853)
Amplitude	1.0	2.3	2.2	1.0	2.8	2.4
Rising Slope	0.46	1.95	1.76	0.51	1.91	2.10

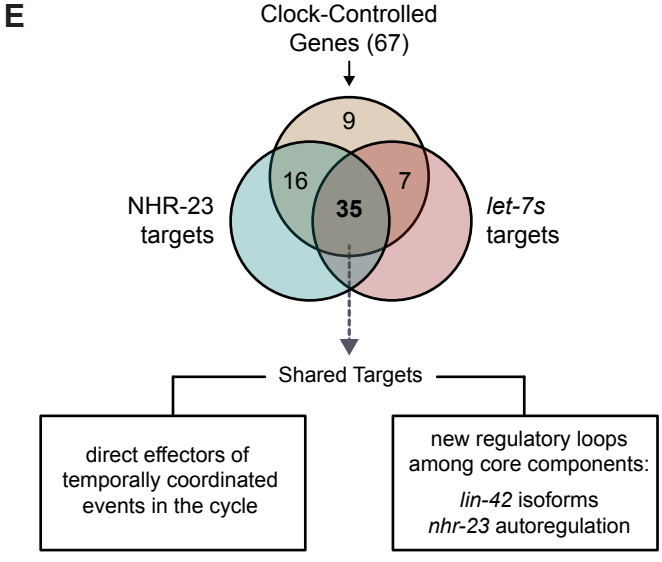

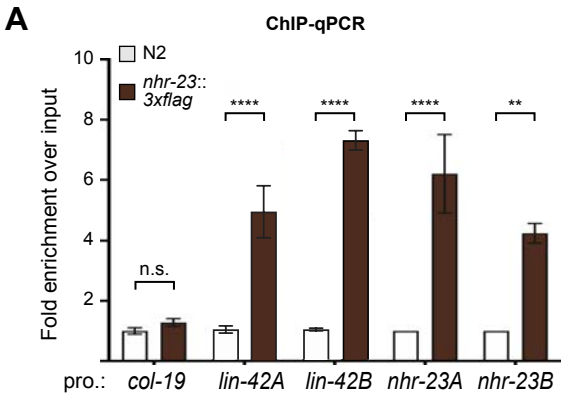

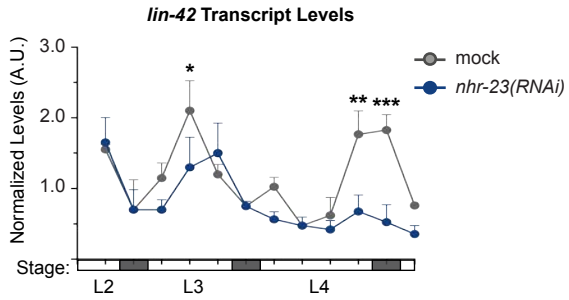

Stage	L3		L4	
RNAi	mock	nhr-23(RNAi)	mock	nhr-23(RNAi)
Amplitude	0.7	0.5	0.6	0.2
Rising Slope	0.35	0.15	0.60	0.10

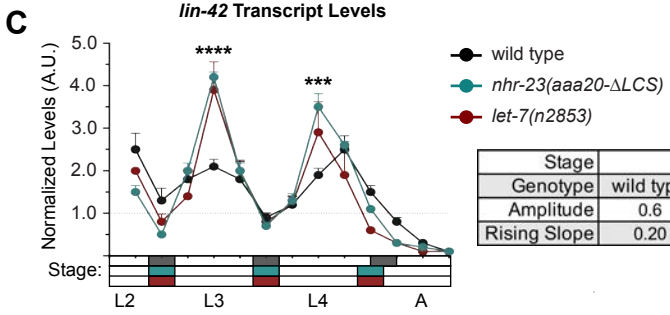

Stage	L3			L4		
Genotype	wild type	nhr-23(aaa20)	let-7(n2853)	wild type	nhr-23(aaa20)	let-7(n2853)
Amplitude	0.6	1.7	1.5	0.8	1.6	1.2
Rising Slope	0.20	0.93	0.78	0.27	0.70	0.53

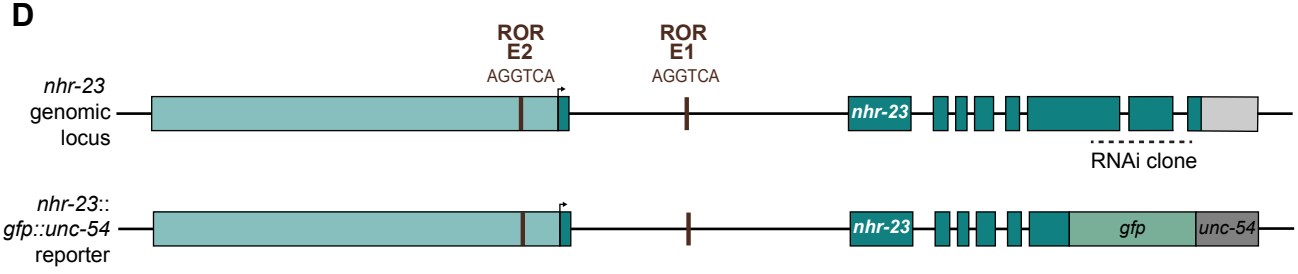

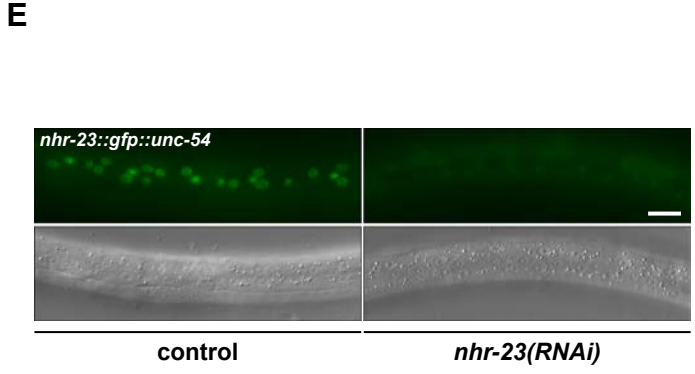

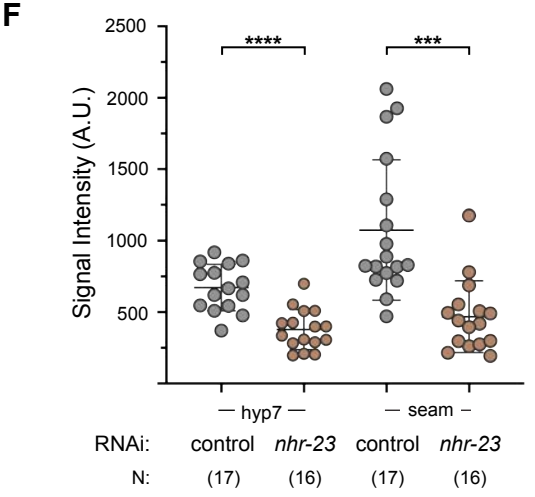

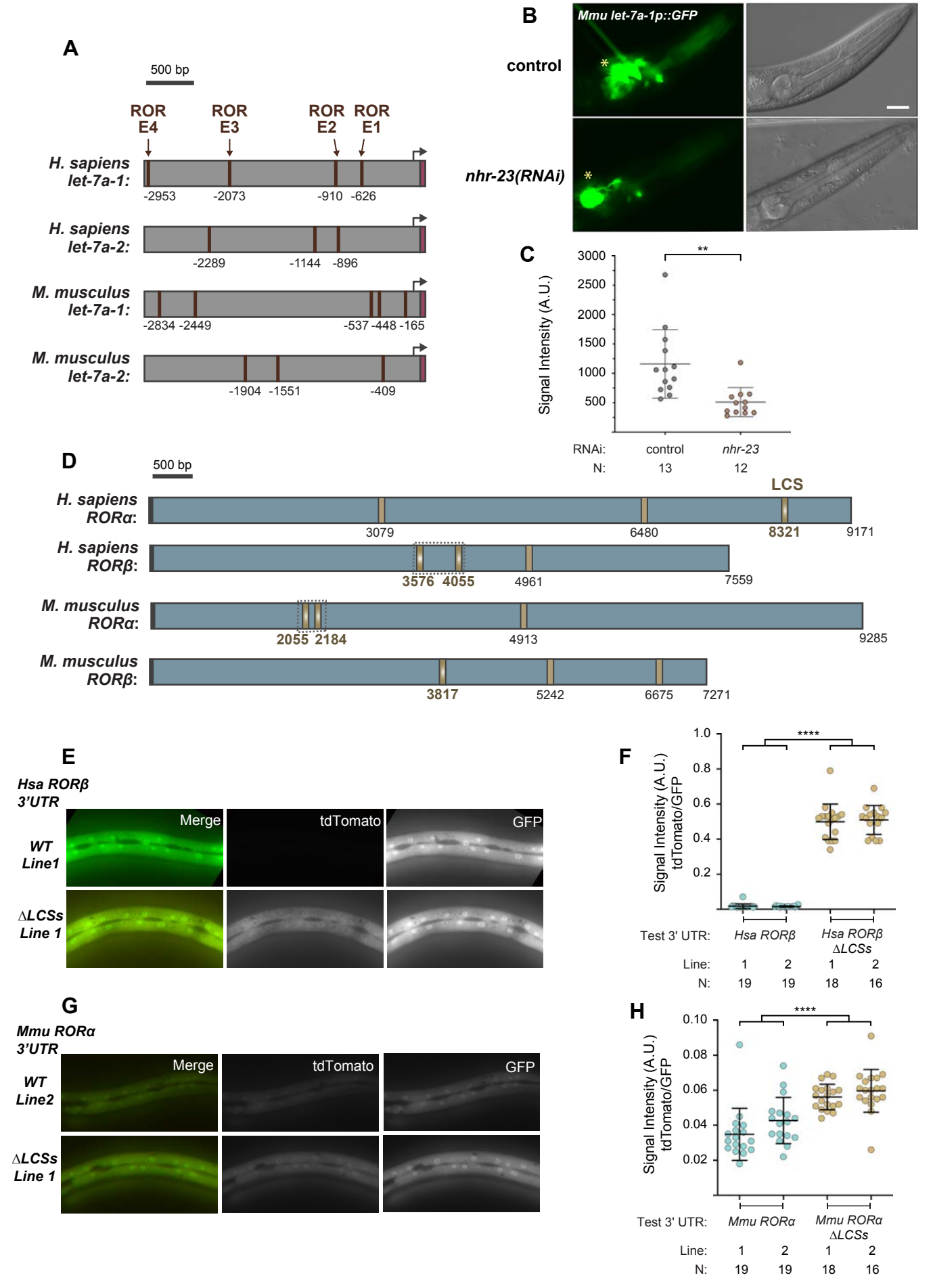
A
500 bp
ROR E4
ROR E3
ROR E2
ROR E1
H. sapiens let-7a-1:
-2953 -2073 -910 -626
H. sapiens let-7a-2:
-2289 -1144 -896
M. musculus let-7a-1:
-2834 -2449 -537 -448 -165
M. musculus let-7a-2:
-1904 -1551 -409
B
Mmu let-7a-1p::GFP
control
nhr-23(RNAi)
C
Signal Intensity (A.U.)
3000
2500
2000
1500
1000
500
**
RNAi: control nhr-23
N: 13 12
D
500 bp
LCS
H. sapiens RORα:
3079 6480 8321 9171
H. sapiens RORβ:
3576 4055 4961 7559
M. musculus RORα:
2055 2184 4913 9285
M. musculus RORβ:
3817 5242 6675 7271
E
Hsa RORβ 3'UTR
Merge
tdTomato
GFP
WT Line1
ΔLCSs Line 1
F
Signal Intensity (A.U.) tdTomato/GFP
1.0
0.8
0.6
0.4
0.2
****
Test 3' UTR: Hsa RORβ Hsa RORβ ΔLCSs
Line: 1 2 1 2
N: 19 19 18 16
G
Mmu RORα 3'UTR
Merge
tdTomato
GFP
WT Line2
ΔLCSs Line 1
H
Signal Intensity (A.U.) tdTomato/GFP
0.10
0.08
0.06
0.04
0.02
****
Test 3' UTR: Mmu RORα Mmu RORα ΔLCSs
Line: 1 2 1 2
N: 19 19 18 16

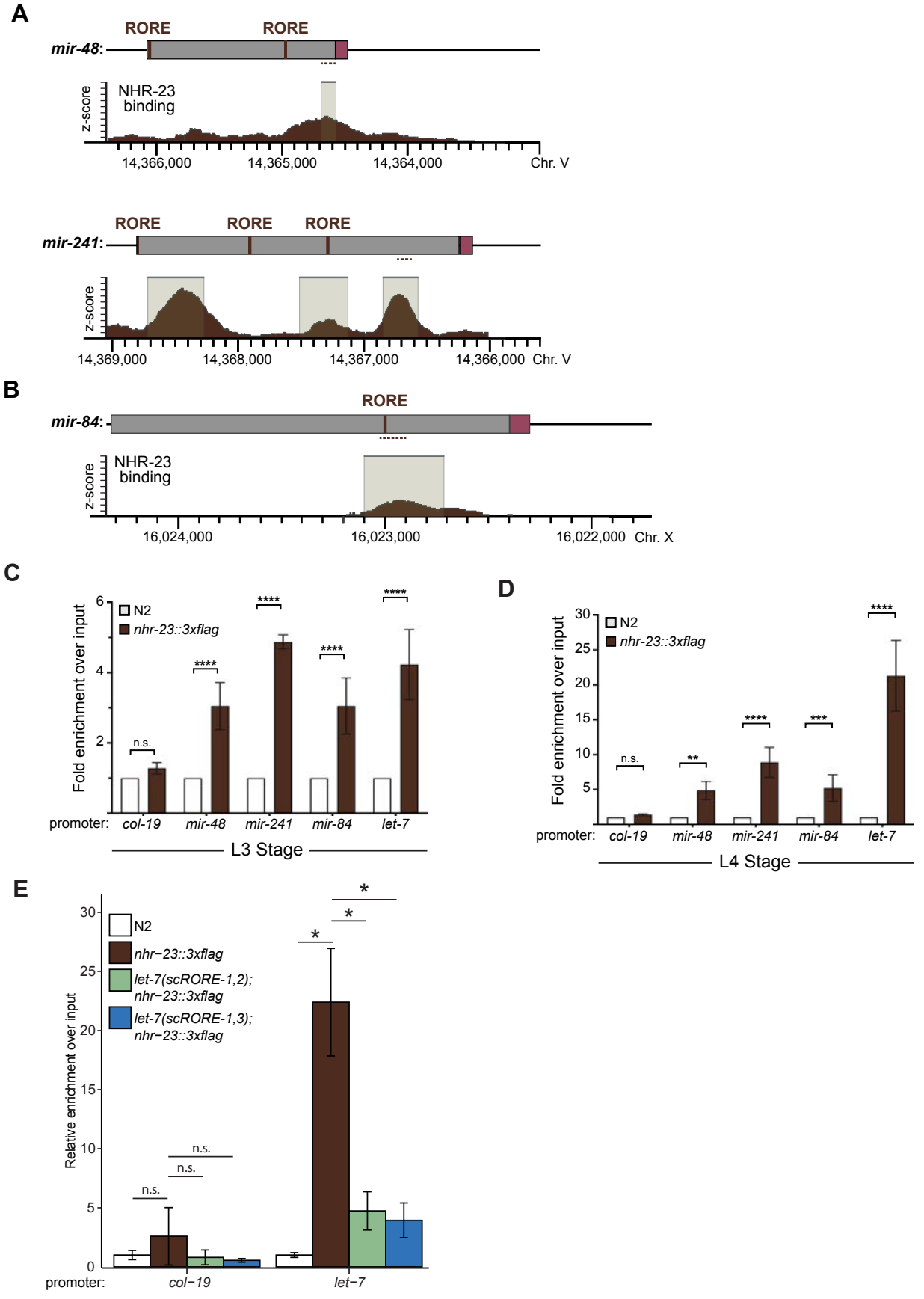
A
RORE
RORE
mir-48:
NHR-23 binding
z-score
14,366,000
14,365,000
14,364,000
Chr. V
RORE
RORE
RORE
mir-241:
z-score
14,369,000
14,368,000
14,367,000
14,366,000
Chr. V
B
RORE
mir-84:
NHR-23 binding
z-score
16,024,000
16,023,000
16,022,000
Chr. X
C
N2
nhr-23::3xflag
Fold enrichment over input
n.s.
****
promoter:
col-19
mir-48
mir-241
mir-84
let-7
L3 Stage
D
N2
nhr-23::3xflag
Fold enrichment over input
n.s.
**
****
***
promoter:
col-19
mir-48
mir-241
mir-84
let-7
L4 Stage
E
N2
nhr−23::3xflag
let-7(scRORE-1,2); nhr−23::3xflag
let-7(scRORE-1,3); nhr−23::3xflag
Relative enrichment over input
n.s.
*
promoter:
col−19
let−7

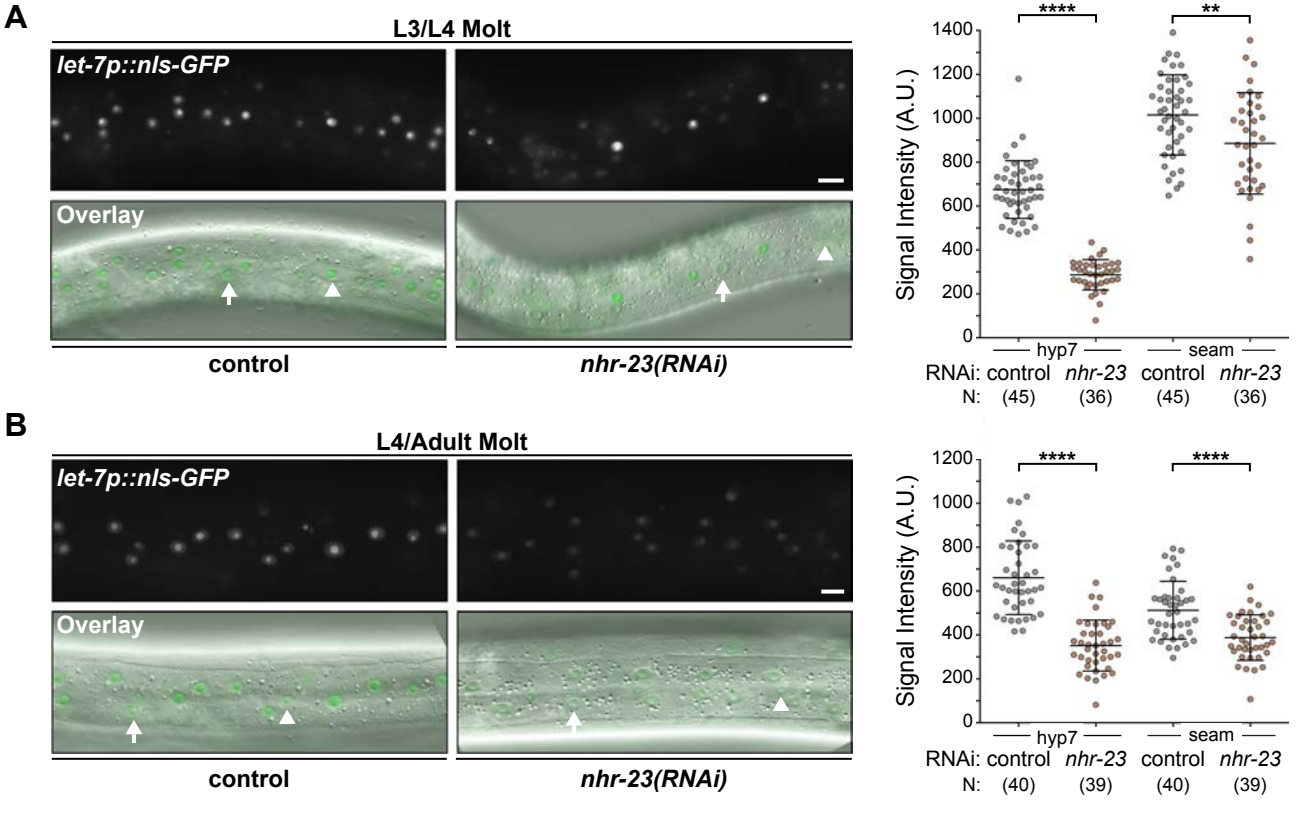
A
L3/L4 Molt
let-7p::nls-GFP
Overlay
control
nhr-23(RNAi)
Signal Intensity (A.U.)
hyp7
seam
RNAi: control nhr-23 control nhr-23
N: (45) (36) (45) (36)
B
L4/Adult Molt
let-7p::nls-GFP
Overlay
control
nhr-23(RNAi)
Signal Intensity (A.U.)
hyp7
seam
RNAi: control nhr-23 control nhr-23
N: (40) (39) (40) (39)
C
mock
nhr-23(RNAi)
primary mir-48
primary mir-241
primary mir-84
Normalized Levels (A.U.)
Stage: L2 L3 L4
D
mock
nhr-23(RNAi)
mature mir-48
mature mir-241
mature mir-84
Normalized Levels (A.U.)
Stage: L2 L3 L4

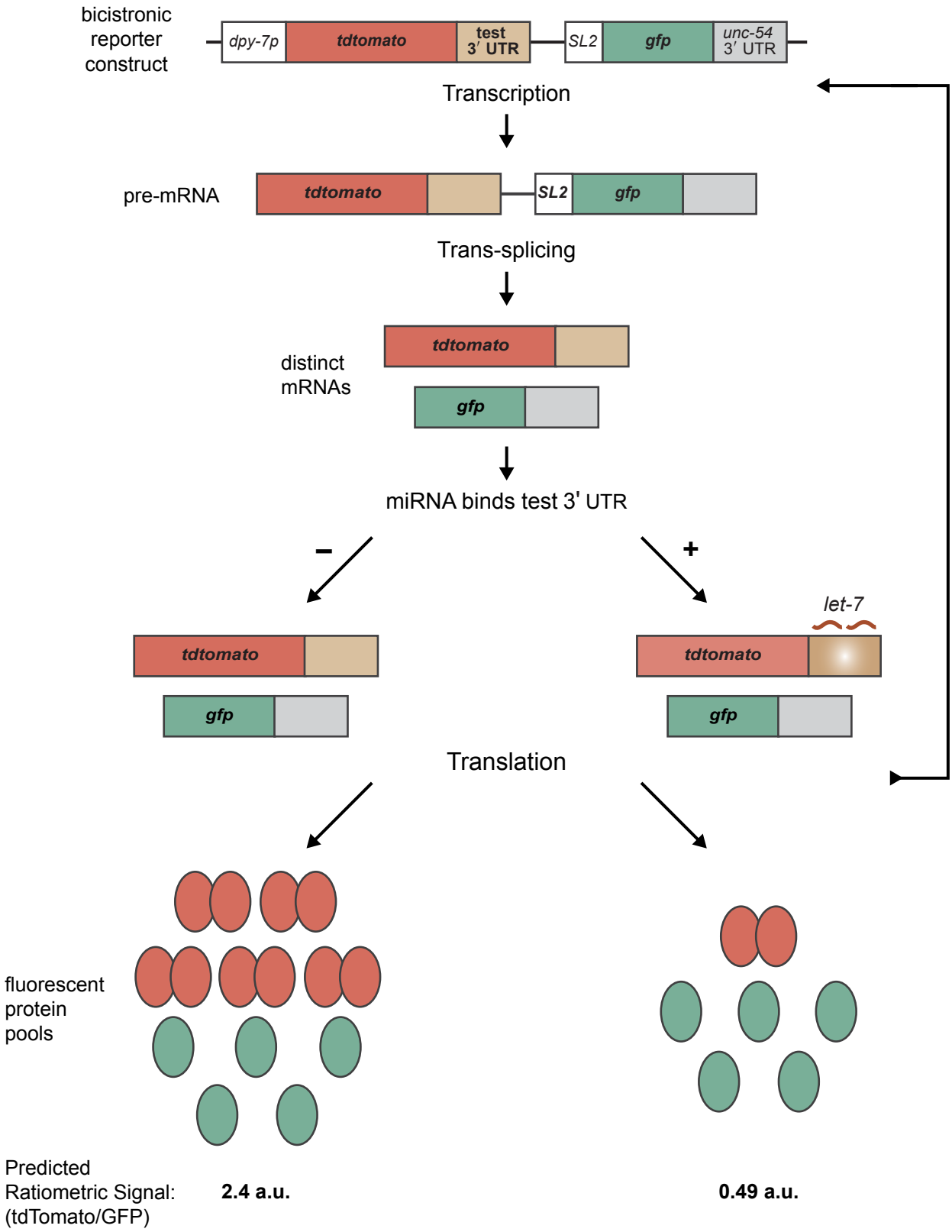
bicistronic reporter construct
dpy-7p
tdtomato
test 3′ UTR
SL2
gfp
unc-54 3′ UTR
Transcription
pre-mRNA
tdtomato
SL2
gfp
Trans-splicing
distinct mRNAs
tdtomato
gfp
miRNA binds test 3' UTR
–
+
let-7
tdtomato
gfp
tdtomato
gfp
Translation
fluorescent protein pools
Predicted Ratiometric Signal: (tdTomato/GFP)
2.4 a.u.
0.49 a.u.

A

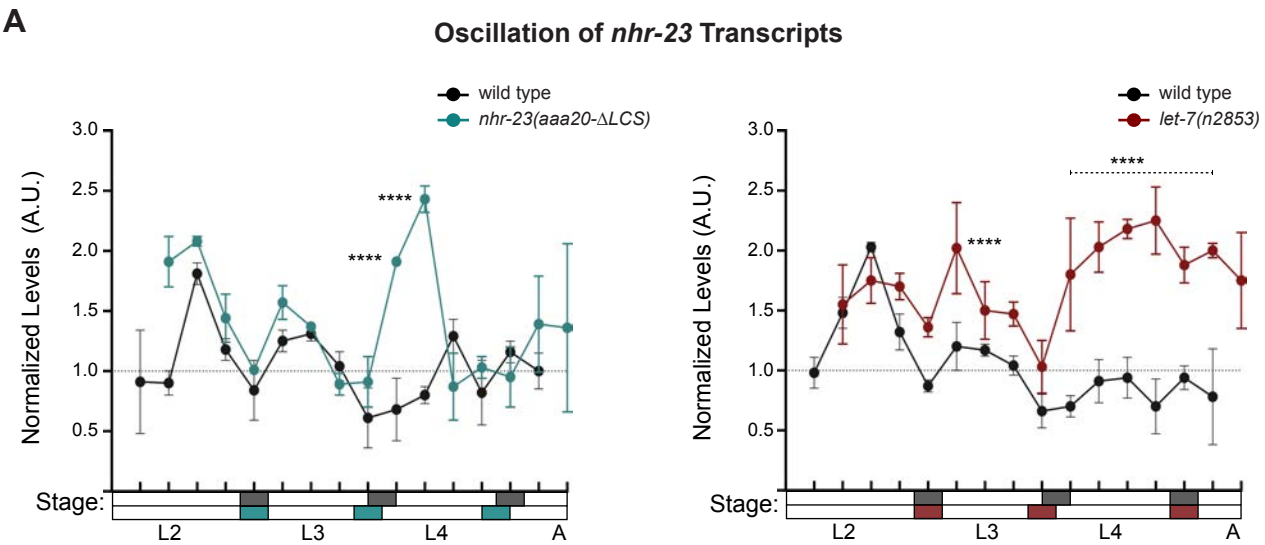

A′

Stage	L3				L4			
Genotype	wild type	*nhr-23(aaa20)*	wild type	*let-7(n2853)*	wild type	*nhr-23(aaa20)*	wild type	*let-7(n2853)*
Amplitude	0.3	0.4	0.2	0.3	0.2	0.7	0.1	0.3
Rising Slope	0.12	0.30	0.17	0.33	0.11	0.40	0.05	0.25

B

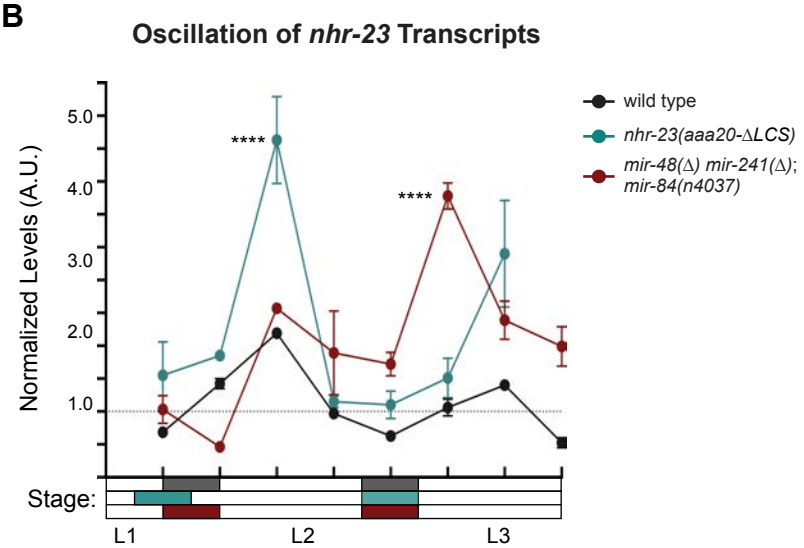

B′

Stage	L2		
Genotype	wild type	*nhr-23(aaa20)*	*mir-48(Δ) mir-241(Δ); mir-84(n4037)*
Amplitude	0.7	1.6	0.6
Rising Slope	0.38	1.64	1.10

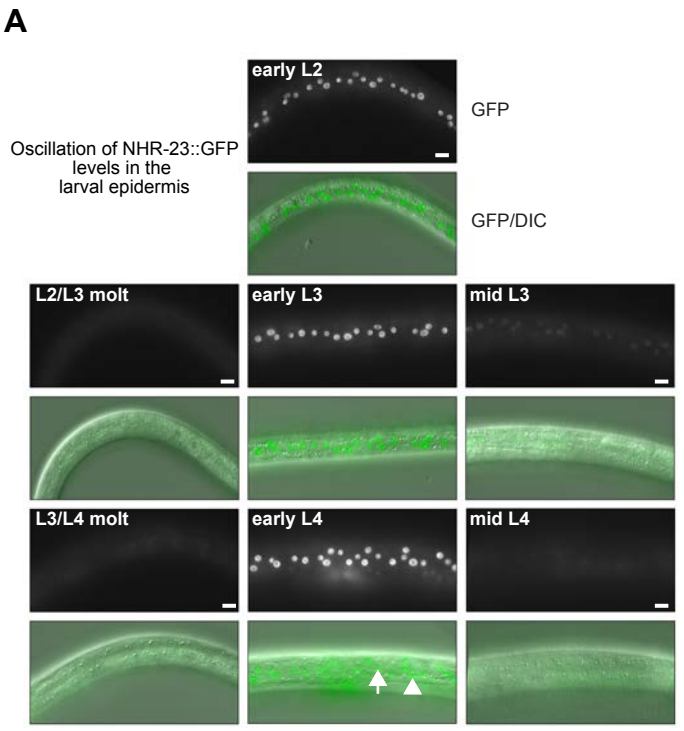
A
Oscillation of NHR-23::GFP levels in the larval epidermis
early L2
GFP
GFP/DIC
L2/L3 molt
early L3
mid L3
L3/L4 molt
early L4
mid L4

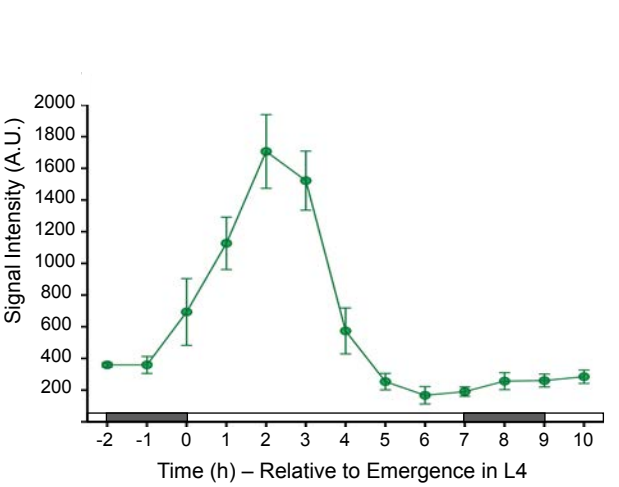
B
Signal Intensity (A.U.)
2000
1800
1600
1400
1200
1000
800
600
400
200
-2
-1
0
1
2
3
4
5
6
7
8
9
10
Time (h) – Relative to Emergence in L4

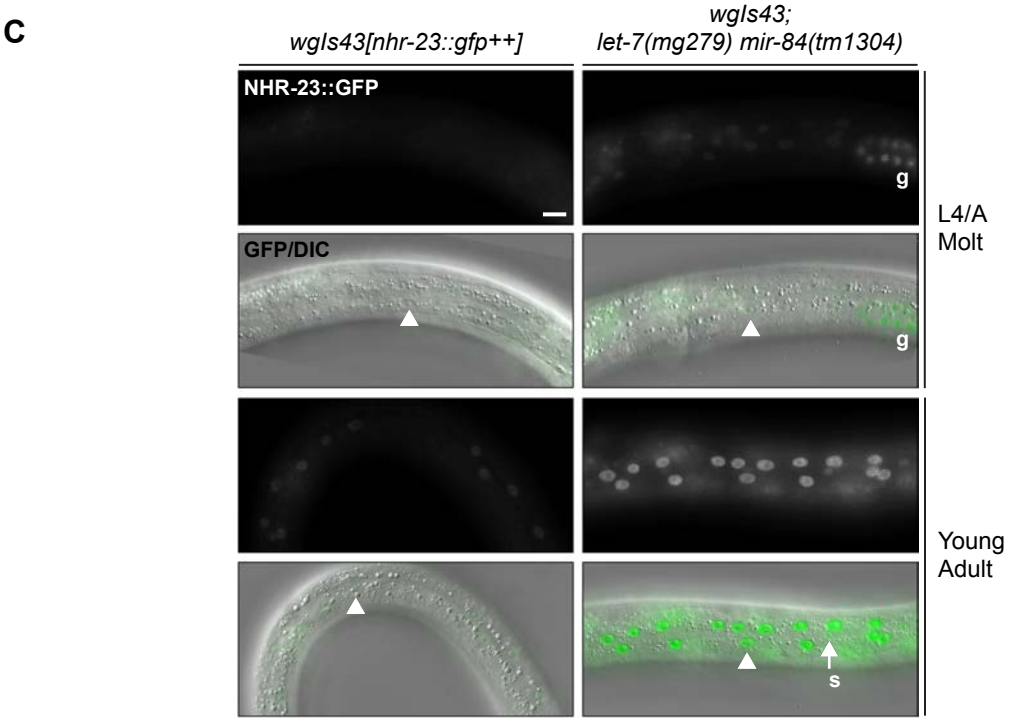
C
wgIs43[nhr-23::gfp++]
wgIs43; let-7(mg279) mir-84(tm1304)
NHR-23::GFP
g
L4/A Molt
GFP/DIC
g
Young Adult
s

A

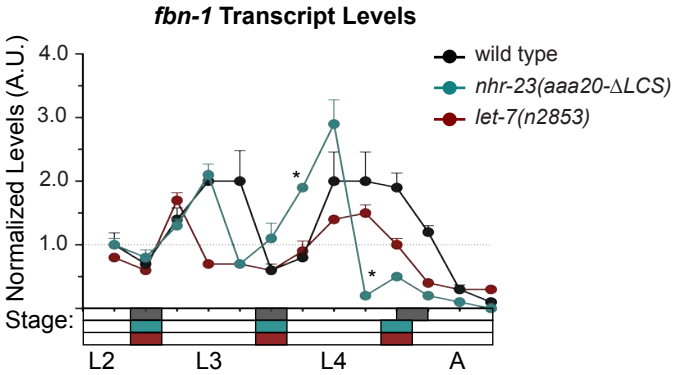

Stage	L3			L4		
Genotype	wild type	*nhr-23(aaa20)*	*let-7(n2853)*	wild type	*nhr-23(aaa20)*	*let-7(n2853)*
Amplitude	0.7	0.6	0.5	0.6	0.8	0.7
Rising Slope	0.33	0.33	1.10	0.30	0.37	0.20

B

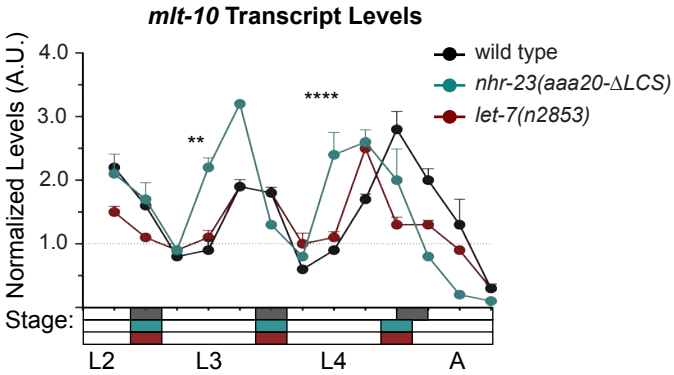

Stage	L3			L4		
Genotype	wild type	*nhr-23(aaa20)*	*let-7(n2853)*	wild type	*nhr-23(aaa20)*	*let-7(n2853)*
Amplitude	0.8	0.9	0.2	0.8	1.0	0.6
Rising Slope	0.28	0.58	0.40	0.37	0.45	0.38

A

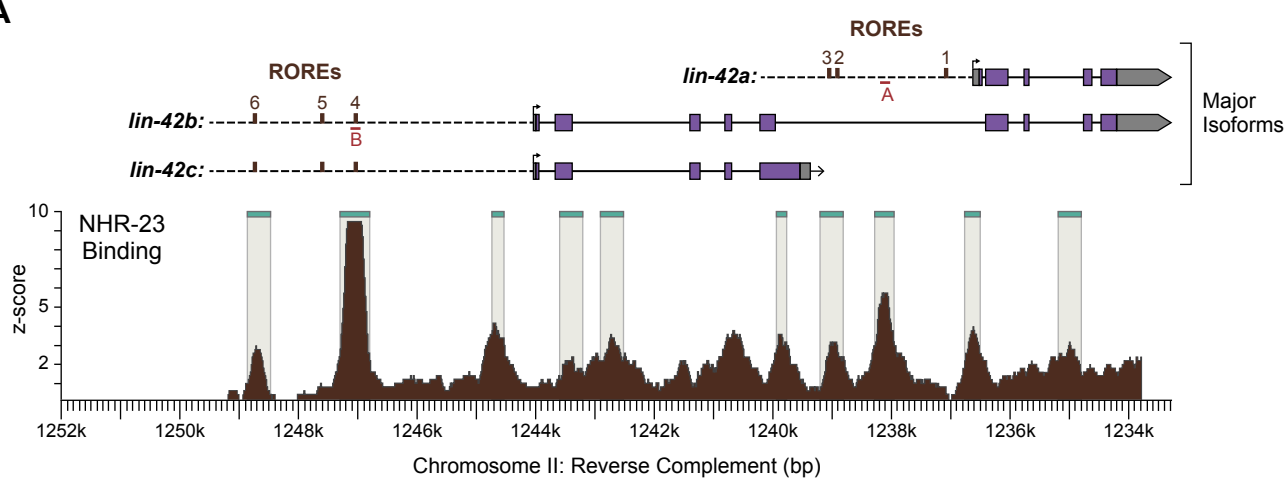

B

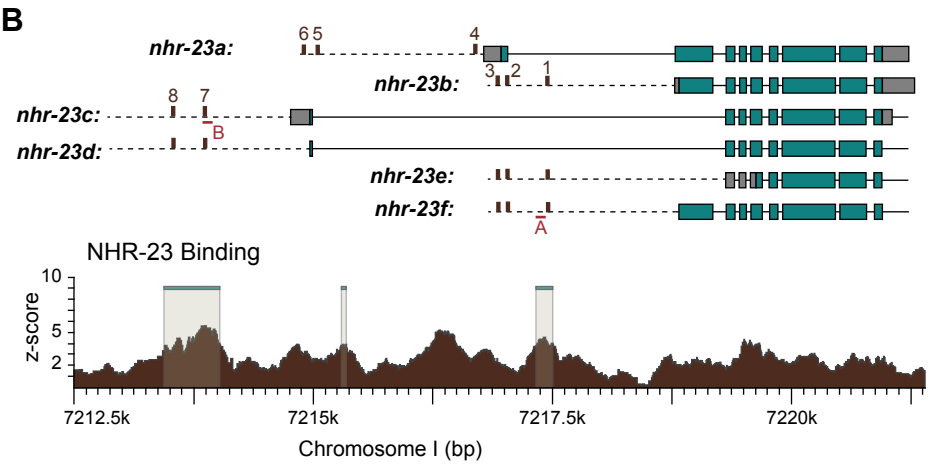

C

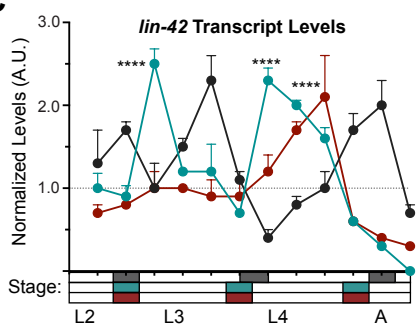

Stage	L3			L4		
Genotype	wild type	*nhr-23(aaa20)*	*let-7(n2853)*	wild type	*nhr-23(aaa20)*	*let-7(n2853)*
Amplitude	0.4	0.6	-	0.6	0.8	0.7
Rising Slope	0.33	0.80	-	0.20	0.80	0.20

D

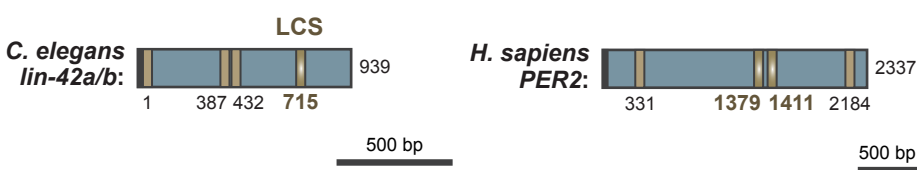

A

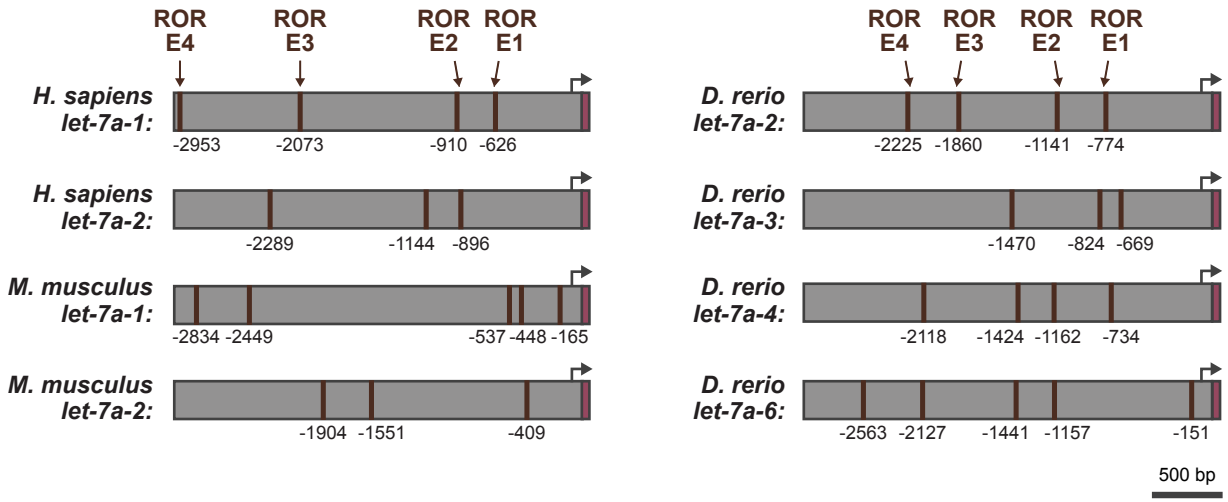
ROR E4
ROR E3
ROR E2
ROR E1
H. sapiens let-7a-1:
-2953 -2073 -910 -626
H. sapiens let-7a-2:
-2289 -1144 -896
M. musculus let-7a-1:
-2834 -2449 -537 -448 -165
M. musculus let-7a-2:
-1904 -1551 -409
D. rerio let-7a-2:
-2225 -1860 -1141 -774
D. rerio let-7a-3:
-1470 -824 -669
D. rerio let-7a-4:
-2118 -1424 -1162 -734
D. rerio let-7a-6:
-2563 -2127 -1441 -1157 -151
500 bp

B

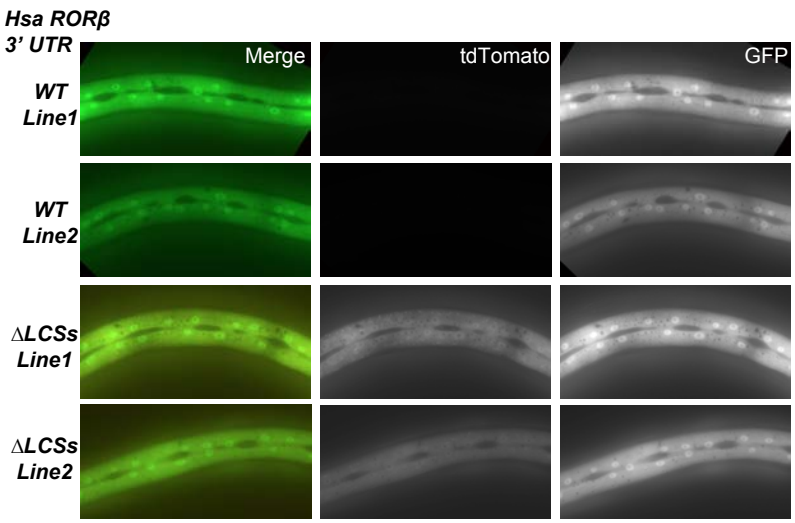
Hsa RORβ 3' UTR
Merge
tdTomato
GFP
WT Line1
WT Line2
ΔLCSs Line1
ΔLCSs Line2

C

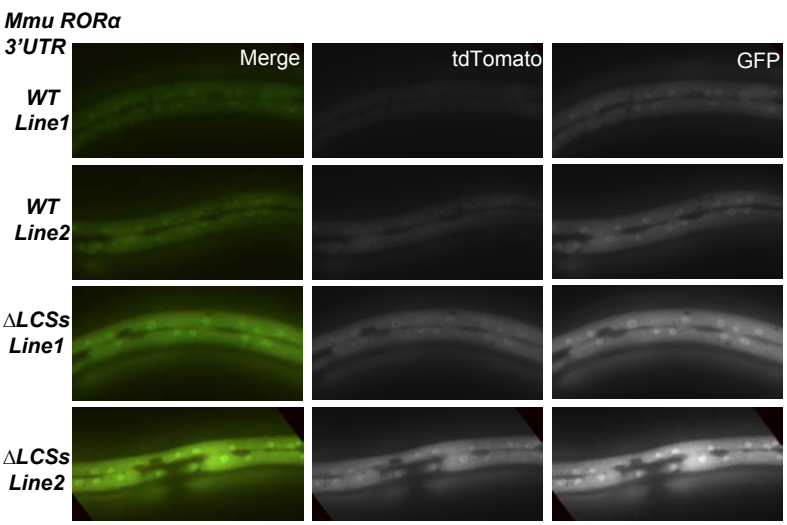
Mmu RORα 3'UTR
Merge
tdTomato
GFP
WT Line1
WT Line2
ΔLCSs Line1
ΔLCSs Line2

1988 **Supplemental Table 1 – Relates to Figures 2, 4 and 6**
1989

Metrics of the Molting Biorhythm Associated with Specific Genotypes															
			Interval (h)												
L4 stage cohort			Active				Lethargic				Wake-to-Wake				
Strain	RNAi	N	mean	sd	cv	p	mean	sd	cv	p	mean	sd	cv	p	
wild type (N2)	—	16	8.1	0.5	0.06	—	2.2	0.4	0.18	—	10.3	0.4	0.05	—	
wild type	*nhr-23*	17	8.4	0.8	0.09	n.s.	4.6	0.7	0.16	****	13.0	1.1	0.08	****	
let-7(n2853)	—	15	6.3	0.4	0.08	****	1.5	0.5	0.33	*	7.9	0.6	0.08	****	
let-7(n2853)	*nhr-23*	19	6.7	0.6	0.10	****	3.9	0.6	0.16	****	10.6	0.8	0.07	n.s.	
let-7(n2853)†	—	17	6.7	0.6	0.09	****	1.6	0.5	0.30	**	8.4	0.6	0.07	****	
wild type (GR1395)	—	20	7.8	0.5	0.07	—	2.2	0.6	0.18	—	10.0	0.5	0.05	—	
let-7(mg279)	—	20	7.2	0.6	0.08	**	2.2	0.4	0.17	n.s.	9.3	0.6	0.06	**	
let-7(mg279) mir-84(tm1304)	—	18	6.1	0.9	0.15	****	2.4	0.6	0.25	n.s.	8.5	0.9	0.15	****	
wild type (N2)	—	17	7.7	0.5	0.07	—	2.0	0.0	0.00	—	9.7	0.5	0.05	—	—§
let-7(xk41-scRORE1,2)	—	12	6.9	0.7	0.10	*	1.8	0.6	0.36	n.s.	8.7	0.9	0.10	***	***
let-7(xk44-scRORE1,2)	—	8	6.6	0.5	0.08	**	2.3	0.5	0.21	n.s.	8.9	0.4	0.04	*	**
let-7(xk39-scRORE1,3)	—	17	6.5	0.6	0.10	****	2.4	0.6	0.26	n.s.	8.7	0.6	0.07	****	****

let-7(xk42-scRORE1,3)	—	14	6.6	1.1	0.17	***	2.1	0.6	0.30	n.s.	8.6	0.7	0.09	****	****
wild type (N2)	—	12	8.1	0.7	0.08	—	2.0	0.0	0.0	—	10.0	0.7	0.07	—	
wgIs43 [nhr-23++]	—	17	7.2	0.5	0.07	***	2.2	0.6	0.29	n.s.	9.4	0.5	0.05	**	
nhr-23 (aaa20-ΔLCS)	—	25	6.8	0.7	0.1	****	2.1	0.3	0.16	n.s.	8.9	0.6	0.07	****	
L3 stage cohort			Active				Lethargic				Wake-to-Wake				
Strain	RNAi	N	mean	sd	cv	p	mean	sd	cv	p	mean	sd	cv	p	
wild type (N2)	—	17	6.3	0.4	0.07	—	1.6	0.5	0.31	—	7.9	0.7	0.08	—	
wild type	*nhr-23*	12	7.7	1.2	0.15	****	3.8	1.9	0.49	****	11.0‡	1.3	0.12	****	
let-7(n2853)	—	18	5.6	0.6	0.11	*	1.3	0.4	0.36	n.s.	6.8	0.5	0.07	*	
let-7(n2853)	*nhr-23*	18	5.8	0.8	0.13	n.s.	3.8	0.6	0.17	****	9.6	0.9	0.09	****	
wild type (N2)	—	13	6.4	0.7	0.11	—	1.4	0.5	0.37	—	7.8	0.6	0.08	—	
wgIs43 [nhr-23++]	—	15	5.2	0.9	0.18	***	1.7	0.6	0.34	n.s.	6.9	0.6	0.09	**	
nhr-23 (aaa20-ΔLCS)	—	19	5.1	0.7	0.14	***	1.2	0.5	0.44	n.s.	6.3	0.7	0.11	****	
L2 stage cohort			Active				Lethargic				Wake-to-Wake				
Strain	RNAi	N	mean	sd	cv	p	mean	sd	cv	p	mean	sd	cv	p	
wild type (N2)	—	18	5.9	0.3	0.05	—	1.3	0.5	0.36	—	7.2	0.4	0.06	—	
wild type	*nhr-23*	19	6.1	0.6	0.10	n.s.	3.9	1.1	0.28	****	9.9	1.0	0.10	****	

mir-48 mir-241 (nDf51); mir-84(n4037)	—	17	6.3	0.7	0.11	n.s.	1.3	0.5	0.36	n.s.	7.6	0.7	0.10	n.s.
mir-48 mir-241 (nDf51); mir-84(n4037)	*nhr-23*	15	6.4	0.8	0.13	n.s.	3.0	0.4	0.13	****	9.4	0.8	0.09	****

†Entry for the L3 cohort fortuitously observed throughout L4 and depicted by the penultimate actogram in Figure 2C.

‡Value excludes the one and only *nhr-23(RNAi)* larvae that remained lethargic at the final time-sample.

§ p-values of wake-to-wake interval by Mann-Whitney Test

1990

Supplemental Table 2 – Relates to Figures 5 and 10

let-7 Consensus Sites (LCSs) Identified in 3' UTRs of Selected Nematode and Vertebrate Homologs of *ROR*						
Species	Gene	Identifier	3' UTR Length (nt.)	LCS Position (3' nt.)	TS (kcal/mol)	Alignment of LCS (5' to 3') with *let-7* (3' to 5')
C. elegans	*nhr-23*	NM_001025806	868	42	-21.8	5' UU C UG – – C 3' UUAU CA CU CU CCUU GAUA GU GA GA GGAG 3' UU U UG U U U 5'
				249	-15.2	5' U U GAG G U 3' G CUG UGCAG A U CCUCA U GAU AUGUU U A GGAGU 3' U – GGA G U 5'
				594	-17.0	5' UUAA CU CCAUU U 3' AUAU CC UAUUGCCUU UAUG GG AUGAUGGAG 3' UUGA UU ----- U 5'
				646	-17.6	5' C UUAAU – UC – U 3' GCU UAC GCCU UUACC CA UGA AUG UGGA GAUGG GU 3' U U---- U U– A 5'
C. briggsae	*nhr-23*	WBGene 00040598	866	629	-20.7	5' UU C CGCU U C 3' C AUACAACU CUGC CUC G UAUGUUGG GAUG GAG 3' UU A AU-- – U 5'
				835	-21.8	5' UUAC CUUUUUU C 3' AUAUAAUCU CUGCCUC UAUGUUGGA GAUGGAG 3' UUGA U------ U 5'
H. sapiens	*RORβ*	NM_006914	7559	**3576**	-25.9	5' CGC – C 3' GGCU UGCAAUCU CUGCCUC UUGA AUGUUGGA GAUGGAG 3' U-- U U 5'
				4055	-23.1	5' U A UUU AUCAUA G 3' G C GUACA CCU GCUGCCUU U G UAUGU GGA UGAUGGAG 3' U A U-- ------ U 5'
				4961	-23.1	5' C – A U 3' GAU GU CAGCUUGC GCCUC UUG UA GUUGGAUG UGGAG 3' A U A U 5'
M. musculus	*RORβ*	NM_146095	7271	**3817**	-23.8	5' A GC CU U 3' GG UG CAACU UACUGCCUC UU AU GUUGG AUGAUGGAG 3' G AU -- U 5'
				5242	-22.7	5' GUCACA GAUGCUUC G 3' AACUA GCAACC CUGCCU UUGAU UGUUGG GAUGGA 3' A----- AU------ GU 5'
				6675	-26.7	5' AG – C 3' GA GUACAGCUUGCU CCUC UU UAUGUUGGAUGA GGAG 3' GA U U 5'
D. rerio	*RORβ*	NM_001082856	5431	**949**	-21.8	5' AA C U– U 3' U AUAU UCUGCUGCCUU G UAUG GGAUGAUGGAG 3' UU A UU U 5'
				4318	-23.8	5' U AAAAUAAA G 3' A UUGUACA GCU ACUACUUCA U GAUAUGU UGG UGAUGGAGU 3' U -------- A 5'
				4421	-23.3	5'U ACACAGGCAAACA AUCA U 3' GCUAUAU GAC UACUGCCUU UGAUAUG UUG AUGAUGGAG 3'U ---------- G--- U 5'
H. sapiens	*RORα*	NM_134261	9171	3079	-23.7	5' C – CC A 3' ACUGU CAGCC GCUGCU CA UGAUA GUUGG UGAUGG GU 3' U U A– A 5'
				3142	-22.8	5' UU AA AA C 3' UUGUACA GCCUG UACCUU GAUAUGU UGGAU AUGGAG 3' UU -- G– U 5'
				6480	-24.0	5' C UGUCU – U 3' A CUGUAU GCCUGCU CCUU U GAUAUG UGGAUGA GGAG 3' U U---- U U 5'
				8321	-22.2	5' U AAUC UCAUU UA U 3' A ACA CCU ACUGCCUC U UGU GGA UGAUGGAG 3' U GAUA U---- -- U 5'

M. musculus	*RORα*	NM_013646	9285	**2055**	-23.9	5' CC C A C 3' CJ AUGUA CC GCUGCCUC GAUAUGU GG UGAUGGAG 3' UU U A U 5'
				2184	-23.7	5' U U U 3' AACU UAC GACUU CUGCCUUA UUGA AUG UUGGA GAUGGAGU 3' U U 5'
				4913	-22.6	5' C A CAUC G C 3' AC GUGCAGCC UGCUG CUU UG UAUGUUGG AUGAU GAG 3' U A ---- G U 5'

Supplemental Table 3 – Relates to Figures 5, 7, 8 and Supplemental Figures 6 and 7

Comparisons among wild type, *nhr-23(aaa20)* and *let-7(n2853)*

Transcript: *nhr-23*

	Replicate 1							
Stage	L3				L4			
Genotype	wild type	*nhr-23 (aaa20)*	wild type	*let-7 (n2853)*	wild type	*nhr-23 (aaa20)*	wild type	*let-7 (n2853)*
Amplitude	0.4	1.1	0.5	0.9	0.3	0.4	0.1	0.8
Phase	3.2	2.4	3.2	3.0	0.4	3.2	0.04	3.8
Rising Slope	0.19	0.46	0.15	0.71	0.19	0.21	0.11	0.26
Falling Slope	0.50	0.49	0.36	0.45	0.21	0.19	0.20	0.38
Peak Value	1.78	2.93	1.69	2.84	1.14	1.81	1.18	2.65

	Replicate 2							
Stage	L3				L4			
Genotype	wild type	*nhr-23 (aaa20)*	wild type	*let-7 (n2853)*	wild type	*nhr-23 (aaa20)*	wild type	*let-7 (n2853)*
Amplitude	0.3	0.4	0.2	0.3	0.2	0.7	0.1	0.3
Phase	3.1	2.1	4.5	2.0	5.3	4.0	4.5	4.8
Rising Slope	0.12	0.30	0.17	0.33	0.11	0.40	0.05	0.25
Falling Slope	0.14	0.17	0.10	0.14	0.24	0.39	0.12	0.19
Peak Value	1.31	1.57	1.17	2.02	1.30	2.43	0.94	2.25

Transcript: *fbn-1*

	Replicate 1					
Stage	L3			L4		
Genotype	wild type	*nhr-23 (aaa20)*	*let-7 (n2853)*	wild type	*nhr-23 (aaa20)*	*let-7 (n2853)*
Amplitude	1.4	3.0	2.1	1.2	1.7	1.9
Phase	2.1	2.4	2.8	3.6	2.9	2.9
Rising Slope	0.73	1.56	1.85	0.78	1.45	2.35
Falling Slope	0.64	1.59	1.02	0.60	1.00	0.91
Peak Value	3.65	7.15	5.19	4.24	6.63	5.94

	Replicate 2	
Stage	L3	L4

Genotype	wild type	*nhr-23 (aaa20)*	*let-7 (n2853)*	wild type	*nhr-23 (aaa20)*	*let-7 (n2853)*
Amplitude	0.7	0.6	0.5	0.6	0.8	0.7
Phase	2.2	1.5	1.6	6.3	4.6	5.2
Rising Slope	0.33	0.33	1.10	0.30	0.37	0.20
Falling Slope	0.70	0.70	0.50	0.40	1.35	0.28
Peak Value	1.90	2.10	1.70	2.00	2.90	1.50

Transcript: ***mlt-10***

	Replicate 1					
Stage	L3			L4		
Genotype	wild type	*nhr-23 (aaa20)*	*let-7 (n2853)*	wild type	*nhr-23 (aaa20)*	*let-7 (n2853)*
Amplitude	1.0	2.3	2.2	1.0	2.8	2.4
Phase	5.4	4.9	5.1	6.2	5.0	4.9
Rising Slope	0.46	1.95	1.76	0.51	1.91	2.10
Falling Slope	0.88	0.95	0.65	0.30	0.69	0.63
Peak Value	3.95	4.36	4.56	1.92	4.31	5.17

	Replicate 2					
Stage	L3			L4		
Genotype	wild type	*nhr-23 (aaa20)*	*let-7 (n2853)*	wild type	*nhr-23 (aaa20)*	*let-7 (n2853)*
Amplitude	0.8	0.9	0.2	0.8	1.0	0.6
Phase	2.7	1.5	2.8	8.6	6.6	6.3
Rising Slope	0.28	0.58	0.40	0.37	0.45	0.38
Falling Slope	0.60	0.60	0.23	0.38	0.40	0.35
Peak Value	1.80	3.20	1.90	2.80	2.60	2.50

Transcript: ***lin-42***

	Replicate 1					
Stage	L3			L4		
Genotype	wild type	*nhr-23 (aaa20)*	*let-7 (n2853)*	wild type	*nhr-23 (aaa20)*	*let-7 (n2853)*
Amplitude	0.6	1.7	1.5	0.8	1.6	1.2
Phase	4.5	3.9	4.2	5.4	4.8	4.7

Rising Slope	0.20	0.93	0.78	0.27	0.70	0.53
Falling Slope	0.30	0.86	0.78	0.37	0.52	0.44
Peak Value	2.12	4.15	3.88	2.50	3.48	2.94

	Replicate 2					
Stage	L3			L4		
Genotype	wild type	*nhr-23 (aaa20)*	*let-7 (n2853)*	wild type	*nhr-23 (aaa20)*	*let-7 (n2853)*
Amplitude	0.4	0.6	-	0.6	0.8	0.7
Phase	1.9	0.3	-	6.20	4.10	5.00
Rising Slope	0.33	0.80	-	0.20	0.80	0.20
Falling Slope	0.48	0.30	-	0.65	0.28	0.30
Peak Value	2.30	2.50	-	2.00	2.30	2.10

Comparisons between vector and *nhr-23(RNAi)*

Transcript: ***fbn-1***

Stage	L3		L4	
RNAi	mock	*nhr-23 (RNAi)*	mock	*nhr-23 (RNAi)*
Amplitude	0.7	0.2	1.0	0.2
Phase	2.0	2.0	1.9	2.1
Rising Slope	0.68	0.14	0.40	0.30
Falling Slope	0.21	0.15	0.42	0.12
Peak Value	1.85	0.90	2.80	1.20

Transcript: ***mlt-10***

Stage	L3		L4	
RNAi	mock	*nhr-23 (RNAi)*	mock	*nhr-23 (RNAi)*
Amplitude	0.7	0.5	0.7	0.5
Phase	5.9	6.1	4.9	4.9
Rising Slope	0.36	0.08	0.40	0.10
Falling Slope	0.58	0.20	0.33	0.15
Peak Value	2.10	0.80	1.90	0.80

Transcript: ***lin-42***

Stage	L3		L4	
RNAi	mock	*nhr-23 (RNAi)*	mock	*nhr-23 (RNAi)*
Amplitude	0.7	0.5	0.6	0.2
Phase	3.2	5.3	4.8	4.1
Rising Slope	0.35	0.15	0.60	0.10
Falling Slope	0.33	0.25	0.50	0.15
Peak Value	2.10	1.30	1.80	0.70

Comparisons among wild type, *nhr-23(aaa20)* and *mir-48 mir-241(nDf51); mir-84(n4037)*

Transcript: *nhr-23*

Stage	L2		
Genotype	wild type	*nhr-23 (aaa20)*	*mir-48 mir-241 (nDf51); mir-84 (n4037)*
Amplitude	0.7	1.6	0.6
Phase	1.8	2.0	1.6
Rising Slope	0.38	1.64	1.10
Falling Slope	0.39	2.00	0.21
Peak Value	2.20	5.10	2.60

Supplemental Table 4 – relates to Figures 8 and 9

Classification of Clock-Controlled Genes (CCGs) as Direct Targets of NHR-23, *let-7s*, neither or both.

Gene Name	Sequence	Criteria for targets of NHR-23:					NHR-23 target (Y/N)	Criteria for targets of *let-7s*:				*let-7s* target (Y/N)	Target class	Cyclic mRNA levels (〰)
		Size of upstream regulatory region & first intron (kb)	RORE#	RORE # Obs. / # Exp.	mRNA levels after *nhr-23* RNAi	NHR-23 ChIP-Seq Peaks (#)		Size of 3' UTR (nt.)	LCS#	LCS # Obs. / # Exp.	ALG-1 iCLIP Peaks (+/-)			
Potential Key Clock Components														
let-7	C05G5.6	1.5	3	5.8	↓	1	Y	N/A	–	–	–	N/A	NHR-23	〰
lin-42a	F47F6.1	3.7	3	2.3	↓	4	Y	939	4	3.2	+	Y	Shared	〰
lin-42b	F47F6.1	5.5	3	1.6	↓	3	Y	939	4	3.2	+	Y	Shared	〰
lin-42c	F47F6.1	5.5	3	1.6	↓	3	Y	156	0	0.0	–	N	NHR-23	〰
mir-48	F56A12.3	1.7	2	3.4	–	1	Y	N/A	–	–	–	N/A	NHR-23	〰
mir-241	F56A12.4	2.0	2	2.9	–	2	Y	N/A	–	–	–	N/A	NHR-23	〰
mir-84	B0395.4	2.8	1	1.1	–	2	Y	N/A	–	–	–	N/A	NHR-23	〰
nhr-23	C01H6.5	6.1	8	3.8	↓	3	Y	868	4	2.6	+	Y	Shared	〰
nhr-25	F11C1.6	6.9	3	1.3	–	3	Y	749	1	1.0	+	Y	Shared	〰
Other Gene Regulatory Factors														
alg-1	F48F7.1	9.9	1 1	3.2	–	3	Y	400	1	1.9	+	Y	Shared	〰
bed-3	F25H8.6	1.7	2	3.4	–	1	Y	459	1	1.6	+	Y	Shared	〰
blmp-1	F25D7.3	6.7	7	3.0	–	4	Y	861	3	2.6	+	Y	Shared	〰
bro-1	F56A3.5	1.2	0	0.0	–	1	N	379	1	2.0	–	N	–	〰

dre-1	K04A8.6	7.5	8	3.1	–	4	Y	376	2	4.0	+	Y	Shared	
mab-10	R166.1	6.0	8	3.9	–	2	Y	374	1	2.0	–	N	NHR-23	
nhr-41	Y104H12A.1	11.1	23	6.0	–	2	Y	332	1	2.3	–	N	NHR-23	
pqn-47	F59B10.1	5.9	7	3.4	–	5	Y	804	2	1.9	+	Y	Shared	
rnt-1	B0414.2	9.2	4	1.3	–	0	N	221	0	0.0	–	N	–	
Signaling Pathway Components														
acn-1	C42D8.5	4.0	4	2.9	↓	3	Y	384	1	2.0	+	Y	Shared	
apl-1	C42D8.8	4.9	4	2.4	–	5	Y	678	1	1.1	+	Y	Shared	
calu-1	M03F4.7	1.7	3	5.1	–	3	Y	256	1	3.0	+	Y	Shared	
cki-1	T05A6.1	1.9	2	3.1	–	1	Y	235	2	6.5	+	Y	Shared	
glf-1	H04M03.4	2.4	1	1.2	↓	1	Y	247	2	6.2	–	N	NHR-23	
lon-1	F48E8.1	4.8	3	1.8	–	5	Y	185	2	8.3	+	Y	Shared	
lrp-1	F29D11.1	7.9	3	1.1	–	6	Y	346	2	4.4	+	Y	Shared	
mlt-8	W08F4.6	3.5	2	1.7	↓	1	Y	270	2	5.6	+	Y	Shared	
nekl-2	ZC581.1	1.1	1	2.6	–	0	N	73	0	0.0	–	N	–	
nlp-22	T24D8.3	0.8	0	0.0	–	0	N	1000	2	1.5	–	N	–	
osm-7	T05D4.4	3.5	1	0.8	–	0	N	121	1	6.5	+	Y	*let-7s*	
osm-11	F11C7.5	2.8	1	1.1	–	3	Y	545	4	5.5	+	Y	Shared	
phi-59	T19B10.2	1.5	0	0.0	↓	1	Y	121	1	6.5	+	Y	Shared	
pod-2a	W09B6.1	3.0	4	3.9	–	2	Y	324	1	2.3	–	N	NHR-23	
ptr-4	C45B2.7	4.5	4	2.6	↓	2	Y	221	2	6.9	–	N	NHR-23	
ptr-23	ZK270.1	2.0	0	0.0	–	2	N	311	3	7.3	+	Y	*let-7s*	
qua-1	T05C12.10	5.7	3	1.5	↓	4	Y	340	1	2.2	+	Y	Shared	
	E03H4.8	3.4	1	0.9	–	0	N	307	1	2.5	–	N	–	
	T19A5.3	4.9	2	1.2	↓	2	Y	347	1	2.2	+	Y	Shared	

	Y47D3B.1	4.9	3	1.8	–	1	Y	98	1	8.1	–	N	NHR-23	
Extracellular Matrix Proteins and Receptors														
adt-2	F08C6.1	7.6	7	2.7	–	6	Y	621	1	1.2	+	Y	Shared	
bli-5	F45G2.5	1.4	0	0.0	–	0	N	300	1	2.5	+	Y	*let-7s*	
bus-8	T23F2.1	3.6	0	0.0	↓	0	N	453	2	3.3	–	N	–	
clc-1	C09F12.1	5.4	0	0.0	–	0	N	101	1	7.8	–	N	–	
col-12	F15H10.1	0.7	0	0.0	–	0	N	101	1	7.8	+	Y	*let-7s*	
dpy-13	F30B5.1	3.8	5	3.8	–	4	Y	63	2	26.1	+	Y	Shared	
dpy-17	F54D8.1	0.4	1	7.3	–	0	N	54	1	15.5	–	N	–	
dpy-4	Y41E3.2	2.4	0	0.0	–	1	N	102	1	7.8	+	Y	*let-7s*	
dpy-5	F27C1.8	0.8	1	3.6	↓	1	Y	39	0	0.0	–	N	NHR-23	
dpy-7	F46C8.6	0.7	2	8.3	↓	1	Y	236	1	3.2	–	N	NHR-23	
fbn-1	ZK783.1	8.3	12	4.2	↓	6	Y	457	1	1.7	+	Y	Shared	
ina-1	Y116A8A.9	8.0	8	2.9	–	2	Y	261	1	2.9	+	Y	Shared	
mam-1	ZC13.3	3.8	3	2.3	–	0	N	243	0	0.0	–	N	–	
mlt-10	C09E8.3	8.6	4	1.3	↓	1	Y	139	2	11.2	+	Y	Shared	
mlt-11	W01F3.3	5.2	11	6.1	↓	4	Y	353	1	2.1	+	Y	Shared	
mlt-7	ZK430.8	11.5	15	3.8	–	1	Y	317	2	4.8	+	Y	Shared	
mlt-9	F09B12.1	3.5	1	0.8	↓	5	Y	313	1	2.4	–	N	NHR-23	
mup-4	K07D8.1	5.8	5	2.5	–	2	Y	394	0	0.0	–	N	NHR-23	
nas-36	C26C6.3	1.1	1	2.6	↓	0	Y	327	5	11.6	+	Y	Shared	
nas-37	C17G1.6	3.6	7	5.6	↓	2	Y	240	4	12.7	–	N	NHR-23	
noah-1	C34G6.6	7.9	9	3.3	↓	5	Y	550	1	1.4	+	Y	Shared	
noah-2	F52B11.3	8.9	3	1.0	↓	6	Y	316	2	4.8	+	Y	Shared	

pan-1	M88.6	2.5	2	2.3	–	2	Y	393	2	3.8	+	Y	Shared	⊠
pat-2	F54F2.1	4.0	4	2.9	–	2	Y	292	2	5.2	+	Y	Shared	⊠
rol-6	T01B7.7	3.4	2	1.7	↓	4	Y	117	1	6.7	+	Y	Shared	⊠
pat-3	ZK1058.2	5.0	0	0.0	–	2	N	400	1	1.9	+	Y	*let-7s*	⊠
Cytoskeletal Components														
ifa-2	W10G6.3	1.7	1	1.7	–	1	Y	186	2	8.3	–	N	Shared	⊠
ifc-2	M6.1	3.0	0	0.0	–	0	N	536	2	2.8	+	Y	*let-7s*	⊠
nmy-2	F20G4.3	1.8	6	9.7	–	1	Y	448	2	3.4	+	Y	Shared	⊠
Genes linked to the molting cycle whose expression is not known to oscillate														
daf-9	T13C5.1	1.1	0	0.0	↓	1	Y	214	2	7.2	+	Y	Shared	–
daf-12	F11A1.3	17.0	12	2.0	–	7	Y	1393	5	2.7	+	Y	Shared	–
gei-8	C14B9.6	1.8	1	1.6	–	3	Y	449	4	6.7	+	Y	Shared	–
let-767	C56G2.6	0.6	1	4.8	–	1	Y	87	1	9.2	+	Y	Shared	–
lin-3	F36H1.4	5.5	5	1.9	–	0	N	442	5	8.5	+	Y	*let-7s*	–
nhr-67	C08F8.8	5.5	5	2.6	–	0	N	241	3	9.5	–	N	–	–
skn-1	T19E7.2	5.1	2	1.1	–	2	Y	677	1	1.1	+	Y	Shared	–
Non-CCGs (Randomly Selected)														
acs-13	Y65B4BL.5	4.9	3	1.8	–	2	Y	424	1	1.8	+	Y	Shared	–
ced-8	F08F1.5	0.7	0	0.0	–	0	N	85	0	0.0	–	N	–	–
cyp-33C12	Y5H2B.6	1.5	0	0.0	–	0	N	148	0	0.0	–	N	–	–
ech-5	F56B3.5	0.5	0	0.0	–	1	N	602	1	1.2	–	N	–	–
map-2	Y116A8A.9	1.5	1	1.9	–	0	N	274	2	5.6	–	N	–	–
mpst-7	R186.6	1.0	0	0.0	–	1	N	84	0	0.0	+	N	–	–
nhr-176	F14H3.11	0.2	0	0.0	–	0	N	54	1	15.5	–	N	–	–

nlp-37	F48B9.4	2.9	3	3.0	–	0	N	302	2	5.0	–	N	–	–
nuo-2	T10E9.7	0.2	0	0.0	–	1	N	109	1	14.5	–	N	–	–
srz-10	ZK1037.11	1.1	1	2.6	–	0	N	16	0	0.0	–	N	–	–
ttll-12	D2013.9	0.1	0	0.0	–	0	N	175	1	4.4	+	Y	*let-7s*	–
unc-112	C47E8.7	2.8	1	1.1	–	1	Y	295	1	2.6	+	Y	Shared	–
viln-1	C10H11.1	7.0	3	1.1	–	0	N	119	2	13.2	–	N	–	–
	C01G6.9	0.1	0	0.0	–	0	N	76	1	10.6	–	N	–	–
	F44E5.5	0.4	0	0.0	–	1	N	39	0	0.0	–	N	–	–
	R10E8.6	1.3	0	0.0	–	0	N	31	0	0.0	–	N	–	–
	R12B2.2	0.5	0	0.0	–	0	N	115	0	0.0	–	N	–	–
	T06D4.1	2.3	3	3.8	–	0	N	234	0	0.0	–	N	–	–
	W02D7.3	2.0	1	1.3	–	0	N	78	0	0.0	–	N	–	–
	Y53C10A.6	6.3	0	0.0	–	0	N	201	2	7.6	–	N	–	–

Supplemental Table 5. Oligonucleotides used in this study		
PCR Primer	**Nucleotide Sequence (5' to 3')**	**Application**
HM01	GAAGAACGCCTCACCGAAGGAAGGAAGCATGCGGGATTGGCCAAAGGACCCAAAGGTATGTTT CGAATGATACTAACATAACATAGAACATTTTCAGGAGGACCCTTGGAGGGTAGAAAAAATGGTG AGCAAGGGCGAGGAGGTCATCAAAG	Construction of the bicistronic reporter for *cis*-regulatory elements in the 3' UTR of *unc-54* (pHR011 and *aaaEx97*)
SL2::GFP *::* *unc-54* cassette	GCTGTCTCATCCTACtttcacctagttaactgcttgtcttaaaatctatgcttctctttagtatctaaaattttcctagaagcttacaagtatat aaatggtctcttctcaataaaggttgtatatttattcatcttattgaatctgccatttcctcgtttttgcgagtttatataccttccaattttctttctattgtatttt caacttctaattttaattcagggaaactgctgTACCGGTAGAAAAAATGAGTAAAGGAGAAGAACTTTTCACTGGA GTTGTCCCAATTCTTGTTGAATTAGATGGTGATGTTAATGGGCACAAATTTTCTGTCAGTGGAGA GGGTGAAGGTGATGCAACATACGGAAAACTTACCCTTAAATTTATTTGCACTACTGGAAAACTAC CTGTTCCATGGGTAAGTTTAAACATATATATACTAACTAACCCTGATTATTTAAATTTTCAGCCAA CACTTGTCACTACTTTCTGTTATGGTGTTCAATGCTTCTCGAGATACCCAGATCATATGAAACGG CATGACTTTTTCAAGAGTGCCATGCCCGAAGGTTATGTACAGGAAAGAACTATATTTTTCAAAGA TGACGGGAACTACAAGACACGTAAGTTTAAACAGTTCGGTACTAACTAACCATACATATTTAAAT TTTCAGGTGCTGAAGTCAAGTTTGAAGGTGATACCCTTGTTAATAGAATCGAGTTAAAAGGTATT GATTTTAAAGAAGATGGAAACATTCTTGGACACAAATTGGAATACAACTATAACTCACACAATGTA TACATCATGGCAGACAAACAAAAGAATGGAATCAAAGTTGTAAGTTTAAACATGATTTTACTAACT AACTAATCTGATTTAAATTTTCAGAACTTCAAAATTAGACACAACATTGAAGATGGAAGCGTTCAA CTAGCAGACCATTATCAACAAAATACTCCAATTGGCGATGGCCCTGTCCTTTTACCAGACAACCA TTACCTGTCCACACAATCTGCCCTTTCGAAAGATCCCAACGAAAAGAGAGACCACATGGTCCTT CTTGAGTTTGTAACAGCTGCTGGGATTACACATGGCATGGATGAACTATACAAATAGgagctcCGC ATCGGCCGCTGTCATCAGATCGCCATCTCGCGCCCGTGCCTCTGACTTCTAAGTCCAATTACTC TTCAACATCCCTACATGCTCTTTCTCCCTGTGCTCCCACCCCCTATTTTTGTTATTATCAAAAAAA CTTCTTCTTAATTTCTTTGTTTTTTAGCTTCTTTTAAGTCACCTCTAACAATGAAATTGTGTAGATT CAAAAATAGAATTAATTCGTAATAAAAAGTCGAAAAAAATTGTGCTCCCTCCCCCCATTAATAATA ATTCTATCCCAAAATCTACACAATGTTCTGTGTACACTTCTTATGTTTTTTTTACTTCTGATAAATT TTTTTTGAAACATCATAGAAAAAACCGCACACAAAATACCTTATCATATGTTACGTTTCAGTTTAT GACCGCAATTTTTATTTCTTCGCACGTCTGGGCCTCTCATGACGTCAAATCATGCTCATCGTGAA AAAGTTTTGGAGTATTTTTGGAATTTTTCAATCAAGTGAAAGTTTATGAAATTAATTTTCCTGCTTT TGCTTTTTGGGGGTTTCCCCTATTGTTTGTCAAGAGTTTCGAGGACGGCGTTTTTCTTGCTAAAA TCACAAGTATTGATGAGCACGATGCAAGAAAGATCGGAAGAAGGTTTGGGTTTGAGGCTCAGTG GAAGGTGAGTAGAAGTTGATAATTTGAAAGTGGAGTAGTGTCTATGGGGTTTTTGCCTTAAATGA CAGAATACATTCCCAATATACCAAACATAACTGTTTCC	Construction of the bicistronic reporter for *cis*-regulatory elements in the 3' UTR of *unc-54* (pHR011 and *aaaEx97*)

HM04	ATGGTGAGCAAGGGCGAGG	
HM27	GCGGCCGCTTACTTGTACAGCTCGTCC	
HM28	GGACGAGCTGTACAAGTAAGCGGCCGCGTCCAATTACTCTTCAACATCCC	
HM37	GGTACCATGGTATTGAGCTGTCTCATCC	
HM29	CCGCGCACATTTCCCCGAAAAGTGCCACGGTACCCAAAAAAATTTATCAGAAG	Construction of pHR011 and *aaaEx97*
HM32	GTGGCACTTTTCGGGGAAATG	
HM34	CCTTTTCTGTACATGTCCTGGCCGGCCGGCCAGCAAAAGGCCAGGAACC	
RA31	GATGGCCGGCCTGATCGAAAGTCTCTCCGG	
RA32	CTAGTGATATCCATTTATCTGGAACAAAATGTAAG	
RA101	GGATCCCTGAATCCATATATCATC	Construction of *nhr-23* 3' UTR reporter (pHR017 and *aaaEx129*)
RA102	GGTACCGAGACGTTTTATCACTG	
RA190	GGATCCACACTTTCTTCTTGCTCTTTACC	Construction of *lin-41* 3' UTR reporter (pHR023 and *aaaEx146*)
RA191	GGTACCAATTTCGCAGTGAAATTTGCG	
RA169	TTAAAACTCGTATCATTCCAGTGTCTGC	Deletion of LCS from *nhr-23* 3' UTR reporter (pHR021 and *aaaEx131*)
RA170	TTAATAAAATAAAAATTAGTGCGCCTAGAAATCC	
RA171	TTTGATCCAACCATTTTCTCGTTTATGG	Deletion of nucleotides 623-646 from *nhr-23* 3' UTR reporter (pHR022 and *aaaEx165*)
RA172	GCAGACACTGGAATGATACGAGTTTTAA	
RA184	TTCTTTCTCTCCTTTTCCTGTTTTTAAAG	Deletion of nucleotides 227-249 from *nhr-23* 3' UTR reporter (pHR026 and *aaaEx166*)
RA185	GACTACAATTATTTTTCTATTAATTTTCTG	
RA168	AACTATTGATGATATATGGATTCAGGGATCC	Deletion of nucleotides 26-42 from *nhr-23* 3' UTR reporter (pHR020 and *aaaEx130*)
RA167	CCCTATCCCCGTCCATGAATC	
RA227	CACGGGTACAAAACCACAAATTTCC	Genotype *nhr-23(aaa20) I*

RA228	GCGACCACTACACCATAAACG	
RA272	AGATGAGATGACTAATGAAAGTCCTCG	Genotype *dpy-10 II*
RA273	AGTGAAGAAAGTCCTGCCTTATCC	
RA202	GGTGACAGCCCACTTGGTGCC	Genotype *let-7(n2853) X*
RA203	TCCTTCTAAATTCGTCTAGGCGTCG	
RA277	GGGATAAATGATAAAATGATAACG	Genotype *nDf51 V*
RA278	GGCCGAAAGGCTTCTTACAC	
RA246	GCTCAATTCTTGGAGCCAGC	Genotype *mir-84(n4037) X*
RA247	GATTTTCTGCTCCGACAGATTAACATG	
RA173	TGCCAGACGGCATTCCCTAG	Genotype *let-7(mg279) X*
RA174	AATCAAGTGTGCACTGACCACTC	
RA109	GCAACGGGAAGCTCTGTTACAGG	Genotype *mir-84(tm1304) X*
RA110	GTTCCTCCATTCGACCATAAAGCC	
oHG206	GCTCTTCAAAACTTCCGAATGTCTG	Genotype *nhr-23(xk22) I*
oHG207	AATAACCGGAGGAAACGAGATTCAT	
oHG280	CACTGCGTGACACCCGATTAA	Genotype *let-7(xk39) X*, *let-7(xk41) X, let-7(xk42) X, let-7(xk43) X, let-7(xk44) X*
oHG281	TACATGCCCATTTCAAATGTTTCTT	
oHG290	CTCGAAGAACACAACATGTTATTTCAC	Sanger sequencing of *let-7(xk39) X*, *let-7(xk41) X, let-7(xk42) X, let-7(xk43) X, let-7(xk44) X*
oHG281	TACATGCCCATTTCAAATGTTTCTT	
oHG227	ACTGCGTGACACCCGATTAAA	ChIP-qPCR for *let-7* promoter
oHG228	CAAAATCCAGGTCACCGCAA	
oHG235	TCCATCTCTCTTGGAAACACAT	

oHG236	ACACCTTCAAACCTAACCAGTGT	ChIP-qPCR for *col-19* promoter
oHG294	GCCTGACTCAGACTTCTCCATAGAT	ChIP-qPCR for *mir-84* promoter
oHG295	AGAAGAGGAAAGGAAAAAAACAAGTTA	
oHG298	GCTCGGTGCCGTGTACTTTTATA	ChIP-qPCR for *mir-241* promoter
oHG299	CCAACTTTCCATCTCTGTCGTCT	
oHG300	AAGCGGATCGAGGGAAAAGA	ChIP-qPCR for *mir-48* promoter
oHG301	CCTCTCTAGTTCCTTCTGACTCTCTTG	
oHG373	GGACAGACTGTGGACATCCGA	ChIP-qPCR for *let-7* promoter in the *let-7(scRORE)* mutants
oHG374	GCACGGAACCAACTTGCACT	
oHG251	CACCACCATCATCGCAAACC	ChIP-qPCR for *nhr-23* promoter, amplicon A
oHG252	AACGGTACGGTATGCCTCC	
oHG253	CTGAGGGTCAGTGGTGTGAAA	ChIP-qPCR for *nhr-23* promoter, amplicon B
oHG254	ACACAAAACACCTGCGTTCTC	
oHG306	CCCTTTCATGCACTATTCCGAGA	ChIP-qPCR for *lin-42* promoter, amplicon A
oHG307	CCACCACCGCTAAACCTTTTG	
oHG304	GCGGAGACGCAGAGTACAG	ChIP-qPCR for *lin-42* promoter, amplicon B
oHG305	TGCGAGACATGCCTACAGC	
oHG193	CAAGCAGGCGATTGGTGGA	qPCR primers for *pri-let-7*
oHG194	GACGCAGCTTCGAAGAGTTCTGTC	
oTH1269	acgctcgtgatgagttcaag	qPCR primers for *eft-2*
oTH1270	atttggtccagttccgtctg	
CRISPR	**Nucleotide Sequence (5' to 3')**	**Application**
dpy-10 crRNA	GCUACCAUAGGCACCACGAGGUUUUAGAGCUAUGCUGUUUUG	Edit the *dpy-10* locus

RA226	CACTTGAACTTCAATACGGCAAGATGAGAATGACTGGAAACCGTACCGCATGCGGTGCCTATGG TAGCGGAGCTTCACATGGCTTCAGACCAACAGCCTAT	*dpy-10* ssODN
nhr-23 crRNA	GAGUUUUAAAAGGCAAUAAAGUUUUAGAGCUAUGCUGUUUUG	Edit the 3' UTR of *nhr-23*
tracrRNA	AACAGCAUAGCAAGUUAAAAUAAGGCUAGUCCGUUAUCAACUUGAAAAAGUGGCACCGAGUC GGUGCUUUUUUU	Trans-activation of CAS9
RA225	CTGGATTTCTAGGCGCACTAATTTTTATTTTATTAATTAAAACTCGTATCATTCCAGTGTCTGCGC TTTAA	Repair template (ssODN) for excision of the LCS from 3' UTR of *nhr-23*
oHG202 crRNA	AUGAUAUAUGGAUUCAGUCA	Edit the final exon of *nhr-23*
oHG257	TAGGGAAGGAGAGCATGGATAAAACTATTGATGATATATGGATTCAGTCATCCCTTGTCGTCGT CGTCCTTGTAGTCGATATCATGGTCCTTGTAATCTCCGTCGTGATCTTTATAGTCCGATCCCGAT CCTCCTGAGCCTCCAGGCCGATCTGCAGTGAATAGCTCTTTGTAGAGGGCAGGAAGCTTTTCA G	Repair template (ssODN) for insertion of the coding sequence for 3xFLAG between the last coding codon and the stop codon of *nhr-23*
oHG278 crRNA	GGTATTTTATTGCGGTGACC	Edit RORE3 in the promoter of *let-7*
oHG291	CTTTTGTTCCACTTTTGATGGTATTTTATTGCGGgtctacGGATTTTGCAACATGTGCATTCGAGGG TAAAGGAAG	Repair template (ssODN) for scrambling RORE3 in the promoter of *let-7*
oHG282 crRNA	CGCAGTGCTAGCCGTTGCAC	Edit RORE2 in the promoter of *let-7*
oHG292	CAAAAAAACAGTGCAAGTTGGTTCCGTGCAAACAAgtctacGTGCAACGGCTAGCACTGCGTGACA CCCGATTAAA	Repair template (ssODN) for scrambling RORE2 in the promoter of *let-7*
oHG287 crRNA	AAACTATCTAGGAGGGAACT	Edit RORE1 in the promoter of *let-7*
oHG293	AGGAATTGAAAGTGGACAGACTGTGGACATCCGAGgcctaCAGTTCCCTCCTAGATAGTTTTTTTT CGCTTTCAA	Repair template (ssODN) for scrambling RORE1 in the promoter of *let-7*
oHG3	TCCGAGgcctaCAGTTCCCTCCTAGATAGTTTTTTTTCGCTTTCAACTCCGCCCACAAAAAAACAGT GCAAGTTGGTTCCGTGCAAACAAgtctacGTGCAACGGCTAGCACTGCGTGACACCCGATTAAA	Repair template (ssODN) for scrambling RORE1 and RORE2 in the promoter of *let-7*